

The role of SUN4 and related proteins in sperm head formation and fertility

Dissertation

zur Erlangung des naturwissenschaftlichen Doktorgrades
der Julius-Maximilians-Universität Würzburg

vorgelegt von

Elisabeth Pasch

aus Weimar

Würzburg, 2016



Eingereicht am: _____

Mitglieder der Promotionskommission:

Vorsitzender: _____

Erstgutachter: Prof. Dr. Manfred Alsheimer

Zweitgutachter: Prof. Dr. Dr. Manfred Schartl

Tag des Promotionskolloquiums: _____

Doktorurkunde ausgehändigt am: _____

Table of contents

2.2.3 SUN4 depletion alters the distribution of other LINC complex components and NE associated structures	39
2.2.4 SUN4 depletion causes disruption of the posterior nucleocytoplasmic junction.....	41
2.3 Investigation of SUN4 binding partners.....	46
2.3.1 SUN4 has the potential to interact with SUN3, Nesprin1 and itself.....	46
2.3.2 <i>In vivo</i> binding potential of SUN4	49
3 Discussion	51
3.1 SUN4 is critical for sperm head formation and male mice fertility	53
3.2 <i>Sun4</i> ^{-/-} spermatozoa become encircled by their tail	56
3.3 SUN4 is a posterior LINC complex component.....	57
3.4 SUN4 deficiency influences the distribution of other NE components	61
3.5 SUN5 reveals a unique localization pattern in developing spermatids	63
3.6 SUN4 is crucial for the correct localization and assembly of the spermatid-specific manchette	64
3.7 Localization of the basal body is not affected by the absence of SUN4	66
3.8 Future perspectives.....	68
4 Materials.....	70
4.1 Biological material	70
4.1.1 Bacteria	70
4.1.2 Cell lines.....	70
4.1.3 Animals	71
4.1.4 Antibodies	71
4.2 Molecular material	74

4.2.1 Plasmids.....	74
4.2.2 Oligonucleotides.....	74
4.2.3 Recombinant DNA constructs	75
4.3 Chemicals	76
4.4 Equipment and Software.....	76
5 Methods.....	78
5.1 Microbiological methods.....	78
5.1.1 Culturing of bacteria	78
5.1.1.1 Liquid culture	78
5.1.1.2 Preparation of a glycerol stock	78
5.1.1.3 Culturing bacteria on agar plates.....	78
5.1.2 Production of competent bacteria	79
5.1.3 Transformation of bacteria with plasmid DNA.....	79
5.1.3.1 Determination of the transformation efficiency	80
5.2 Cell culture	81
5.2.1 Culturing of COS-7 cells.....	81
5.2.2 Transfection of COS-7 cells	81
5.3 Mouse husbandry.....	82
5.4 Tissue and organ isolation	83
5.4.1 Testis tissue dissection	83
5.4.1.1 Preparation of testicular cell suspension.....	83
5.4.1.2 Preparation of whole protein tissue samples.....	84
5.5 Molecular methods.....	85
5.5.1 Purification of genomic DNA	85

5.5.2 Purification of plasmid DNA	85
5.5.3 RNA extraction	86
5.5.4 Generation of cDNA by reverse transcription.....	86
5.5.5 Polymerase chain reaction (PCR).....	86
5.5.5.1 Amplification of cDNA with <i>PhusionTM</i> DNA polymerase.....	87
5.5.5.2 Amplification of genomic DNA/ genotyping	88
5.5.5.3 Colony PCR.....	89
5.5.6 DNA electrophoresis	90
5.5.7 Preparative DNA electrophoresis and gel extraction.....	91
5.5.8 DNA cloning	91
5.5.8.1 StrataClone.....	92
5.5.8.2 Restriction digest	92
5.5.8.3 Ligation	92
5.5.9 DNA sequencing	93
5.6 Biochemical methods	94
5.6.1 SDS-PAGE.....	94
5.6.2 Coomassie blue staining	96
5.6.2.1 Drying of Coomassie blue stained acrylamide gels.....	96
5.6.2.2 Measuring protein concentrations in Coomassie blue-stained SDS gels ...	97
5.6.3 Western blot analysis	97
5.6.3.1 Stripping of a nitrocellulose membrane	99
5.6.4 Co-immunoprecipitation	100
5.6.5 Expression and purification of a HIS-tagged fusion protein	103
5.6.6 Precipitation of proteins.....	105

5.6.7 Concentration of proteins	106
5.6.8 Dialysis of proteins	106
5.6.9 Generation of SUN4-specific antibodies	107
5.7 Microscopic methods	111
5.7.1 Mouse tissue preparation for immunohistochemistry	111
5.7.1.1 Smear preparation of germ cells or spermatozoa	111
5.7.1.2 Paraffin tissue embedding and sectioning.....	111
5.7.1.3 Frozen tissue embedding and sectioning	112
5.7.2 Immunofluorescence analysis	113
5.7.2.1 Immunofluorescence analysis on paraffin tissue sections	113
5.7.2.2 Immunofluorescence analysis on frozen tissue sections, germ cell or spermatozoa smear, and cultured COS-7 cells	114
5.7.3 Hematoxylin and Eosin staining	115
5.7.4 Tissue preparation for electron microscopy	116
5.7.4.1 Tissue embedding	116
5.7.4.2 Embedding of testicular cells according to Russell et al. (1991).....	117
5.7.4.3 Sectioning and contrasting of Epon-embedded tissue samples	118
5.8 Image acquisition and analysis	119
5.8.1 Confocal laser scanning microscopy.....	119
5.8.2 Structured illumination microscopy	119
5.8.3 Transmission electron microscopy.....	119
5.8.4 Image processing	120
5.9 Statistics	120
6 References	121

7 Appendix	133
7.1 Abbreviations	133
Erklärung	134
Danksagung.....	135

Summary

Spermiogenesis describes the differentiation of haploid germ cells into motile, fertilization-competent spermatozoa. During this fundamental transition the species-specific sperm head is formed, which necessitates profound nuclear restructuring coincident with the assembly of sperm-specific structures and chromatin compaction. In the case of the mouse, it is characterized by reshaping of the early round spermatid nucleus into an elongated sickle-shaped sperm head. This tremendous shape change requires the transduction of cytoskeletal forces onto the nuclear envelope (NE) or even further into the nuclear interior. LINC (linkers of nucleoskeleton and cytoskeleton) complexes might be involved in this process, due to their general function in bridging the NE and thereby physically connecting the nucleus to the peripheral cytoskeleton.

LINC complexes consist of inner nuclear membrane integral SUN-domain proteins and outer nuclear membrane KASH-domain counterparts. SUN- and KASH-domain proteins are directly connected to each other within the perinuclear space, and are thus capable of transferring forces across the NE. To date, these protein complexes are known for their essential functions in nuclear migration, anchoring and positioning of the nucleus, and even for chromosome movements and the maintenance of cell polarity and nuclear shape.

In this study LINC complexes were investigated with regard to their potential role in sperm head formation, in order to gain further insight into the processes occurring during spermiogenesis. To this end, the behavior and function of the testis-specific SUN4 protein was studied. The SUN-domain protein SUN4, which had received limited characterization prior to this work, was found to be exclusively expressed in haploid stages during germ cell development. In these cell stages, it specifically localized to the posterior NE at regions decorated by the manchette, a spermatid-specific structure which was previously shown to be involved in nuclear shaping. Mice deficient for SUN4 exhibited severely disorganized manchette residues and gravely misshapen sperm heads. These defects resulted in a globozoospermia-like phenotype and male mice infertility. Therefore, SUN4 was not only found to be mandatory for the correct assembly and anchorage of the manchette, but also for the correct localization of SUN3 and Nesprin1, as well as of other NE components. Interaction studies revealed that SUN4 had the potential to interact with SUN3, Nesprin1, and itself, and as such is likely to build functional LINC complexes that anchor the manchette and transfer cytoskeletal forces onto the nucleus.

Summary

Taken together, the severe impact of SUN4 deficiency on the nucleocytoplasmic junction during sperm development provided direct evidence for a crucial role of SUN4 and other LINC complex components in mammalian sperm head formation and fertility.

Zusammenfassung

Die Spermiogenese beschreibt die Differenzierung haploider Keimzellen zu beweglichen, fortpflanzungsfähigen Spermatozoen. Während dieses fundamentalen Entwicklungsabschnittes wird neben dem Aufbau von spermien spezifischen Strukturen und der Kompaktierung des Chromatins auch der speziell spezifische Spermienkopf geformt. Im Falle der Maus ist dies eine aktive Umformung des runden Zellkerns in einen gestreckten, sichelförmigen Spermienkopf. Eine derart gravierende Formveränderung erfordert eine Kraftweiterleitung aus dem Zytoskelett auf die Kernhülle und das Kerninnere. In diesem Zusammenhang könnten LINC (linkers of nucleoskeleton and cytoskeleton) Komplexe eine Rolle spielen, da ihre grundlegende Funktion darin besteht die Kernhülle zu überbrücken und somit den Kern mit dem peripheren Zytoskelett zu verbinden.

LINC Komplexe werden aus SUN und KASH Domänen Proteinen aufgebaut, welche in die innere beziehungsweise äußere Kernmembran eingelagert sind. Diese membranintegralen Proteine sind direkt miteinander verbunden, so dass sie einen Komplex bilden, der zur Kräfteübertragung geeignet ist. LINC Komplexe besitzen vielfältige Funktionen in Prozessen wie nuklearer Migration, Verankerung und Positionierung des Zellkerns, Chromosomenbewegungen und in der Aufrechterhaltung der Zellpolarität oder der Kernform.

Um ein größeres Verständnis der Prozesse während der Spermiogenese zu gewinnen, wurden in dieser Studie die Funktionen von LINC Komplexen in der Spermiogenese und ihre spezifische Rolle bei der gerichteten Spermienkopfstrukturierung untersucht. Dabei wurde insbesondere das Verhalten und die Funktion des bisher wenig charakterisierten SUN Domänen Proteins SUN4 erforscht. Entsprechend der Ergebnisse dieser Studie ist SUN4 ein hodenspezifisches Protein, das ausschließlich in haploiden Keimzellen exprimiert wird. In diesen lokalisiert es in der posterioren Kernhülle, spezifisch in Regionen, an die sich die spermatidenspezifische Manschette anlagert. Dies ist eine Struktur, für die bereits gezeigt wurde, dass sie an der Verformung des Kerns beteiligt ist. SUN4 defiziente Mäuse zeigten ausschließlich Spermatiden mit stark desorganisierten Manschettenüberresten und einen gravierend verformten Spermienkopf. Insgesamt führten die Fehlbildungen zu einem globozoospermieartigen Phänotyp und männlicher Sterilität bei Mäusen. Dabei zeigte sich, dass SUN4 nicht nur zwingend erforderlich ist für den korrekten Aufbau und die Verankerung der Manschette, sondern auch für die korrekte Lokalisation von SUN3 und Nesprin1, wie auch für weitere Komponenten der

Zusammenfassung

posterioren Kernhülle. Interaktionsstudien zeigten, dass SUN4 sowohl mit SUN3 und Nesprin1 als auch mit sich selbst interagieren kann, vermutlich um funktionsfähige LINC Komplexe zu bilden, die die Manchette verankern und Kräfte aus dem Zytoskelett auf den Kern übertragen.

Zusammenfassend zeigen die schwerwiegenden Auswirkungen auf die kernzytoplasmatische Verbindung während der Spermienentwicklung, die durch den Verlust von SUN4 entstanden, einen direkten Nachweis einer entscheidenden Rolle von SUN4 und anderen LINC-Komplex-Komponenten für die Spermienkopfentwicklung und Fertilität bei Säugetieren.

1 Introduction

Today we recognize a declining birth rate in developed countries, which is increasingly becoming a serious social problem (The ESHRE Capri Workshop Group, 2010). In 2010 the absolute number of involuntarily childless couples reached 48.5 million registered cases (Mascarenhas et al., 2012). The reasons for infertility are tremendously variable, and vary from lifestyle and environmental contributions to genetic abnormalities. Male infertility accounts for up to 50% of the infertility-affected couples, which means that approximately 7% of all men have fertility problems (Krausz, 2011). In 15% of the cases this condition is related to genetic disorders - chromosomal or single gene alterations (Krausz, 2011; Krausz et al., 2015). However, even after a complete diagnostic work-up 40% of these patients are still diagnosed with “idiopathic infertility”, which means that the etiology simply remains unknown (Krausz et al., 2015). In the last one-and-a-half decades substantial progress has been made in the reproductive field. In particular, work on mutant mouse models with reproductive phenotypes has led to significant advances in the understanding of fertility regulation (Matzuk and Lamb, 2008).

Reproduction is the fundamental basis for life, the production of offspring sharing the parental genetic material. In mammals, specialized germ cells need to be developed within male and female organisms. Gametogenesis is the development of haploid gametes from diploid precursor cells through cell division and differentiation. The developmental process of creating fertilization-competent gametes in males (spermatogenesis) is highly complex. It has been estimated that approximately 4% of the genes in the mouse genome are male germ cell-specific transcripts that are expressed during or after meiosis (Schultz et al., 2003). This underlines the high degree of complexity in the processes occurring during meiosis and spermiogenesis, the postmeiotic sperm cell differentiation. Furthermore, this vast number of potential participants in male germ cell development might be a central reason why the detailed mechanisms of these processes remain poorly understood.

1.1 Spermatogenesis – the male basis for sexual reproduction

For sexual reproduction it is essential to reduce the chromosomal content from diploid to haploid. This allows the resulting male gamete to fertilize a female gamete and produce a zygote with diploid chromosomal content. The production of haploid gametes from diploid precursor cells is termed oogenesis in females and spermatogenesis in males. While during oogenesis a mature egg is created, spermatogenesis describes the development of mobile fertilization-competent spermatozoa. The extremely high complexity of this process is evidenced by the fact that about 4% of the mouse genome is expressed specifically in male germ cells. It furthermore has been shown that the overall abundance of transcribed genes increases with the onset of meiosis, with one fifth of the genes apparently expressed only in male germ cells (Schultz et al., 2003).

During spermatogenesis, undifferentiated spermatogonial stem cells develop into spermatocytes. Spermatocytes become haploid spermatids and finally differentiate into mature spermatozoa, all in the company of Sertoli cells, which support and nourish the developing germ cells (Hermo et al., 2010a; Hermo et al., 2010b). Therefore, spermatogenesis is generally divided into three functional phases occurring within the seminiferous epithelium. The first phase is termed the mitotic phase, in which the spermatogonia undergo several rounds of mitotic division. After spermatogonial renewal and proliferation, some of the cells differentiate into primary spermatocytes and enter the meiotic phase. In this phase the spermatocytes undergo two successive rounds of highly specialized meiotic divisions to become haploid spermatids. Thereafter, the round spermatids differentiate into elongated, mobile fertilization-competent spermatozoa, a process which is called spermiogenesis (Oakberg, 1956a; Fawcett, 1975). Finally the spermatozoa are released into the lumen of the seminiferous tubules, from where they are carried into the epididymis for further maturation.

In mice and rats the epithelium of the seminiferous tubules is composed of concentric layers of developing germ cells, which are more or less associated and/or embedded in their supporting Sertoli cells. The outermost layer consists of spermatogonia with subsequent layers carrying germ cells that are progressively more advanced - first spermatocytes, then early round spermatids, and finally the late elongated spermatids in the innermost layer. In this way spermatogenesis is staged within a cycle of the seminiferous epithelium, which is a synchronous sequential appearance of cellular associations that occur over time in a certain area of the seminiferous tubules (Figure 1.1). The exact number of stages within the seminiferous

epithelial cycle is species-specific. There are 14 different stages described for the rat (Leblond and Clermont, 1952a), 12 stages for the mouse (Oakberg, 1956b; Oakberg, 1957), and 6 stages in humans (Clermont, 1963; Heller and Clermont, 1963). The duration of a cycle varies in different species as well: 13 days in the rat; 8.65 days in the mouse; 16 days in humans. The cycles of different species and the analysis of their stages has been exhaustively reviewed (Russell et al., 1990). In the mouse, the first meiotic cell stages appear by day 10 of postnatal development; starting from day 18, when the first two meiotic divisions are completed, haploid spermatids can be detected. It takes another 14 days until the first round of spermiogenesis is completed and the first mature spermatozoa are released into the epididymis (Bellve et al., 1977; Nebel et al., 1961).

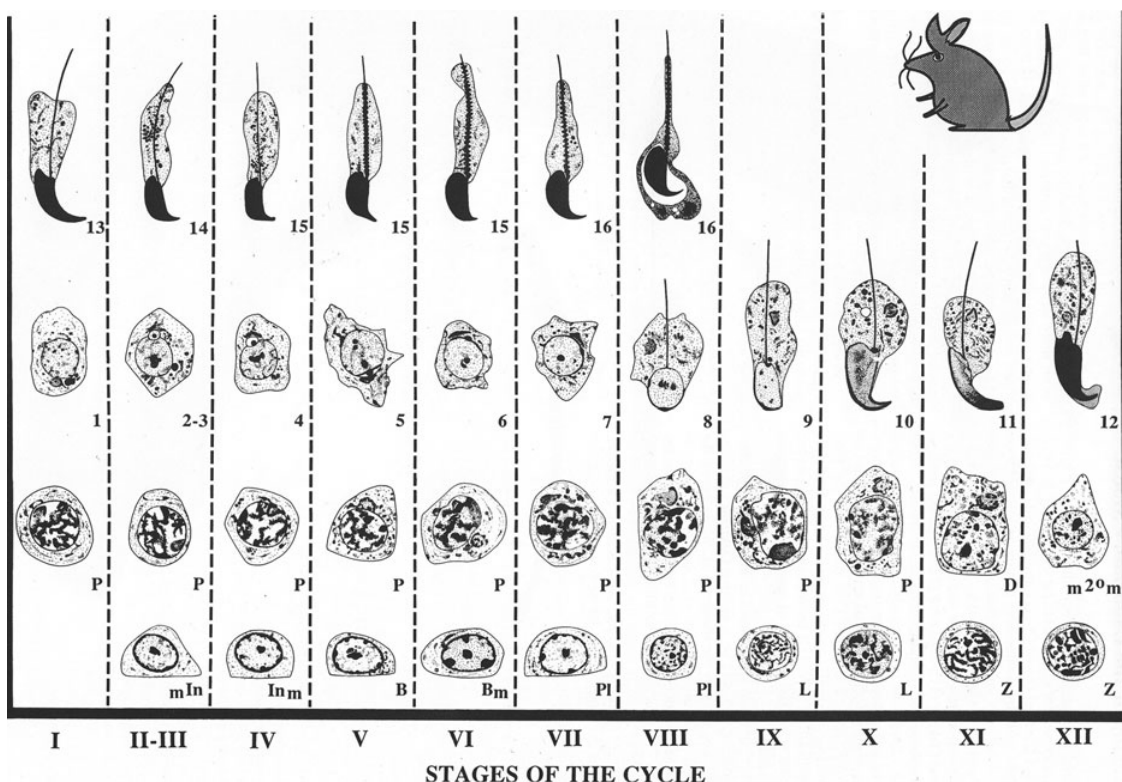


Figure 1.1: Cycle of the mouse seminiferous epithelium.

Schematic representation of the 12 stages (roman numerals I–XII) of the seminiferous epithelium in mice. The vertical columns indicate the different cell types in each of the stages. The illustrated cells show the consecutive germ cell types - the spermatogonia during proliferation (m^{In} – B^m), the spermatocytes during meiotic divisions (Pl– $m^{20}m$), and finally spermiogenesis, which is divided into 16 steps in mice (1–16). Steps 1–8 represent round spermatids and steps 9–16 elongated ones. Figure from Russell et al. (1990).

However, there is not only a temporal organization within the seminiferous tubules, but also a spatial one. This is referred to as the wave of the seminiferous epithelium, which describes the arrangement of the stages in a sequential order along the length of the seminiferous tubules (Perey et al., 1961).

1.2 Spermiogenesis – a unique male germ cell restructuring

Spermiogenesis is characterized by a profound cellular remodeling which is unique to haploid male germ cells. The formation of functional sperm requires complex cellular mechanisms to assemble sperm-specific structures like the flagellum and the acrosome. Furthermore it includes cellular and nuclear polarization, chromatin compaction, and a profound reshaping of the nucleus from an initially round morphology to a characteristic species-specific elongated form (Fawcett, 1975; Russell et al., 1991; Kierszenbaum et al., 2003; Toshimori and Ito, 2003; Kierszenbaum and Tres, 2004; Hermo et al., 2010a; Hermo et al., 2010b). Taking this fundamental cellular restructuring into account, it is not surprising that at least half of the testis-specific genes are exclusively expressed during spermiogenesis (Schultz et al., 2003; Yan, 2009). Failures affecting the formation of the spermatozoa, which often lead to nonfunctional sperm with structural abnormalities, quite frequently cause male infertility (Yan, 2009; de Boer et al., 2015).

Mouse spermiogenesis is subdivided into 16 steps of which the main cytoplasmic and nuclear changes are summarized in Figure 1.1. Haploid germ cells of steps 1-8 are called early or round spermatids, while those of steps 9-16 are referred to as elongating or late spermatids. The subdivision of the 16 steps is based on a periodic acid-Schiff acrosome staining, also called periodic acid-fuchsin sulfurous technique (Leblond and Clermont, 1952b). The acrosome is one of the most prominent structures that are formed during spermiogenesis. It is a lysosome-like membrane-bound organelle on the anterior side of the spermatid (Figure 1.2), and is important for fertilization as it is needed for the sperm to penetrate the zona pellucida of the egg (Hermo et al., 2010b; Hermo et al., 2010c). In the initial phase of acrosome formation, the Golgi phase, vesicles derived from the trans-Golgi stacks fuse to proacrosomic granules that associate with the anterior pole of the nuclear surface (Figure 1.2). In the next phases, the cap phase and the acrosomic phase, the acrosome increases in size and spreads over the anterior nuclear side. It reaches its final shape on top of the elongated nucleus of the late spermatid in the maturation phase (Leblond and Clermont, 1952a; Clermont and Leblond, 1955). The acrosome is maintained at the

nuclear anchoring site by the acroplaxome (Figure 1.2), a cytoskeletal plaque between the acrosome and the nucleus. The marginal ring marks the edge of the acroplaxome and contains F-actin and keratin5 (Kierszenbaum et al., 2003). Disruption of correct acrosome assembly often leads to severe malformations, called globozoospermia, as it features a phenotype with misshaped round-headed spermatozoa (Yan, 2009).

Caudally to the acrosome, the manchette, a girdle of microtubules, develops in close association with the elongating spermatid nucleus (Figure 1.2). In this process, tubulins and microtubule associated proteins assemble at a perinuclear ring, a scalloped ring margin associated with the nuclear envelope (NE) in proximity to the marginal ring of the acroplaxome. In total the manchette consists of the perinuclear ring and a mantle of microtubules, which radiates from it along the anterior-posterior axis of the nucleus in close association with the NE (Fawcett et al., 1971; Russell et al., 1991; Kierszenbaum and Tres, 2004). The manchette forms at the onset of nuclear elongation during step 8 of spermiogenesis, and disassembles right after the completion of the elongation of the nucleus and the compaction and condensation of the nuclear chromatin in step 14 (Clermont et al., 1993; O'Donnell and O'Bryan, 2014). It seems to play a role in trafficking proteins within the spermatid cytoplasm via an intramanchette transport system, and in maintenance and formation of the sperm head (Kierszenbaum and Tres, 2004).

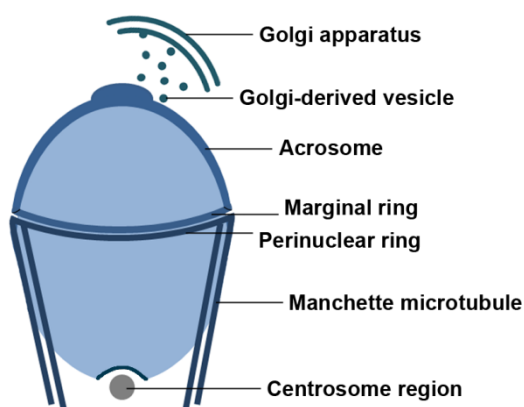


Figure 1.2: Elongating sperm head with associated acrosome and manchette.

Schematic drawing of the differentiating nucleus during spermiogenesis. Represented are: (I) the Golgi apparatus; (II) the vesicles derived from it that generate the acrosome; (III) the acrosome with its marginal ring covering the anterior side of the spermatid nucleus; (IV) and the perinuclear ring with its associated manchette microtubules (indicated by single microtubules) surrounding the posterior part of the nucleus during elongation. At the posterior pole the flagellum is initiated in the centrosome region.

Another prominent structure which assembles during spermiogenesis is the flagellum, which is the drive unit required to transport the male germ cell to the egg and penetrate the zona pellucida. The flagellum is composed of a neck region (or connecting piece) and the tail, which is divided into 3 parts - the mid, principal and end pieces (Figure 1.3). They all share the same central element: the axoneme. The axoneme is the functional unit to produce progressive movement and is composed of nine microtubule doublets that are arranged in a circle around two inner microtubules. In the mid and principal pieces the axoneme is paralleled by outer dense fibers (ODF) (Hermo et al., 2010c). In the mid piece, the axoneme is enveloped by a mitochondrial sheath, while in the principal piece it is surrounded by a fibrous sheet. The formation of the flagellum is initiated by the centrosome/basal body, which consists of the paired centrioles and several associated proteins that form the connecting piece. This structure in turn finally nucleates the flagellum. The shallow dent in the posterior pole of the nucleus is called the implantation fossa; here the connecting piece is associated with the nucleus (Fawcett and Phillips, 1969; Hermo et al., 2010c).

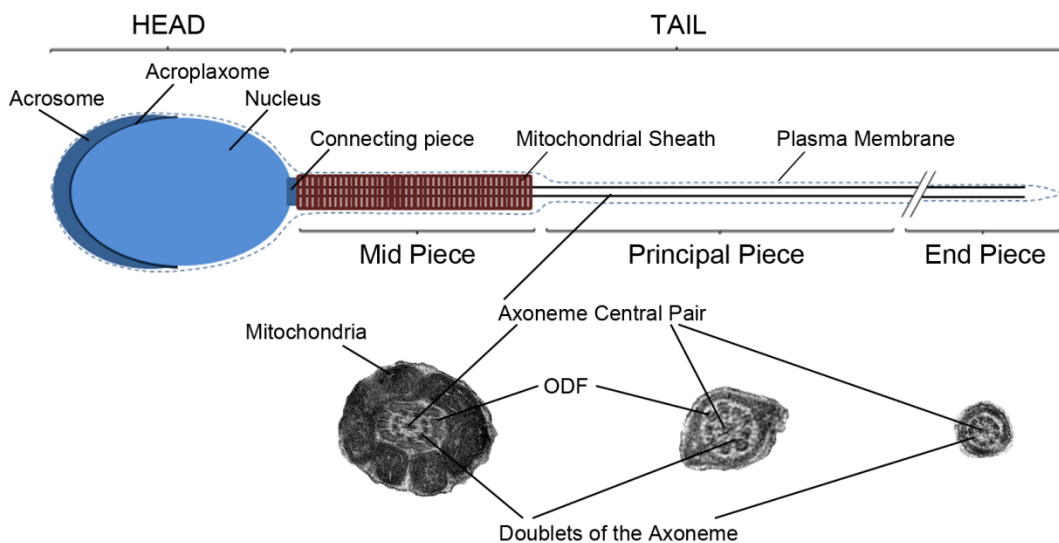


Figure 1.3: A mammalian spermatid during late spermiogenesis.

Schematic drawing of an elongated spermatid during the final differentiation stages in spermatogenesis. The mammalian sperm is shown with major spermiogenesis-specific structural adaptations: the acrosome and acroplaxome at the anterior nucleus, and the tail, which is formed at the posterior pole in late spermiogenesis. The tail is separated into a mid, a principal, and an end piece, which all contain the axoneme as the central element required for mobility. Representative electron micrograph cross sections of the sperm tail are shown below the schematic. The mid piece additionally contains outer dense fibers (ODF) and a mitochondrial sheath, which provides the needed energy for the progressive tail movements. The principal piece additionally contains ODF and a fibrous sheet surrounding the central axoneme.

Further changes which can be observed during spermatogenesis are the topographical and extensive structural changes of the endoplasmic reticulum (ER), e.g. the formation of new structures like the radial body and the annulate lamellae (Clermont et al., 1993). In addition the chromatoid body is a characteristic structure of developing spermatids; it is thought to be involved in RNA storing and processing (Hermo et al., 2010b).

One of the most eye-catching changes during rodent spermatogenesis, however, is the nuclear restructuring of the sperm head. It is an extensive species-specific structural shape change, which in the case of the mouse ultimately leads from an initially round form to an elongated sickle-shaped nucleus, the main component of the sperm head (Figure 1.1) (Russell et al., 1990). The restructuring of the nucleus will be described in more detail below. Sperm head formation is accompanied by nuclear compaction and chromatin condensation. Chromatin compaction is achieved by gradually replacing the histones, first with transition proteins and finally by highly basic protamines (Ward and Coffey, 1991; Dadoune, 2003; Hermo et al., 2010b). At the same time the nucleus migrates from the center of the cell towards the periphery with the acrosome in close vicinity to the plasma membrane, facing the Sertoli cell (Clermont et al., 1993). This close association is an ectoplasmic specialization, which is a contact site for interactions between the germ and the Sertoli cell (Hermo et al., 2010d).

At the end of spermatogenesis, after the completion of all structural and functional modifications, the excess cytoplasm together with unnecessary cellular components and organelles, (such as the Golgi and ER cisternae), are eliminated. The resulting residual body and cytoplasmic droplet is phagocytized by the surrounding Sertoli cells (Clermont, 1972).

1.3 Nuclear remodeling and the nuclear envelope

The process of sperm head formation requires a complex nuclear restructuring, concomitant with a substantial modulation of the nuclear envelope (NE). The NE surrounds the genome and functions as a highly regulated double membrane barrier to separate the nuclear interior from the cytoplasm (Figure 1.4) (Hetzer, 2010). It consists of an outer nuclear membrane (ONM), an inner nuclear membrane (INM), the underlying nuclear lamina and the nuclear pore complexes (NPCs). The ONM and INM are linked by the NPCs, which form a highly regulated channel to transport molecules in and out of the nucleus (Strambio-De-Castillia et al., 2010). The ONM is continuous

with the ER, which in turn connects the lumen of the ER with the perinuclear space (PNS), a cytoplasmic gap between the ONM and INM. In somatic cells this lumen is evenly spaced with a cell-specific width between 30 and 50 nm (Liu et al., 2007; Hetzer and Wente, 2009, Sosa et al., 2013). The INM comprises many different integral membrane proteins (Schirmer and Gerace, 2005), some of which bind to the nuclear lamina as well. The lamina is a protein meshwork with a thickness of 20 to 50 nm (Liu et al., 2007), which underlies the INM and interacts with nuclear proteins and chromatin to fulfill a variety of different functions, e.g. in nuclear architecture, chromatin organization, gene expression and signaling, and cell development and differentiation (Gruenbaum et al., 2000; Gruenbaum et al., 2005; Schirmer and Foisner, 2007).

During spermiogenesis the germ cell NE undergoes profound remodeling, which correlates with the shaping of the sperm head. Therefore it is presumed that the reorganized NE is a requirement for force transduction from the cytoskeleton to the nucleus in order to enable directed nuclear shaping (Göb et al., 2010; Kierszenbaum et al., 2011, Kracklauer et al., 2013). One of the main characteristics of this shaping is the reorganization of numerous NE components. Many proteins which are distributed more or less evenly within the entire NE of somatic cells and/or the early round spermatids redistribute and polarize to a certain area of the developing spermatid nucleus. Amongst others, lamins B1 and B3, Lap2 and lamin B receptor relocate to the posterior spermatid NE during differentiation and can no longer be detected once the elongation of the nucleus is completed (Alsheimer et al. 1998; Mylonis et al. 2004; Schütz et al. 2005a). For the spermatid-specific lamin B3, which is a transcript of the *lamin B2* gene that otherwise codes for the somatic lamin B2, a correlation of its properties to the sperm head formation has been found (Schütz et al., 2005b). The lamin B3 transcript is missing the N-terminus and the head part of the α -helical rod domain compared to the somatic lamin B2; this whole region is replaced by an amino acid sequence unique to lamin B3. In this context, it has been demonstrated that the ectopic expression of lamin B3 in somatic culture cells causes nuclear deformations due to this truncated rod domain. Furthermore it was shown that lamin B3 has an increased mobility within the lamina compared to lamin B2. Thus it was concluded that lamin B3 could be involved in nuclear deformations by means of locally reducing the stability of the NE to facilitate sperm head formation due to a more flexible spermatid NE (Schütz et al., 2005b).

Remarkably, during sperm head formation a typical relocation of NPCs towards the posterior NE can be observed as the acrosome enlarges. Ultimately, the NPCs retract into the redundant nuclear envelope (RNE), the excess NE resulting from the reduction of the nuclear volume during sperm head compaction (Ho, 2010). This

retraction might be caused by the spermatid-specific manchette, which assembles in close association with the posterior part of the spermatid nucleus and might therefore assist the redistribution and exclusion of the NPCs from the underlying NE (Ho, 2010).

It is worth noting that the manchette as a perinuclear mantle not only assembles in close association with the NE, but is also physically attached to it via connecting links that lie between the microtubules of the manchette and the NE. These links were first shown by Russell and colleagues (1991), who described them as rod-like elements with a diameter of about 10 nm and a 40-70 nm length linking the innermost microtubules to the outer leaflet of the NE. It was suggested that these links maintain the manchette at a constant distance and position to the NE and due to force transmission enable sperm head elongation and formation of the caudal spermatid nucleus (Russell et al., 1991). Like the manchette on the posterior part of the nucleus, the acroplaxome (and acrosome) enables sperm head elongation and formation of the anterior part, as both are highly polarized cytoskeletal structures in tight contact with the NE (Russell et al., 1991; Kierszenbaum et al., 2003; Kierszenbaum and Tres, 2004; Kierszenbaum et al., 2011). The axroplaxome with its marginal ring and the manchette with its perinuclear ring are suggested to be active players in the formation of the elongated species-specific sperm head form by generating clutching forces that constrict the nucleus at opposing sides (Kierszenbaum et al., 2003; Kierszenbaum and Tres, 2004; Kierszenbaum et al., 2011).

However, besides having a model of a potential mechanism for shaping the nucleus from the outside, very little mechanistic detail is known, especially concerning force transduction from cytoskeletal elements to the nuclear interior during sperm head formation. It is quite striking that the polarization of some of the NE components correlates with the formation of cytoskeletal structures that surround the nucleus. Just recently two spermatid-specific LINC (linker of nucleoskeleton and cytoskeleton) complexes have been found that show a remarkable polarized localization within the spermatid NE. LINC complexes consisting of SUN3 and Nesprin1 were found exclusively in the posterior part of the NE, in regions decorated with the microtubule manchette. Separate complexes consisting of SUN1/SUN1 η and Nesprin3 have been described to specifically localize to the opposite, anterior pole in the late elongating spermatids (Göb et al., 2010). Interestingly, the posterior SUN3/Nesprin1 and the anterior SUN1 η /Nesprin3 complexes retain their strict polarization during nuclear shaping (Göb et al., 2010). It has been suggested that these LINC complexes play a role in nucleocytoskeletal linkage, as they are either adjacent to the posterior spermatid-specific manchette (SUN3/Nesprin1) or to the anterior actin cytoskeleton

adjacent to the acrosome (SUN1 η /Nesprin3) (Göb et al., 2010). Therefore they might represent the connectors of the nucleus to the surrounding cytoskeleton, thus capable of transmitting cytoskeletal forces onto the nucleus. It should however be noted that next to the SUN1 η /Nesprin3 complexes at the anterior cap a parallel localization of these LINC complexes exists at the posterior half of the spermatid nucleus. During differentiation these posterior complexes gradually relocate and concentrate at the posterior pole, excluded from the very posterior implantation fossa (Göb et al., 2010).

In addition to the SUN1/Nesprin3 and the SUN3/Nesprin1 complexes further LINC complex components have been found at the spermatid NE, which currently are rather sparsely characterized. Notably, the distribution of the mammalian Spag4/SUN4 protein and its presumed *Drosophila* ortholog both resemble a posterior NE localization adjacent to the manchette and might therefore also play a role in nucleocytoskeletal linkage (Shao et al., 1999; Kracklauer et al., 2010, Kracklauer et al., 2013). Furthermore, on the opposite anterior site, the potential LINC complex component SUN5 might also have a cooperative function in linking the anterior nuclear structures to the adjacent actin cytoskeleton (Göb et al., 2010; Frohnert et al., 2011; Kracklauer et al., 2013). However, the anterior SUN5 localization is quite controversial, as a recent study suggested that SUN5 is not involved in acrosome attachment due to its exclusion from the NE adjacent to the acrosome within the elongating spermatid nucleus. This recent study described SUN5 to be rather evenly distributed at the posterior side of the elongating nucleus, thereby progressively accumulating towards the posterior pole, where it is still present in the epididymal sperm (Yassine et al., 2015).

1.4 The LINC complex – a protein complex bridging the NE

LINC complexes are part of the NE and have been found in all different kinds of cells. Identified as protein assemblies that connect the nuclear content to the cytoskeleton they span the entire NE. These NE bridges were first mentioned by Crisp et al. (2006) as “LINC” complexes due to the function of particular members of two transmembrane protein families that form a complex to link the nucleoskeleton to the cytoskeleton (Figure 1.4) (McGee et al., 2006; Stewart-Hutchinson et al., 2008; Starr and Fridolfsson, 2010). These evolutionarily highly conserved transmembrane protein families are the SUN- and the KASH-domain proteins. The KASH-domain proteins reside within the ONM, where they interact with different cytoskeletal elements, e.g. actin, microtubules or intermediate filaments (Wilhelmsen et al., 2006). The SUN-

domain proteins are the INM protein partners and interact with the nuclear lamina and the chromatin on the nucleoplasmic side (Razafsky and Hodzic, 2009).

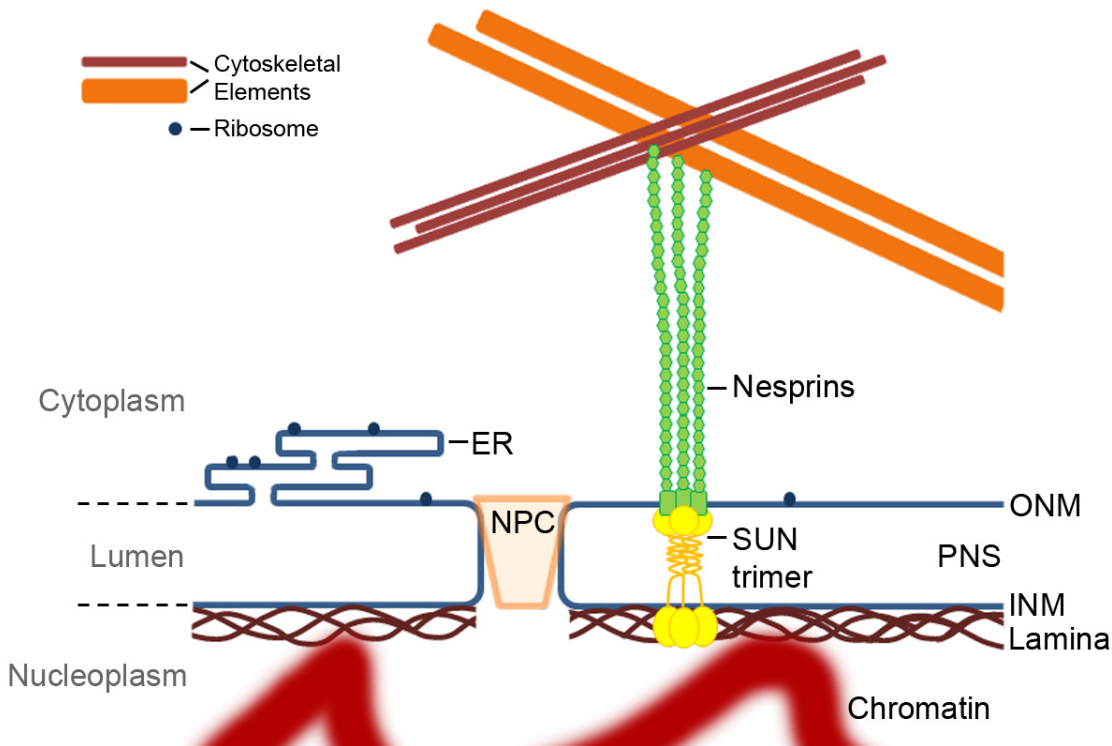


Figure 1.4: The LINC complex bridges the nuclear envelope.

The nuclear envelope (NE) consists of the outer nuclear membrane (ONM), the inner nuclear membrane (INM) and the perinuclear space (PNS) in between. At the sites of the nuclear pore complexes (NPC), which connect the cytoplasm with the nucleoplasm, the NE membranes are joined to one another. Underlying the INM is the lamina. This protein network interacts with the INM and its constituents, nuclear proteins, and chromatin. The ONM is contiguous with the endoplasmic reticulum and both contain ribosomes. The LINC complex is an oligomeric structure bridging the NE and thereby connecting the cytoplasm to the nucleoplasm. The LINC complex is assembled from a SUN trimer spanning the INM that is connected with three Nesprins in the PNS spanning the ONM.

1.4.1 The components of the LINC complex

SUN-domain proteins are the INM constituents of the LINC complexes. Their name derives from a common C-terminal motif, the SUN-domain, which is named after the first two known SUN proteins: Sad1 in *Schizosaccharomyces pombe* and UNC-84 in *C. elegans* (Hagan and Yanagida, 1995; Malone et al., 1999). SUN-domain proteins are evolutionary conserved and can be found in many different organisms: e.g. Sad1 in *S.pombe* (Hagan and Yanagida, 1995), Mps3 in *S. cerevisiae* (Jaspersen et al., 2006), Sun1 in *D. discoideum* (Xiong et al., 2008), UNC-84 and Matefin/SUN-1 in *C. elegans*

(Hagan and Yanagida, 1995; Fridkin et al., 2004), Klaroid, Giacomo and Spag4 in *D. melanogaster* (Kracklauer et al., 2007; Kracklauer et al., 2010), AtSUN1 and AtSUN2 in *A. thaliana* (Graumann et al., 2010), OzSAD1 in rice (Moriguchi et al., 2005), and SUN1 to 5 in mammals (Kracklauer et al., 2013). Concomitant with the increasing complexity of the organism, the number of SUN-domain proteins within the different species increases as well (Kracklauer et al., 2013). This evolutionary diversity can be seen by the fact that compared to yeast, where as yet only one SUN-domain protein (Sad1) was identified, the mammalian genome contains five distinct genes coding for different SUN-domain proteins: the ubiquitously expressed SUN1 and SUN2 (Hodzic et al. 2004; Padmakumar et al. 2005), and the male germ cell-specific SUN3, SUN4/Spag4 and SUN5/Spag4L (Shao et al., 1999; Göb et al., 2010; Frohnert et al., 2011; Kracklauer et al., 2013). Some of the SUN-domain protein coding genes express various splice isoforms, which even further increases the variety of the different SUN-domain proteins. This has been shown for the mammalian SUN1 and SUN5 proteins, for example (Göb et al., 2010; Göb et al., 2011; Liu et al., 2007; Frohnert et al., 2011). Furthermore it is worth noting that more complex species with more than one SUN-domain protein exhibit different expression patterns between the different SUN-domain proteins, e.g. the testis-specific expression of SUN3, SUN4 and SUN5 in mammals (Kracklauer et al., 2013). In turn this evolutionary diversity points to a multiplicity of functions (see below).

SUN-domain proteins have many common characteristics. First of all, they share the common C-terminal SUN-domain of approximately 150 to 200 amino acids in length, which is highly conserved at the amino acid level (Hodzic et al. 2004; Padmakumar et al. 2005; Crisp et al., 2006). The function of the SUN-domain is to interact with the KASH-domain of respective KASH-domain protein partners within the PNS, so together they can span the entire NE (McGee et al., 2006; Starr and Fischer, 2005; Starr and Fridolfsson, 2010; Sosa et al., 2012). Most of the SUN-domain proteins contain at least one coiled-coil motif near the C-terminus (Starr and Fridolfsson, 2010). The amino acid sequence encoding the coiled-coil motif of the different SUN-domain proteins is not very conserved, though the function seems to be the same, i.e. essential to form homo- or heteropolymers of SUN-domain proteins (Zhou et al., 2012b; Sosa et al., 2012). Furthermore, the SUN-domain proteins contain at least one functional transmembrane domain, which enables their localization within the INM (Starr, 2009; Starr and Fridolfsson, 2010). As INM integral membrane proteins, they seem to have the same orientation, with the C-terminus extending into the PNS and the N-terminus into the nuclear interior. The N-terminus of the SUN-domain proteins is not conserved in length and structure, and is rather variable (Starr and Fridolfsson, 2010; Rothballer

et al., 2013). It is presumed that this variability is important for the potential of the different SUN-domain proteins to bind to different nuclear components, though very little is known about such interaction partners (Haque et al., 2006; Mejat and Misteli, 2010; Rothballer and Kutay, 2013). Nonetheless, it is proposed that the retention of the SUN-domain proteins within the INM is due to their N-terminal interaction with the lamina and chromatin (Haque et al., 2006; Hasan et al., 2006; Razafsky and Hodzic, 2009).

KASH-domain proteins have been found in many different model organisms. Just like the SUN-domain proteins, usually at least one KASH-domain protein is expressed nearly ubiquitously within the organism. Even though the KASH-domain proteins can be found from yeast to plants, it is still quite difficult to clearly define their number or detect all of them due to their rather weak conservation at the amino acid level and many splice isoforms (Zhang et al., 2001; Warren et al., 2005; Mellad et al., 2011). Furthermore, although most KASH-domain proteins reside within the ONM, some variants may also be part of the INM or can be found, likely due to the lack of the transmembrane domain, at a variety of other intracellular locations (Mislow et al., 2002; Warren et al., 2005; Starr and Fischer, 2005; Haque et al., 2010; Mellad et al., 2011; Duong et al., 2014). The KASH-domain proteins take their name from a short highly conserved C-terminal “KASH” motif, which points to the homology between representatives of this protein family from different species: Klarsicht (in *D. melanogaster*), UNC-1 (in *C. elegans*) and SYNE (in mammals) homology. Up to now a great variety of KASH-domain proteins have been identified in many different species: e.g. Kms1/2 in *S. pombe* (Shimanuki et al., 1997; Miki et al., 2004; King et al., 2008), Csm4 in *S. cerevisiae* (Conrad et al., 2008), UNC-83, ANC-1 and ZYG-12 in *C. elegans* (Starr et al., 2001; Starr and Han, 2002; Malone et al., 2003), Klarsicht and MSP-300 in *D. melanogaster* (Fischer-Vize and Mosley, 1994; Rosenberg-Hasson et al., 1996), Nesprin1-4 (Syne1-4) and KASH5 in mammals (Zhang et al., 2001; Mellad et al., 2011; Kracklauer et al., 2013). Like SUN-domain proteins, KASH-domain proteins become more diverse with the increasing complexity of the organism. This is matched by their differential expression patterns. In mammals for example Nesprin1, Nesprin2 and Nesprin3 are expressed nearly ubiquitously, while Nesprin4 is specific to epithelial cells and the male germ cell-specific KASH5 is only expressed during meiosis (Mellad et al., 2011; Morimoto et al., 2012). LRMP seems to be another mammalian KASH protein, and was originally described as a lymphoid-restricted protein (Behrens et al., 1994). Interestingly, only recently the zebrafish homolog of LRMP has been found to be expressed in the zygote and early embryo (Lindeman and Pelegri, 2012).

Even though KASH-domain proteins are less conserved, their general structure and arrangement remain very similar. The C-terminus of the ONM integral proteins with their eponymous conserved KASH-domain extends into the PNS. The KASH-domain consists of a transmembrane domain and up to approximately 30 additional amino acids, including a strongly conserved C-terminal motif, the PPPX motif, which are the last 4 amino acids (Mislow et al., 2002; Razafsky and Hodzic, 2009; Starr, 2009; Rothballer et al., 2013). The N-terminal side of these proteins extends into the cytoplasm and includes a variable number of spectrin repeats that determine the size of the splice isoforms (Djinovic-Carugo et al., 2002). The N-terminus further contains one or more cytoskeletal binding domains, which exhibit an extreme variability to bind specifically to different cytoskeletal interaction partners (Starr and Fridolfsson, 2010). While the mammalian proteins Nesprin1 and Nesprin2 are very large and interact with actin and microtubule binding proteins (Zhang et al. 2001; Zhen et al. 2002; Cartwright and Karakesisoglou, 2014; Wilson and Holzbaur, 2015), Nesprin3 is able to bind to plectin (Wilhelmsen et al. 2005; Ketema et al. 2007), Nesprin4 to kinesin (Roux et al. 2009) and the meiosis-specific KASH5 interacts with dynein (Morimoto et al. 2012).

1.4.2 The diverse functions of the LINC complex

The evolutionary conservation of the SUN- and KASH-domain proteins as well as their variability, especially with regard to the variety of potential interaction partners, suggests participation in a wide range of essential biological functions. The core function of the LINC complex appears to be the connection of the components of the nuclear interior to the cytoskeletal system, which further links to the extracellular matrix and its adjacent connections (Meinke and Schirmer, 2015). It is worth noting that LINC complexes not only fulfill different cellular functions due to the specific interaction partners of their different SUN- and KASH-domain proteins, additionally they exhibit a cell type or function-specific partner switching among the SUN and KASH interaction partners as well (Hiraoka and Dernburg, 2009; Chang et al., 2015). UNC-84 in *C. elegans* for example can specifically bind to the KASH-domain protein UNC-83 and via this connection to the microtubule network (Malone et al., 1999). On the other hand it can bind ANC-1, which connects to actin filaments (Starr and Han, 2002). This data points to a selective interaction, where a particular SUN-domain protein can interact with different KASH partners, including their respective cytoskeletal elements, and thereby contribute to different functions (Tzur et al., 2006; Razafsky and Hodzic, 2009; Mejat and Misteli, 2010; Rothballer and Kutay, 2013). Conversely, it was also shown that SUN- and KASH-domain proteins are also partially redundant and therefore might

be able to at least partly compensate for the loss of a particular partner (Lei et al., 2009; Yu et al., 2011; Link et al., 2014).

Fundamental cellular processes, like nuclear migration and positioning as well as nuclear anchorage, were among the first functions to be described for LINC complexes. In fact many founding members of the SUN- and KASH-domain proteins were first characterized in mutant model organisms displaying phenotypes influencing these processes (Starr and Fridolfsson, 2010; Rothballer and Kutay, 2013). Nuclear migration is of utmost importance during development and is directed by force transmission from the microtubule network to the nucleus. In *C. elegans* the LINC complex consisting of UNC-84 and UNC-83 interacts with microtubule motor proteins and thereby participates in nuclear migration of various cell types during developmental processes (Malone et al., 1999; Meyerzon et al., 2009; Fridolfsson et al., 2010). In a similar way, Klaroid and Klarsicht connect to the microtubule network to mediate nuclear migration in the developing eye in *D. melanogaster* (Mosley-Bishop et al., 1999; Kracklauer et al., 2007). Nuclear anchorage on the other hand is maintained by the actin cytoskeleton in order to hold the nucleus at the correct position within the cell. In *C. elegans* for example, LINC complexes consisting of UNC-84 and ANC-1 anchor the nucleus to the actin cytoskeleton (Starr and Han, 2002). A similar function has been identified for mammalian SUN1/2 with Nesprin1/2 (Zhang et al., 2007; Lei et al., 2009). Surprisingly, the LINC complexes are not only a mechanical bridge over the NE, but may also function in the transduction of signals, e.g. for cell regulation pathways, which might even go all the way from an extracellular signal to the genome (Fridkin et al., 2009; Mejat and Misteli, 2010; Chambliss et al., 2013; Isermann and Lammerding, 2013). Furthermore, they are also involved in NE organization and structuring, e.g. NPC and spindal pole body insertion, or maybe even mediators of membrane fusion (Jaspersen and Ghosh, 2012; Rothballer et al., 2013).

Due to their interactions, a key function of LINC complexes is attaching to and repositioning meiotic telomeres within the nuclear interior (Chikashige et al., 2007; Kracklauer et al., 2013). This well-conserved meiotic chromosome movement has been studied in yeast and mice and revealed that LINC complexes are able to transfer forces from the cytoskeleton across the intact NE onto the attached telomeres (Chikashige et al., 2007; Hiraoka and Dernburg, 2009; Kracklauer et al., 2013).

In connecting the cytoplasmic filaments with the inner nuclear components, the LINC complexes also function in a general maintenance of nuclear morphology and shape (Kracklauer et al., 2013; Rothballer and Kutay, 2013). The LINC complex may therefore determine the set distance between the INM and ONM, as co-depletion of

SUN1 and SUN2 revealed expansions of the PNS (Crisp et al., 2006; Sosa et al., 2012). This would in turn imply that the distance between the INM and ONM might be dependent on the different LINC complex assemblies. The size of the C-terminus of the SUN-domain protein might be the decisive factor for the spacing; however it could also just be an adaptation to a given membrane distance (Sosa et al., 2013; Rothbäller et al., 2013). It has at least been shown that in *C. elegans* the SUN-KASH bridges are only required to keep the correct NE spacing in cells under mechanical forces (Cain et al., 2014). This naturally argues against the LINC complexes as the determining factor for the width of the NE and rather for the size and structure of LINC complexes to be an adaptation to the NE width.

Beyond the function in maintaining the NE architecture, LINC complexes play an essential role in nuclear shaping. For example AtSUNs together with their KASH binding partners, AtWIPs, have been shown to be crucial for the elongation of the nucleus in *Arabidopsis* root hairs, likely by transferring cytoplasmic forces to the NE (Oda and Fukuda, 2011; Zhou et al., 2012a; Zhou et al., 2015). In mammals LINC complex components have been suggested to be involved in nuclear shaping as well. On the one hand, Olins et al. (2009) proposed that lacking LINC complexes is an adaptation of differentiated granulocyte nuclei in order to have a malleable nuclear shape to be highly deformable during cell migration. On the other hand, SUN1 η /Nesprin3 and SUN3/Nesprin1 LINC complexes have been proposed to contribute in nuclear elongation, in that they may transfer opposing mechanical forces to elongate and shape the spermatid nucleus during sperm head formation (Göb et al., 2010). Since testis-specific SUN4 and SUN5 proteins polarize within the spermatid nucleus as well, they might also be prime candidates for essential roles in nuclear shaping (Kracklauer et al., 2013). Thus, it was suggested that specialized LINC complexes might be involved in spermatid-specific nuclear shaping. Consistent with this, the proposed *Drosophila* ortholog of the mammalian SUN4, Spag4, has been suggested to be involved in directed nuclear shaping of the sperm head (Kracklauer et al., 2010; Kracklauer et al., 2013). In homozygous *Spag4* deletions sperm nuclei are often deformed (Kracklauer et al., 2010). Whether this is a direct or rather indirect effect of lack of the Spag4 protein is not known. However, it is worth noting that while it was shown that the presumed *Drosophila* ortholog Spag4 localizes to the posterior NE, the murine variant was described to be found in the NE adjacent manchette and furthermore in the axoneme of the flagellum as an outer dense fiber (ODF) –interacting protein (Shao et al. 1999; Kracklauer et al. 2010). Nonetheless SUN4 is considered as an NE protein due to its conserved general structure, including the SUN-domain, the coiled coil motif and the transmembrane domain(s).

1.4.3 The LINC complex - a complex structure

The model of the LINC complex developed over several years. It started with a NE-bridging proposal and evolved, due to several studies demonstrating the SUN-KASH interactions, to the LINC complex model (Malone et al., 1999; Lee et al., 2002; Starr et al., 2001; Starr and Han, 2002; Crisp et al., 2006). According to this model, the INM integral SUN-domain proteins tether the KASH-domain proteins in the ONM via direct interaction (Crisp et al., 2006; Sosa et al., 2012). Thereby the LINC complex spans the PNS and provides a mechanical bridge needed for direct communication between the inner leaflet of the nucleus and cytoskeletal components.

The enormous variety of different functions makes it plausible that some of these are rather an indirect effect of the core function of the LINC complex, the bridging of the NE and the connection of the nuclear content with the cytoskeleton and even the extracellular matrix (Meinke and Schirmer, 2015). To ensure such a core function the SUN- and KASH-domain proteins need to assemble a strong and tight interface in order to bear tension forces and heavy loads. The coiled-coil motifs after the transmembrane region of the SUN-domain proteins point to a LINC complex model with a homo- or heteropolymer structure. A few years ago, a dimerization of the SUN-domain proteins was the favored structure for the LINC complex model (Wang et al., 2006; Lu et al., 2008). In 2012, crystallography based on the SUN2 and Nesprin1/2 structures revealed that the SUN-domain proteins form trimers, which interact with three respective KASH-domain protein partners to form a hexameric complex (Zhou et al., 2012b; Sosa et al., 2012). It was shown that the SUN-domain consists of a beta-sandwich structure and an approx. 20 amino acid β -hairpin extension, the so called KASH-lid, which is critical for KASH binding (Sosa et al., 2012). This core structure is stabilized by the helical extension towards the N-terminus, which together with the neighboring SUN protomers forms a triple stranded coiled-coil to contribute to the higher order organization (Sosa et al., 2012; Sosa et al., 2013). Each of the KASH peptides is bound in a deep and expansive groove created by two adjacent SUN protomers and interacts with a respective KASH-lid (Sosa et al., 2012). The KASH-lid itself seems to be rather flexible before the binding of the KASH-domain protein, suggesting that it facilitates insertion of the KASH-domains into the SUN trimer core complex (Meinke and Schirmer, 2015). The interface of the SUN trimer and the three KASH peptides is further stabilized by the formation of a disulfide bond between two highly conserved cysteine residues, one from the SUN- and one from the KASH-domain protein (Sosa et al., 2012; Sosa et al., 2013). Furthermore, it has been shown that this intermolecular disulfide bond is not only needed for the stability of the SUN-

KASH interactions during physiologically relevant forces, but that it is also crucial for the force transmission through the LINC complex (Jahed et al., 2015). Even though the crystallization so far only revealed a homotrimeric SUN-domain protein structure that is intimately bound with three KASH peptides to form a LINC complex, it has been shown that also SUN1 and SUN2 have the intrinsic property to interact with each other (Wang et al., 2006; Lu et al., 2008). Therefore, it seems plausible that SUN-domain proteins are able to form heterotrimeric structures, which would increase the variability of possible LINC complexes and their amount of interaction partners for one complex.

1.5 Objectives

To date the complex processes during the development of haploid male germ cells have been studied in quite some detail. Still, the exact mechanisms as well as many of the involved proteins are not yet known for the processes of nuclear elongation and shaping during sperm head formation. Interestingly, three out of five mammalian SUN-domain proteins reveal a testis-specific expression pattern: SUN3, SUN4, and SUN5 (Shao et al., 1999; Göb et al., 2010; Frohnert et al., 2011). As LINC complex components, SUN-domain proteins in general play a vital role in many fundamental cellular processes in all organisms (Razafsky and Hodzic, 2009; Starr and Fridolsson, 2010; Kracklauer et al., 2013). For SUN3, the hypothesis that it might be involved in sperm head shaping has previously been suggested according to its localization (Göb et al., 2010). The roles of SUN4 and SUN5 on the other hand remain rather elusive and their localization controversial (Shao et al., 1999; Frohnert et al., 2011; Kracklauer et al., 2013; Yassine et al., 2015).

The aim of this study was to analyze the testis-specific SUN-domain protein SUN4 and to evaluate its potential role in fertility. Therefore the actual expression pattern and subcellular localization of SUN4 were analyzed in detail. A previous study indicated that SUN4 localizes in the NE adjacent manchette and that it furthermore is associated with the axoneme of the spermatid flagellum (Shao et al., 1999). This was surprising, because as a SUN-domain protein and potential LINC complex component SUN4 would rather be expected to reside within the INM and, together with its respective KASH-domain protein partner, span the germ cell NE. However, such a localization was shown for Spag4, the presumed *Drosophila* ortholog of mammalian SUN4, which was detected in the posterior NE of differentiating spermatids (Kracklauer et al., 2010).

As NE bridging protein complexes, which connect the cytoskeletal elements to the nuclear interior, the spermatid-specific LINC complexes are prime candidates for being involved in force transmission to shape the spermatid nucleus in order to reach the fertilization-competent form of the spermatozoa. To study SUN4 with regard to its properties and function during spermiogenesis, not only its detailed behavior, but also its potential binding partners were investigated. Mechanistic insights were gained by characterizing *Sun4* knockout mice, from which the spermatids were analyzed at the ultrastructural level to further evaluate the network in which SUN4 functions.

2 Results

2.1 Expression and localization of SUN4

At the beginning of the project, only a little published information about the SUN-domain protein SUN4 was available and some of it was quite controversial as well. Therefore, a general characterization of the protein was performed using different methods in order to clarify its actual expression pattern and intracellular localization.

2.1.1 Generation of SUN4-specific antibodies

In order to investigate the potential role of SUN4 in sperm head shaping, as well as for a general characterization of the protein, SUN4-specific antibodies were generated. To create reliable antibodies, two different SUN4 epitopes were selected - a short one within the perinuclear domain, and one within the N-terminus, corresponding to amino acids 246 to 260 and 11 to 127 of full length murine SUN4 respectively (Figure 2.1) (for generation and purification see methods under 5.6.9). It is worth noting that the polyclonal antibodies that were generated against the N-terminal epitope were raised in two different host species, a guinea pig and a rabbit, to be able to combine them with different antibodies in co-detection immunofluorescence analyses. Altogether, three different antibodies, including different epitopes and different host species, were provided for internal controls and verification of the results of the experiments.

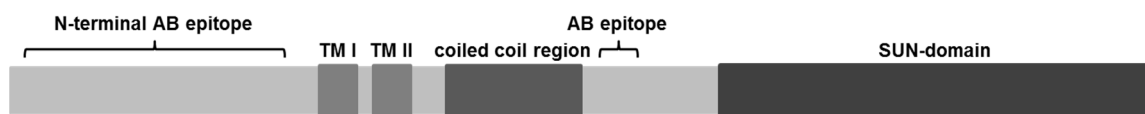


Figure 2.1: Murine SUN4.

Schematic representation of the SUN4 protein including the putative transmembrane domains (TM I and TM II), the coiled coil region and the SUN-domain. The two antibody (AB) epitope sites are marked as well.

2.1.2 *Sun4* expression is restricted to spermiogenesis

To analyze the expression pattern of *Sun4*, RT-PCR was performed on a broad range of different mouse tissues. For the detection of the *Sun4* mRNA expression sequence-specific primers (Sun4_cc_5'; Sun4_cc_3'; see also Table 4.3 under 4.2.2) flanking the putative coiled coil region of *Sun4* were used. PCR amplification revealed the presence of the *Sun4* transcript in the testis, but not in any other somatic tissue or in the ovarian sample (Figure 2.2 A). To confirm this finding a western blot using the affinity-purified SUN4 antibodies was carried out with the same representative mouse tissues. The antibody detection also recognized a single protein band with the expected molecular weight of 49kDa in only the testis tissue sample and none of the other tissues tested (Figure 2.2 B).

For a more detailed analysis of the testis-specific expression pattern, RT-PCR was performed on RNA from testis tissue of 8-, 12-, 15-, 18-, 21- and 25-day old mice. Within this timeframe the first wave of mouse spermatogenesis occurs, which allowed for temporal classification of *Sun4* expression (Bellve et al., 1977; Malkov et al., 1998; Schütz et al., 2005a). From day 8 to day 15, a period that only contains premeiotic and meiotic germ cell stages, no *Sun4* transcript was observed. A first faint signal was detected at day 18 postpartum, a timepoint when spermiogenesis is initiated and first postmeiotic stages appear. Accordingly, at day 21 to 25, when round and elongated spermatids accumulate in the testis, the *Sun4* signal was stronger, suggesting that *Sun4* is expressed during spermiogenic differentiation (Figure 2.2 C). To confirm this result at the protein level, testicular suspensions of mice from the corresponding time points were used for western blot analysis. A strong signal could be detected at day 25 only, when postmeiotic spermatids are abundant within the testis (Figure 2.2 D). Taken together, these results demonstrate expression of SUN4 during spermiogenesis only and therefore suggest a solely postmeiotic expression profile of this potential LINC complex component.

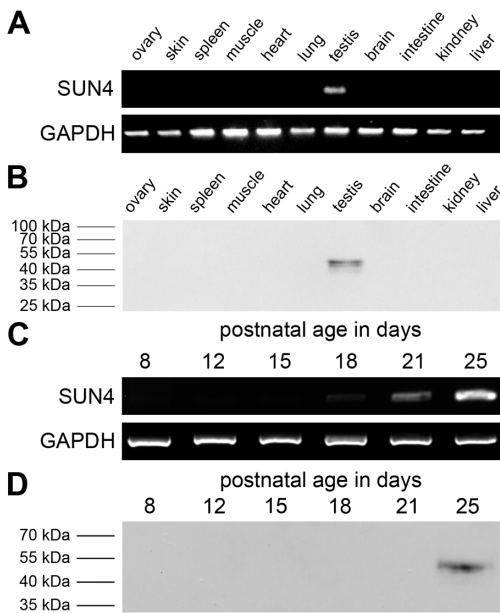


Figure 2.2: Expression of *Sun4*.

(A, B) Expression of *Sun4* is restricted to the testis tissue, shown by (A) RT-PCR and (B) western blot analysis using *Sun4*-specific primers and affinity purified anti-SUN4 antibodies, respectively. (C, D) Analysis of the temporal expression pattern of the testis-specific *Sun4* during mouse spermatogenesis. Spermiogenesis-specific expression was revealed by (C) RT-PCR analysis from RNA of testicular cells at different age stages (day 8 to 25) and by (D) western blot analysis using equivalent amounts of testicular cells of the same stages, as well. Figure adapted from Pasch et al. (2015).

Using paraffin-embedded testis tissue sections, immunofluorescence analysis of SUN4 localization further confirmed the spermatid-specific expression pattern, as spermatogonia and spermatocytes were negative for SUN4 and a clear signal was observed at the NE of the postmeiotic spermatids only (Figure 2.3). In common with other NE components during spermiogenesis (Alzheimer et al., 1998; Mylonis et al., 2004; Schütz et al., 2005a), SUN4 appeared to have a polarized localization pattern as well.

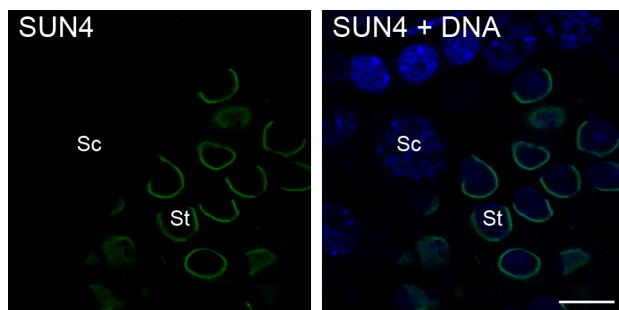


Figure 2.3: Immunostaining of SUN4.

Immunofluorescence localization of SUN4 on paraffin-embedded testis tissue sections using SUN4-specific antibodies shows a staining signal restricted to spermatids (St). Sc, Spermatocyte; Scale bar: 10 µm. Figure adapted from Pasch et al. (2015).

This polarized localization pattern was detected with all three SUN4-specific antibodies. The higher magnifications of the immunofluorescence images revealed the anti-SUN4 signals restricted to only one side of the early and late spermatids (Figure 2.4). Furthermore, co-staining of the SUN4-specific antibodies raised against different epitopes always revealed a congruent localization within the testis tissue (Figure 2.4 A, B), which was also true for the co-staining of the SUN4-specific N-terminal antibodies that were raised in different host species (Figure 2.4 C). The co-localization of the different anti-SUN4 antibodies, and the exclusive staining of postmeiotic germ cells with no recognizable background staining, further demonstrates the specificity of the anti-SUN4 antibodies and is consistent with the expression analysis.

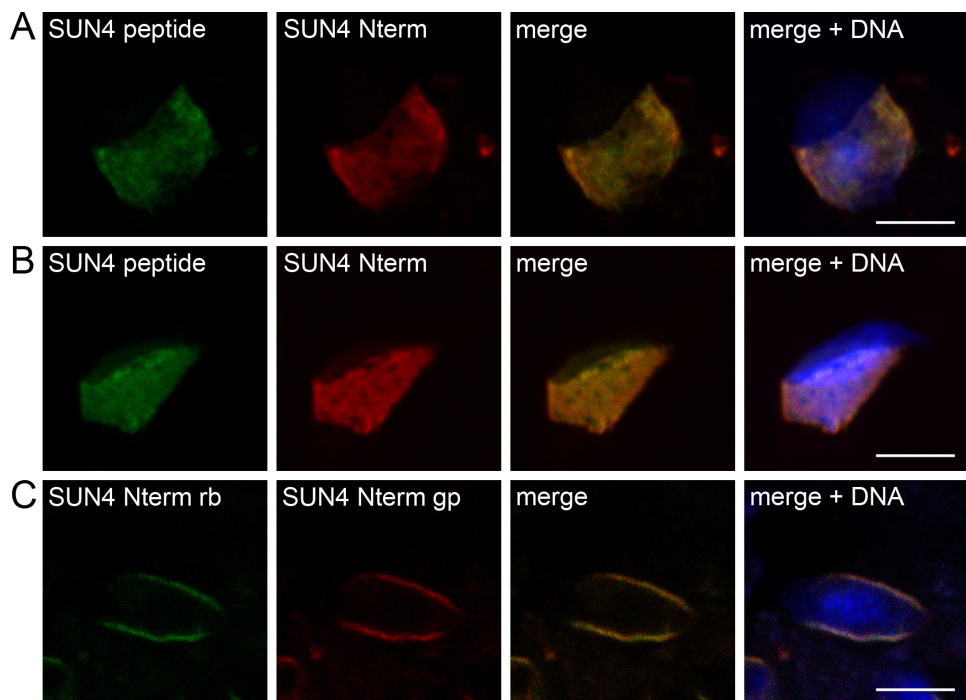


Figure 2.4: Congruent and polarized localization pattern of the different SUN4-specific antibodies.

(A, B, C) Immunofluorescence analyses of the different SUN4-specific antibodies used on either testicular cell suspension spreads (A, B) or paraffin-embedded testis tissue sections (C) revealed a polarized localization pattern. (A, B) Co-staining of the anti-SUN4 antibodies directed against different SUN4 epitopes: the SUN4-specific peptide antibodies against the perinuclear region are stained in green and the guinea pig SUN4-specific N-terminal antibodies in red. (C) Co-staining of the SUN4-specific N-terminal antibodies raised in different species: rabbit (green) and guinea pig (red). Merges are shown on the right with the yellow color indicating a perfect overlay. DNA is stained in blue. Scale bars: 5 µm.

Despite the fact that SUN4 was labeled with three different antibodies, including different antibody epitopes and different host species, an immunofluorescence signal was never detected at spermatozoa from the epididymis (Figure 2.5). Therefore the subcellular distribution pattern of the SUN4 antibodies so far revealed that SUN4 is localized to one side of the NE during spermiogenesis only and is actually not present in the sperm tail, neither during spermiogenesis (Figure 2.4, Figure 2.6), nor during epididymal maturation (Figure 2.5).

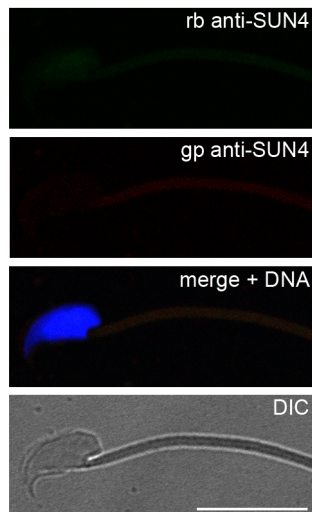


Figure 2.5: Spermatozoa are negative for SUN4.

Immunofluorescence localization of SUN4 on epididymal cell suspension smear. Absence of SUN4 in spermatozoa was revealed by double-staining the spermatozoa with the rabbit anti-SUN4 peptide antibody (green) and the guinea pig anti-SUN4 N-terminal antibody (red). Overlay is depicted third from top, together with DNA stained in blue. Corresponding DIC (differential interference contrast) image is presented on the bottom. Scale bar: 10 µm. Figure adapted from Pasch et al. (2015).

2.1.3 SUN4 localizes to the posterior side of spermatids adjacent to the microtubule manchette

To gain more precise insight into the localization and behavior of the murine SUN4 during the postmeiotic germ cell development, detailed immunofluorescence analyses were performed on paraffin-embedded testis tissue sections of adult mice. Thereby the exact distribution of the protein was investigated by performing co-localization studies using proteins with known distributions to obtain conclusive information about the polarized SUN4 signal.

SUN4 was first co-stained with CAGE1, an acrosomal protein, which covers the anterior pole of the developing spermatid nucleus (Alzheimer et al., 2005). This analysis revealed that SUN4 is completely excluded from the anterior pole, where CAGE1 is present, as no overlap of these proteins was found (Figure 2.6 A). SUN4 obviously localizes to the opposite side of the acrosome in round and elongating spermatids, where it is present at the lateral regions and excluded from the very

posterior pole, i.e. the region of the implantation fossa. This exclusion from the fossa region could be confirmed by co-staining SUN4 with γ -tubulin, which stains the basal body adjacent to the implantation fossa. No SUN4 signal was detected here (Figure 2.6 B).

To narrow down the exact localization of SUN4 it was further co-stained with β -tubulin, a major component of the spermatid-specific manchette, which as a prominent collar-like microtubule structure covers the posterior part of the elongating nucleus (Toshimori and Ito, 2003). This revealed that SUN4 is constrained to the regions associated with the manchette microtubules only. Therefore, it seems that SUN4 is rather a component of the NE instead of being localized within the manchette itself, because the SUN4 signal was present at regions adjacent to the inner nuclear side of the manchette (Figure 2.6 C).

The localization of SUN4 quite strikingly resembled that of SUN3, which had recently been characterized as a posterior NE component that together with Nesprin1 forms a LINC complex adjacent to the manchette microtubules (Göb et al., 2010). Therefore SUN4 was co-stained with either SUN3 or Nesprin1 on paraffin-embedded testis tissue sections. Immunofluorescence analyses of these sections revealed a virtually identical localization pattern of SUN4 and SUN3, as the signals of SUN4 and SUN3 (Figure 2.6 D), as well as the signals of SUN4 and Nesprin1 (the LINC complex partner of SUN3) (Figure 2.6 E), appeared to entirely overlap.

Taken together, the subcellular distribution pattern obtained with the anti-SUN4 antibodies revealed that SUN4 is exclusively localized in the NE of the posterior nucleocytoplasmic junction, where it not only aligns with the spermatid-specific manchette, but also co-localizes with SUN3 and Nesprin1 during spermiogenesis.

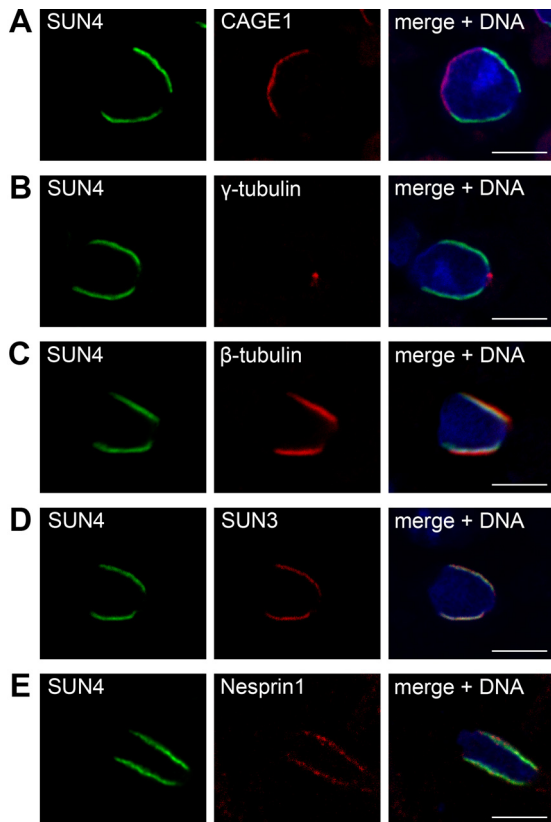


Figure 2.6: SUN4 localizes at the lateral posterior NE.

(A-E) Localization analysis of SUN4 in elongating spermatids using immunofluorescence analyses. Immunolocalization presented by co-staining of SUN4 with (A) CAGE1, (B) γ -tubulin, (C) β -tubulin, (D) SUN3 and (E) Nesprin1 on paraffin-embedded testis tissue sections. Overlays are depicted on the right, together with DNA stained in blue. The asterisks designate the region of the implantation fossa. The arrows point to the basal body. Scale bars: 5 μ m. Figure adapted from Pasch et al. (2015).

Additionally, the distribution of SUN4 was also compared with that of SUN5, another testis-specific potential LINC complex component. For the immunofluorescence detection of SUN5, an antibody against the murine SUN5 epitope from AA 95 to 170 was used. This revealed that in early spermatid stages SUN5 partially co-localizes with the Golgi marker GM130 but is in addition localized within the NE at the opposite side of the nucleus as well (Figure 2.7 A). A diffuse cytoplasmic signal of the anti-SUN5 antibody could also be detected in early spermatid stages.

Closer inspection of co-labeled paraffin-embedded and frozen, tissue embedded testis tissue sections using SUN4- and SUN5-specific antibodies revealed dramatic results. Interestingly, although the stainings of the different tissue embedding methods showed mainly the same results, they differed in the SUN5 signal of the late spermatids. The first SUN5 signal that could be detected was the diffuse cytoplasmic signal in postmeiotic germ cells. This appeared in early spermatid stages where neither SUN4 nor SUN5 could be detected at the NE. Then SUN5 seemed to be relocated to the posterior NE, where it was detected evenly distributed slightly before the SUN4 signal appeared in the NE of the round spermatid stages (Figure 2.7 B). Thereafter the SUN4 and SUN5 signals co-localized in the posterior NE for a rather short period of time within early spermiogenesis (Figure 2.7 C). As soon as the elongation of the

spermatid nucleus started, at step eight to nine of spermiogenesis (according to the spermatogenic cycle), the SUN5 signal seemed to relocate from its localization area at the posterior side towards the center of the nucleus (Figure 2.7 D). In the elongated spermatid, when SUN4 was still evenly distributed at the lateral posterior side of the nucleus, the SUN5 signal was visible as a circular structure surrounding the center of the elongated nucleus, which corresponded to the anterior border of the SUN4 signal (Figure 2.7 E). At this point it should be noted that the observed SUN5 signals could be reliably repeated, although the SUN5 signal in the elongated spermatids, which reveals the rather circular appearance was only visible using tissue tek-embedded cryo sections. In the paraffin-embedded tissue sections no SUN5 signal could be detected after the elongation of the nucleus began. However, the SUN5 signal detected in the early round spermatids was visible using both methods: immunofluorescence staining of paraffin- as well as of tissue tek-embedded testis tissue sections.

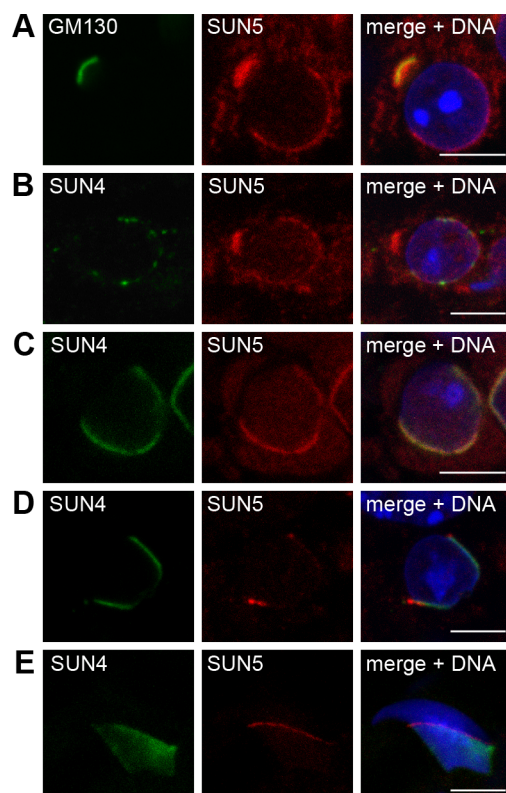


Figure 2.7: SUN5 co-localizes with SUN4 in early spermatids.

Immunofluorescence analysis of SUN5 revealed a differential localization pattern depending on the spermatid stages (A-E). (A) Co-staining of the Golgi marker GM130 and SUN5 showed that SUN5 might be processed within the Golgi. (B-E) Co-staining of SUN4 and SUN5 showed co-localization in the posterior NE of early spermatid stages (B, C). During nuclear differentiation the SUN5 signal shifted towards the anterior edge of the SUN4 signal (D, E). Scale bars: 5 µm.

2.2 Analyzing SUN4 function using a SUN4 deficient knockout model

In order to gain information about the central function and role of SUN4 as a component of the posterior NE, further work was conducted using a SUN4 deficient mouse strain. Here the consequences of the ablation of the SUN4 protein were analyzed by focusing on the relevance of SUN4 for the spermiogenic development of male germ cells.

2.2.1 Absence of SUN4 leads to male infertility

On our behalf a SUN4 deficient mouse strain was generated by the KOMP Repository (www.komp.org; 4.1.3) under the name *Spag4^{tm1(KOMP)Mbp}*. This mouse line was established and kept under adequate and stable conditions in the animal facility at the Biocenter of the University of Würzburg. The mutant animals carry a deletion of exon two to exon ten within the *Sun4* gene, which leads to the loss of the coding regions of important functional domains, like the transmembrane region(s), the coiled coil region and the SUN-domain (Figure 2.8 A). To verify correct gene targeting and for general genotyping of the offspring of the *Spag4^{tm1(KOMP)Mbp}* mouse strain, specific wild type and knockout 5'-primers and a common 3'-primer were generated for PCR analyses. By using a common 3'-oligonucleotide in the PCR it was possible to co-detect the wild type and the knockout alleles in one reaction. Correspondingly either a single 446 bp fragment for the wild type, a single 593 bp fragment for the knockout or both fragments in the heterozygous situation would be amplified (Figure 2.8 B).

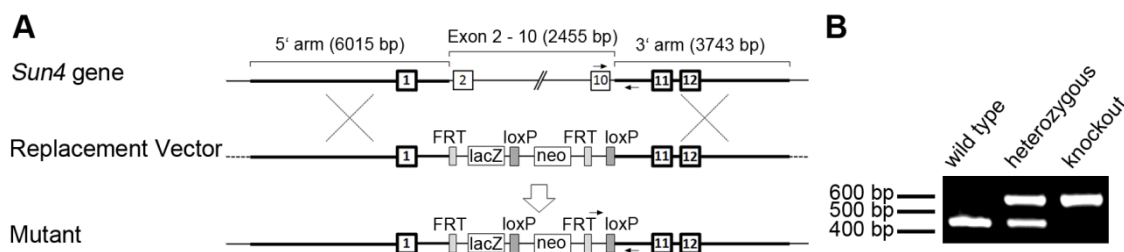


Figure 2.8: Generation and verification of the *Spag4^{tm1(KOMP)Mbp}* mouse strain.

(A) Schematic drawing of the *Sun4* gene, the replacement vector, which is missing exons two to ten, and the resulting mutant allele. Little arrows at the *Sun4* gene and mutant scheme indicate the primer sites for genotyping. (B) Genotyping of the *Spag4^{tm1(KOMP)Mbp}* mice by PCR analysis using the in (A) indicated primers for the wild type and mutant alleles (Table 4.3 under 4.2.2). Figure adapted from Pasch et al. (2015).

To verify the *Sun4* gene disruption on the mRNA expression level *Sun4_cc_5'* and *Sun4_cc_3'* (Table 4.3 under 4.2.2) primers were used in RT-PCR analysis. In purified RNA from testicular cell suspensions, *Sun4*-specific fragments could only be amplified from the wild type and heterozygous material. In the knockout sample no amplicon could be generated, which clearly confirmed the *Sun4* deletion in the homozygous *Sun4* knockout mice (*Sun4^{-/-}*) (Figure 2.9 A). This result was also verified at the protein level by performing western blot analysis. Here SUN4-specific antibodies were able to detect the protein in the wild type and heterozygous testis tissue samples, but not in the *Sun4^{-/-}* testis sample (Figure 2.9 B). Immunofluorescence analysis on paraffin-embedded testis tissue sections further demonstrated the absence of the protein in the mutant animals as well, as no staining signal could be observed in the homozygous *Sun4* knockout tissue section (Figure 2.9 C).

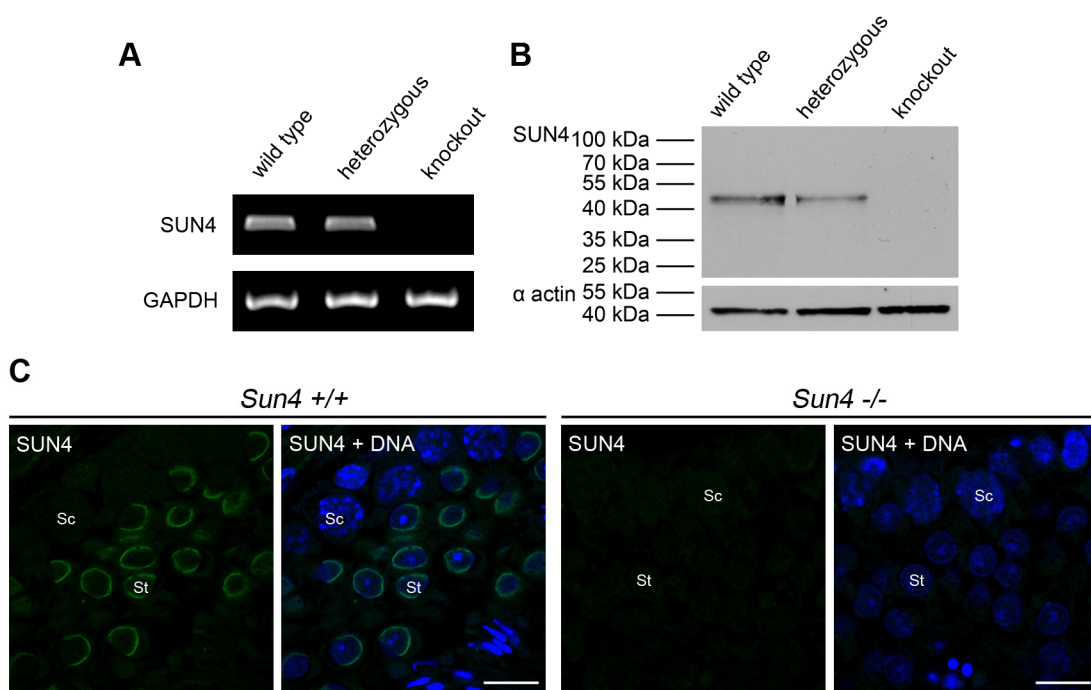


Figure 2.9: Confirmation of the SUN4 deletion in the *Sun4* knockout mouse line.

(A) RT-PCR and (B) western blot analysis revealed the presence of SUN4 in wild type and heterozygous testicular material, but absence in the homozygous knockout mice. (C) Immunofluorescence staining of SUN4 in paraffin-embedded *Sun4^{+/+}* and *Sun4^{-/-}* testis tissue sections show a normal distribution in the wild type and absence in the *Sun4* knockout mice. DNA is stained in blue. Sc, spermatocyte; St, spermatid; Scale bars: 10 µm. Figure adapted from Pasch et al. (2015).

Breeding of *Spag4^{tm1(KOMP)Mbp}* heterozygous males with heterozygous females produced offspring with normal litter size carrying the mutated locus according to Mendelian ratios. None of the offspring, including the *Sun4* knockout mice, showed any visible somatic phenotype, in terms of size and behavior, which demonstrated a normal embryonic development. Beyond this, this illustrated that SUN4 heterozygosity had no overt negative effect on fertility. Next the *Sun4^{-/-}* mice were tested regarding their fertility. The mating attempts of *Sun4^{-/-}* males with *Sun4^{+/+}* females were repeated several times, but this combination never produced any offspring, demonstrating that the *Sun4^{-/-}* males were infertile. As expected, the mating of *Sun4^{-/-}* females with either *Sun4^{+/+}* or *Sun4^{-/+}* males had no negative effect on litter size and viability, which is consistent with the testis-specific expression of *Sun4*.

2.2.2 Absence of SUN4 severely interferes with spermiogenesis

Since *Sun4^{-/-}* male mice were infertile, their germ cell development was analyzed in more detail. In the literature many mouse mutant models for male infertility can be found showing overt differences regarding their testis size and weight, due to the loss of germ cells (Yan, 2009). Interestingly, no overt difference could be observed regarding the testis size of the *Spag4^{tm1(KOMP)Mbp}* male mice, indicating a rather regular number of germ cells within the three different genotypes. To verify this result, a statistical evaluation was performed comparing the testis weight of wild type (n=14; mean value: 89.85), heterozygous (n=16; mean value: 87.5) and homozygous (n=12; mean value: 91.83) *Sun4* knockout mice (Figure 2.10). No significant difference between these groups could be found using the Kruskal-Wallis-Test ($p=0.4018$) after checking the data for normal distribution with the Shapiro-Wilk-Test (*Sun4^{+/+}*: $p=0.067$; *Sun4^{-/+}*: $p=0.041$; *Sun4^{-/-}*: $p=0.221$).

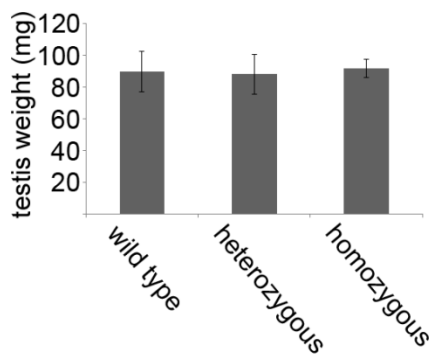


Figure 2.10: Comparison of the testis weight of the *Spag4^{tm1(KOMP)Mbp}* mouse strain males.

The graph shows no difference between the mean values of the testis weight of wild type (n=14), heterozygous (n=16) and homozygous (n=12) *Sun4* knockout mice. The error bars indicate standard deviations. Figure adapted from Pasch et al. (2015).

To analyze whether absence of SUN4 affects male germ cell development, histological analyses were performed on adult *Sun4^{+/+}*, *Sun4^{+/-}* and *Sun4^{-/-}* littermates. Just as expected for a protein expressed in postmeiotic stages only, the comparison of the hematoxylin and eosin staining of paraffin-embedded testis tissue sections between the three different genotypes revealed no overt differences in somatic cells, spermatogonia nor in spermatocytes (Figure 2.11 A-A''). In later spermatid stages, however, dramatic differences could be seen between the sections of wild type and heterozygous *Sun4* knockout littermates, which showed nicely elongated late spermatids, and the homozygous knockout sections that revealed only aberrant roundish late spermatids (Figure 2.11 A-A''). Although SUN4 deficiency seemed to induce a quite striking abnormality in the sperm development these aberrant shaped spermatozoa were still delivered into the epididymis, where they can be found in the caput (Figure 2.11 B'') and the cauda region (Figure 2.11 C'').

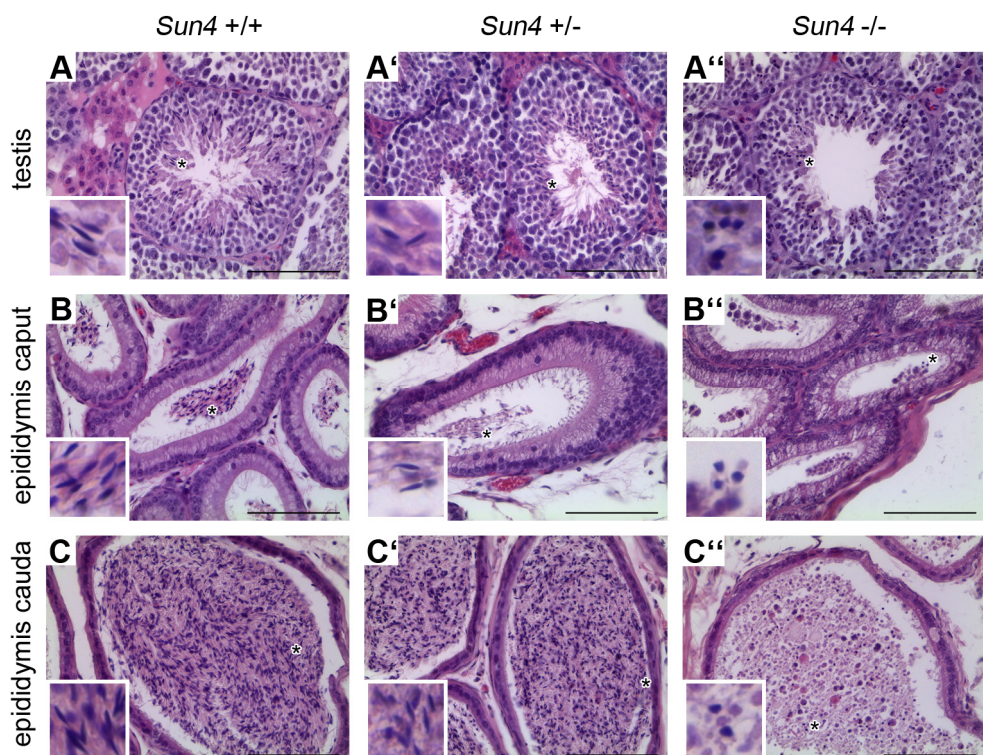


Figure 2.11: SUN4 depletion alters germ cell development.

Histological analysis of *Sun4^{+/+}* (A, B, C), *Sun4^{+/-}* (A', B', C') and *Sun4^{-/-}* (A'', B''; C'') testis (A-A''), epididymis caput (B-B'') and epididymis cauda (C-C'') tissue sections. Hematoxylin and eosin staining show normally developed somatic cells, spermatogonia and spermatocytes in the testis of all three different genotypes (A-A''). In contrast, normally elongated late stages of spermatids or spermatozoa could be detected in *Sun4^{+/+}* (A, B, C) and *Sun4^{+/-}* (A', B', C') tissue sections only, but were absent from the *Sun4^{-/-}* samples. Instead aberrant roundish late spermatids or spermatozoa were observed in the SUN4 deficient tissues (A'', B''; C''). Insets on the bottom left of every image show higher magnifications of the areas marked with an asterisk. Scale bars: 50 µm. Figure from Pasch et al. (2015).

This germ cell phenotype was further analyzed at the ultrastructural level to gain more detailed insight into the defects provoked by SUN4 deficiency in mammals. Electron microscopy (EM) analyses of ultrathin sections from testicular material of wildtype and SUN4 deficient littermates generally verified the initial histological findings. In agreement with the results of the hematoxylin and eosin staining, no differences in the premeiotic and meiotic germ cell stages between the two genotypes could be detected. The samples furthermore revealed no phenotypic abnormalities in early round spermatid stages in *Sun4^{-/-}* male mice. Early spermatids still displayed round cell nuclei with the acrosome properly attaching to and expanding over the anterior pole of the NE, as visible for wild type spermatids at the same stages as well (Figure 2.12 A-A’).

Beginning from step eight to nine of spermiogenesis according to the spermatogenic cycle (Figure 1.1; Russell et al., 1990), the homozygous *Sun4* knockout spermatids showed a dramatically changed appearance when compared to the wild type spermatids (Figure 2.12 B’, B’’). While in a proper functioning germ cell the nucleus develops into a typically flattened and elongated form, which can be easily detected (Figure 2.12 C), the later stages of the *Sun4^{-/-}* spermatids showed completely misshapen nuclei (Figure 2.12 C’, C’’). Closer inspection of the aberrant nuclei revealed quite consistent phenotypes in the differentiating spermatids in the absence of SUN4. These nuclei are not only roundish and misshaped, but also show frequent nuclear membrane evaginations.

Despite the unusual appearance of the nuclei, chromatin compaction appeared not to be affected by SUN4 deficiency, as mutant sperm cell nuclei exhibited visually normal condensed chromatin. Likewise, the acrosome seemed to remain unaffected in *Sun4^{-/-}* spermatids. This prominent structure not only attaches properly in the early spermatid stages, but also expands over the anterior side of the sperm nuclei, where it can be seen aligned with the deformed NE in late spermatid stages as well (Figure 2.12 B’, B’’, C’, C’’). The flagellum as another spermatid-specific prominent structure also appeared to retain a wild type-like development in the *Sun4* knockout spermatids (Figure 2.12 C), as it was correctly localized at the posterior pole and showed a normal development within the testis (Figure 2.12 C’, C’’). Taking the appearance of the anterior positioned acrosome and the posterior positioned flagellum into account, the mutant spermatids clearly maintain their general anterior-posterior polarity (see also 2.2.3).

At the nucleocytoplasmic junction, where in the later spermatid stages the microtubule manchette can be found as a bundle-like structure connected to the

posterior lateral NE in the wild type (Figure 2.12 B), for the most part nothing could be seen in the mutant spermatids. There were a few rare cases, where a severely disorganized microtubule structure was detected in close proximity to a late spermatid nucleus in the SUN4 deficient germ cells (Figure 2.12 B').

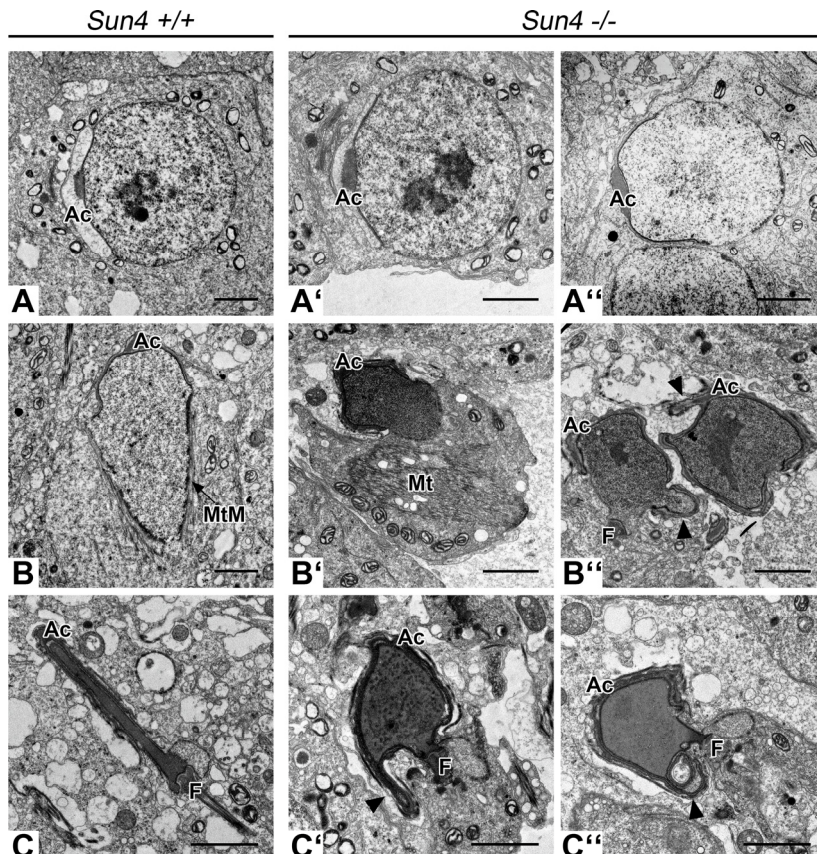


Figure 2.12: Sperm head formation is severely disturbed in *Sun4* knockout spermatids.

Ultrastructural analysis comparing the spermiogenic development of wild type (A, B, C) and SUN4 deficient (A', A'', B', B'', C', C'') spermatid stages. The electron microscopic images revealed no difference in the early round spermatids between the different genotypes (A, A', A''). In contrast, the later stages of the *Sun4*^{-/-} spermatids (B', B'', C', C'') displayed severe malformations compared to the wild type (B, C). Ac, Acrosome; F, Flagellar structures; MtM, Microtubule-containing manchette; Mt Microtubule structure. Scale bars: 2 μm. Figure from Pasch et al. (2015).

Ultrastructural analysis of *Sun4*^{-/-} epididymis tissue sections confirmed the results from the histological analyzes of the testis samples. Compared to wild type spermatozoa with their typically elongated sperm heads (Figure 2.13 A, A'), all nuclei of the spermatozoa that could be detected in the homozygous *Sun4* knockout epididymal tubules appeared severely misshaped (Figure 2.13 B-G). Mutant spermatozoa seemed to change their occurrence during maturation in different sectors of the epididymis

(from caput to cauda). While in the caput region of the epididymis numerous spermatozoa with rather straight appearing tails could be found (Figure 2.13 B), there was a clear tendency that tails coil around the nucleus during epididymal maturation, as most nuclei towards the cauda region were encircled by their tail (Figure 2.13 D horizontally, E vertically). Consistent with a study by Suzuki-Toyota et al. (2007), who investigated the sperm tail coiling in *Gopc*^{-/-} mice, the coiling of the tails in *Sun4*^{-/-} mice seemed to start with the pathological bending of the nucleus towards the mid piece of the flagellum, where cytoplasmic residues are still attached (Figure 2.13 C). In some cases sperm heads could be found in large constrictions together with other cytoplasmic residues (Figure 2.13 F and G). Interestingly the EM analysis presented here also revealed a partial detachment of the acrosome from the NE of most of the *Sun4*^{-/-} spermatozoa that were delivered into the epididymis (Figure 2.13 B-E). This appearance resembled that of a globozoospermia-like phenotype, marked by the roundish sperm nuclei and detached acrosomes (Dam et al., 2011).

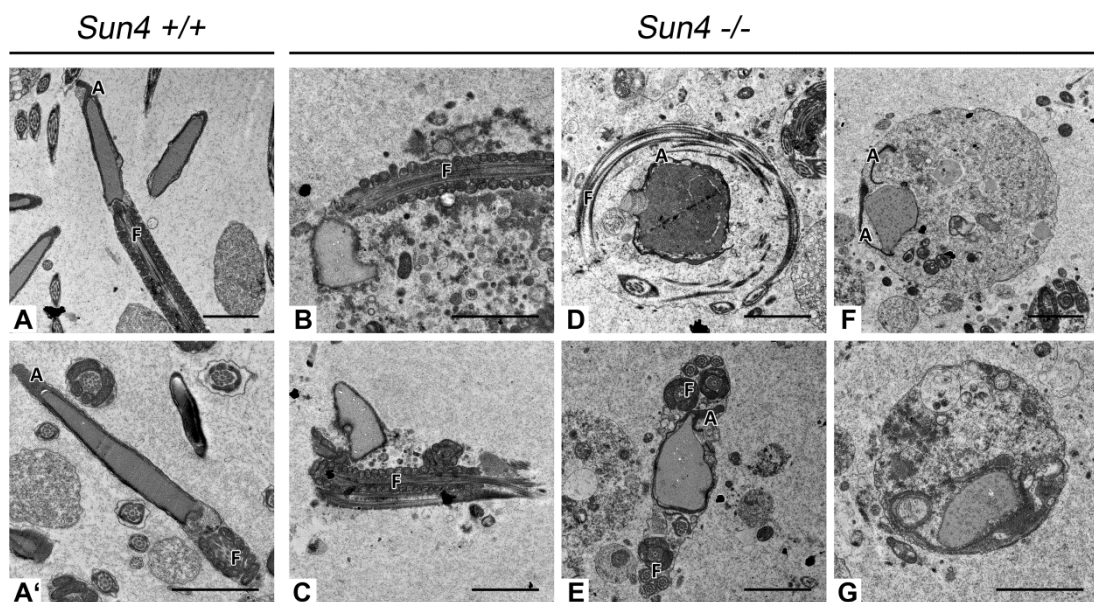


Figure 2.13: *Sun4*^{-/-} spermatozoa reveal a globozoospermia-like phenotype.

Electron microscopy analysis of *Sun4*^{+/+} (A, A') and *Sun4*^{-/-} (B-G) spermatozoa within the epididymis. Compared to the wild type, the SUN4 deficient spermatozoa show severely misshapen nuclei (B-G) and a tendency to coil the flagellum around their head (D, E). In the absence of SUN4 the malformed nuclei were also regularly found in large constrictions (F, G). The malformed roundish nuclei together with the often partially detached acrosomes in the *Sun4*^{-/-} spermatozoa resembled a globozoospermia-like phenotype. Ac, Acrosome; F, Flagellum. Scale bars: 2 μm. Figure adapted from Pasch et al. (2015).

2.2.3 SUN4 depletion alters the distribution of other LINC complex components and NE associated structures

To gain further insights into the role of SUN4 in the nucleocytoplasmic junction, the impact of the absence of this protein within this structure was studied in more detail. Therefore the localization of other LINC complex components and NE associated structures that might be involved in the posterior nucleocytoplasmic junction was investigated. As mentioned earlier, in the wild type background SUN4 distribution completely overlaps with that of SUN3 and Nesprin1, suggesting that they may interact with each other. To see whether the distribution of SUN3 and/or Nesprin1 changes in SUN4 deficient spermatids, testis tissue sections were double-labeled with SUN3 or Nesprin1 and the anterior marker CAGE1. Compared to the wild type spermatids, where SUN3 is localized in the lateral posterior NE, hardly any antibody signal could be found in this region in the SUN4 deficient spermatids (Figure 2.14 A, A'). Instead SUN3 was severely mislocalized and relocated to the cytoplasm, where it showed a tendency to accumulate in cytoplasmic aggregations (Figure 2.14 A'). Localization of Nesprin1, the interaction partner of SUN3, seemed to be affected as well, as it could no longer be detected at the posterior NE of the *Sun4^{-/-}* spermatid nuclei (data not shown). This demonstrated that SUN4 is necessary for the correct localization of SUN3 and probably also of Nesprin1 to the posterior NE in spermatids.

Next, the impact of SUN4 on the localization of the SUN1/Nesprin3 or SUN1 η /Nesprin3 complex was investigated. As previously described by Göb et al. (2010), in the wild type the distribution of these LINC complexes varies depending on spermiogenic progression. In early round spermatids the SUN1/SUN1 η and Nesprin3 signals can be observed more or less evenly distributed over the posterior half of the spermatid nuclei, excluding the implantation fossa, and as a cap like structure at the anterior pole of the acrosome. During spermiogenesis the posterior signals retract towards the posterior pole until they disappear completely in the late spermatids, when only the signals at the anterior side remain (Göb et al., 2010). In general the SUN1/SUN1 η and Nesprin3 signals in the SUN4 deficient spermatids maintained their dual localization at the anterior acrosomal cap and at the posterior half (Figure 2.14 B, B'). However, closer inspection revealed that the posterior SUN1/SUN1 η and Nesprin3 signals stayed more or less evenly distributed over the posterior half during spermiogenic progression in *Sun4^{-/-}* spermatids instead of retracting towards the posterior pole (Figure 2.14 B', D'). This showed a mild but significant effect in which the posterior SUN1 η /Nesprin3 complexes remained extended to more apical regions of the

posterior side, suggesting that SUN4 is also required for the correct localization of these LINC complexes as well.

Due to their function in anchoring the nucleus to cytoskeletal elements it has been suggested that the posterior LINC complexes might be involved in connecting the manchette to the posterior NE as part of the nucleocytoplasmic junction (Göb et al., 2010; Kierszenbaum et al., 2011; Kracklauer et al., 2013). Since the immunofluorescence signal of the potential LINC complex component SUN4 appeared only at regions closely associated with the manchette microtubules, it was of importance to analyze if the manchette as a component of the posterior nucleocytoplasmic junction is affected by the absence of SUN4. While in the wild type background the β -tubulin signal aligned with the posterior NE, representing the manchette as a collar-like structure neighboring the posterior NE (Figure 2.14 C), in the absence of SUN4 the β -tubulin signal was completely mislocalized, which indicated that the spermatids failed to organize a typical manchette. In most cases the anti- β -tubulin antibodies could not detect any microtubule-containing structures in the *Sun4*^{-/-} spermatids. However, degenerated filamentous arrays could sometimes still assemble, but could be seen more or less distant from the posterior NE of the differentiating mutant spermatids (Figure 2.14 C'), which is consistent with the results from the ultrastructural analysis (Figure 2.12 B').

In *Drosophila* it has been shown that the absence of Spag4 (the presumed fly ortholog of the mammalian SUN4), causes the dissociation of the basal body from the posterior pole of the NE. This often occurred together with a sideways shift of the structure (Kracklauer et al., 2010). Therefore Spag4 has been suggested to be critical for the correct positioning and NE attachment of the basal body at least in the fly. To investigate if this is also true for the mammalian SUN4, paraffin-embedded testis tissue sections of SUN4 deficient mice were co-stained for γ -tubulin and SUN1. Compared to the wild type spermatids, γ -tubulin staining in the *Sun4* knockout spermatids revealed no visual difference in the localization of the basal body in relation to the posterior NE (Figure 2.14 D, D'). It is worth noting however that the position of the posterior pole was not as easily estimated in the mutant spermatids due to the extension of SUN1/SUN1 η towards more apical regions, and consequently an expansion of the comparable posterior pole region.

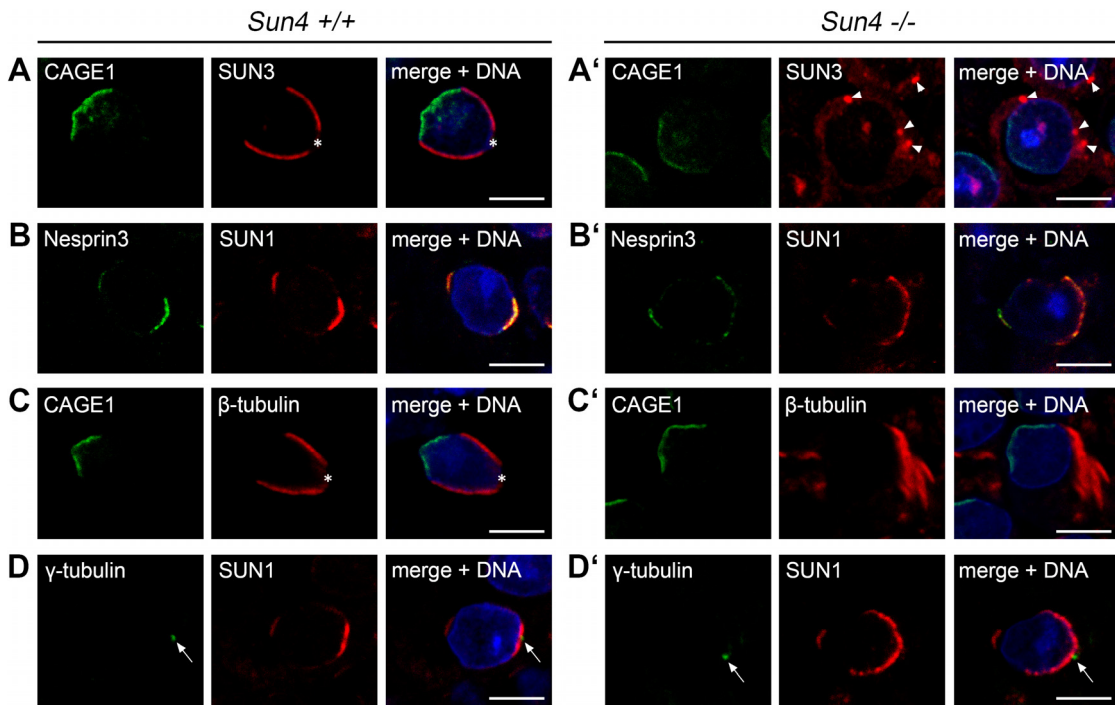


Figure 2.14: LINC complex components and NE associated structures reveal an altered localization in the absence of SUN4.

Representative images of spermatids from immunofluorescence analysis of paraffin-embedded testis tissue sections of *Sun4^{+/+}* (A-D) and *Sun4^{-/-}* (A'-D') littermates. The tissue sections were co-stained for CAGE1 and SUN3 (A, A'), Nesprin3 and SUN1 (B, B'), CAGE1 and β -tubulin (C, C') and γ -tubulin and SUN1 (D, D'). Arrowheads indicate the SUN3 aggregations typically found in *Sun4^{-/-}* spermatids. Overlays are shown on the right side with the DNA stained in blue. Asterisks mark the implantation fossa. Arrows indicate the basal body. Scale bars: 5 μ m. Figure from Pasch et al. (2015).

2.2.4 SUN4 depletion causes disruption of the posterior nucleocytoplasmic junction

Since the current study provided clear evidence that the SUN4 deficient spermatids fail to organize a typical manchette, the posterior nucleocytoplasmic junction was investigated in more detail. CLIP-50, a member of the Clip-170 family of microtubule-binding proteins, has been described as a component of the perinuclear ring from which the manchette microtubules emerge (Tarsounas et al., 2001). Therefore it was of importance to investigate if the perinuclear ring as a potential microtubule organizing center (MTOC) was also affected by the absence of SUN4 (Brinkley, 1985; O'Donnell and O'Bryan, 2014). For this analysis immunofluorescence co-staining with anti- β -tubulin and anti-CLIP1 antibodies was performed. The mammalian CLIP1 (also called CLIP-170) binds to the plus ends of microtubules and plays a role in microtubule dynamics and growth (Perez et al., 1999; Akhmanova et al.,

2005). Due to its close sequence identity the anti-CLIP1 antibodies also detect CLIP-50.

In the wild type background, the anti-CLIP1 antibody signal could be detected evenly distributed at the posterior NE adjacent to the manchette microtubules in the early spermatids (Figure 2.15 A, C). During spermiogenic progression the antibody signal at the posterior side neighboring the manchette weakened with a strong signal remaining only at the anterior rim of the posterior localization area. In accordance with the study by Tarsounas et al. (2001) this circular signal marks the perinuclear ring at the anterior edge of the manchette and therefore clearly resembles the CLIP-50 labeling pattern (Figure 2.15 B, D). In the SUN4 deficient spermatids the anti-CLIP1 antibody signal could no longer be detected evenly distributed around the posterior NE and no specific signal was observed (Figure 2.15 C'). In rare cases, where an anti-CLIP1 antibody signal could still be found in proximity to the *Sun4*^{-/-} spermatid nuclei, this signal was found at the probable anterior end of a peculiar microtubule assembly correlating to the CLIP-50 presence at the minus ends of the manchette microtubules (Figure 2.15 A') (Tarsounas et al., 2001). Sometimes degenerated microtubule arrays could be observed emanating from a strong anti-CLIP1 antibody signal (Figure 2.15 B'). These results clearly demonstrated that the perinuclear ring was indeed severely affected by the deletion of SUN4. Absence or apparent fragmentation of the perinuclear ring, marked by either no or a patchy anti-CLIP1 antibody signal in differentiating mutant spermatids, respectively, suggested that no correct manchette as a nucleus surrounding structure could be assembled anymore.

Interestingly, in the current study the SUN5 signal seemed to closely resemble the one of CLIP-50 in elongated wild type spermatids, as it also revealed a circular structure at the anterior edge of the SUN4 signal, which in general is closely associated to that of the manchette microtubules (Figure 2.7 E). Therefore an immunofluorescence analysis co-staining with anti-SUN5 and anti-CLIP1 antibodies was performed to investigate if the SUN5 localization was altered as well. In wild type testis tissue sections both signals could indeed be seen co-localizing in the posterior side of early spermatids, although the SUN5 signal seemed to vanish during spermiogenic progression, while the anti-CLIP1 antibody signal was still clearly visible (Figure 2.15 C). In elongated spermatids this analysis also revealed remarkably accurately fitting signals, whereby the SUN5 signal always appeared to be adjacent to the anterior side of the anti-CLIP1 antibody signal (Figure 2.15 D). Interestingly, while usually no anti-CLIP1 antibody signal could be detected in the early spermatids of SUN4 deficient mice, the SUN5 signal was still visible at the posterior side (Figure 2.15 C'). In late

Sun4^{-/-} spermatids, in contrast, the localization of SUN5 was just as severely influenced as that of CLIP-50. In SUN4 deficient testis sections neither anti-CLIP1 nor anti-SUN5 antibody signals could easily be detected. Nonetheless, in the rare cases where anti-CLIP1 and anti-SUN5 antibody signals could be seen in late mutant spermatids, they appeared severely mislocalized. Their signals remained closely associated however (Figure 2.15 D'). This clearly indicated that SUN4 was not only necessary for the correct localization and assembly of the perinuclear ring but also for the localization of SUN5, at least in late spermatid stages. In these stages, it was always closely associated to the perinuclear ring or its remaining fragments. These results also suggest that SUN5 interacts with the perinuclear ring in elongating spermatids.

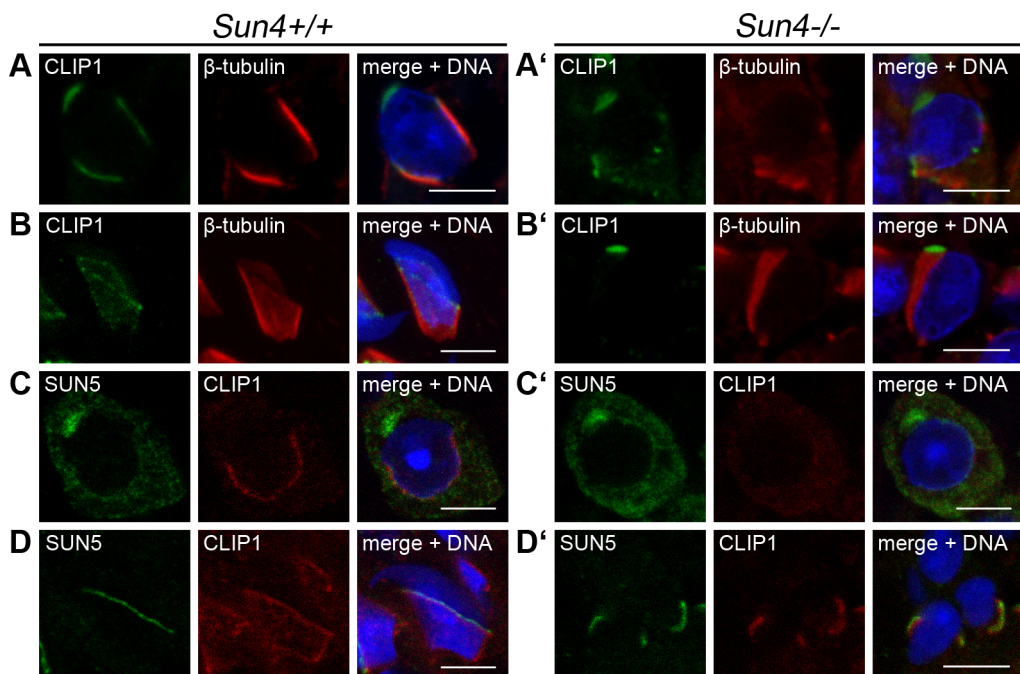


Figure 2.15: The manchette formation is severely influenced in the *Sun4^{-/-}* mice.

Immunofluorescence analysis on paraffin- and tissue tek-embedded testis tissue sections of wild type (A-D) and SUN4 deficient (A'-D') littermates. Tissue sections were co-labeled with either CLIP1 and β-tubulin (A, A', B, B') or SUN5 and CLIP1 (C, C', D, D'). Compared to the wild type, where the manchette surrounds the posterior side of the NE, where CLIP1 and SUN5 signals can be found associated to this area as well, the staining of the SUN4 deficient tissue sections revealed mislocalized CLIP1 and SUN5 signals and a completely degenerated manchette. Overlays are shown on the right side with the DNA stained in blue. Scale bars: 5 μm.

More than two decades ago, Russell and colleagues (1991) were able to show that the manchette microtubules are linked to the nucleus by small filaments. Since LINC complexes in general function in linking the nuclear interior to cytoskeletal elements it seemed plausible that posterior LINC complexes could represent these filaments and anchor the manchette microtubules to the posterior NE (Göb et al., 2010; Kracklauer et al., 2013). Therefore it was of importance to analyze if these filaments are actually comprised of SUN4-containing or SUN4 dependent LINC complexes. To investigate this question ultrastructural analysis was performed on *Sun4^{-/-}* spermatids according to the protocol of Russell et al. (1991). In the wild type preparations numerous filaments connecting the nuclear surface with the closely associated manchette microtubules were seen (Figure 2.16 A, A'). This result was consistent with the finding of the rod-like elements interconnecting the NE with the manchette described in the study by Russell et al. in 1991. In the absence of SUN4 these thin filaments cannot be seen in the posterior NE, indicating that SUN4 is required for the presence of these linkers (Figure 2.16 B, B', C, C'). The manchette, which in the mutant spermatids was completely disorganized, could only be found as loosely assembled microtubules that were dissociated from the NE (Figure 2.16 B, B'). In most cases, no microtubule structures could be detected in proximity to the posterior nucleus in the *Sun4^{-/-}* spermatids at all (Figure 2.16 C, C'). This demonstrates that SUN4 is not only needed for the basic organization of the manchette, but that it is also important for the anchorage and association of the manchette microtubules to the NE. In fact this actually suggests that SUN4 is a constituent of the filaments that link the manchette microtubules to the posterior NE.

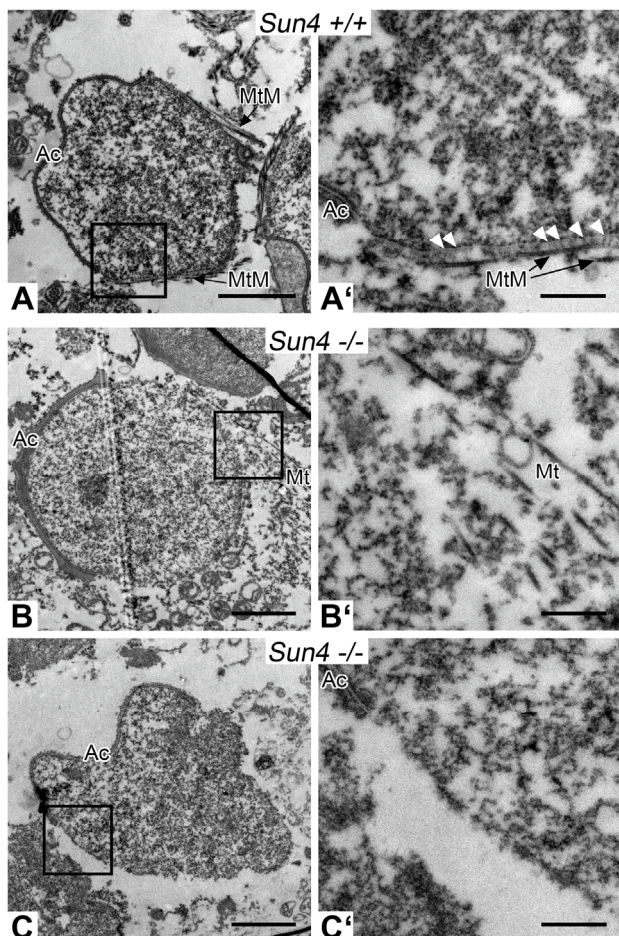


Figure 2.16: The linkers between the nuclear interior and the microtubule manchette are missing in *Sun4^{-/-}* spermatids.

Electron microscopy analysis of the posterior nucleocytoplasmic junction in *Sun4^{+/+}* (A, A') and *Sun4^{-/-}* (B, B', C, C') spermatids. (A, A') In the wild type spermatids the nucleocytoplasmic junction contained rod-like elements (arrow heads) that connected the NE with the closely associated microtubule-containing manchette (MtM). In the absence of SUN4 these filaments were missing and the microtubules (Mt) were rather loosely assembled and disorganized (B, B'), or usually could not be found in proximity to the nucleus at all (C, C'). Ac, Acrosome. Scale bars: 2 μm (A-C) and 500 nm (A'-C'). Figure from Pasch et al. (2015).

2.3 Investigation of SUN4 binding partners

The immunolocalization experiments of SUN4 demonstrated robust co-localization between itself, SUN3 and Nesprin1. SUN3 and Nesprin1 could furthermore not be localized within the posterior NE in the absence of SUN4. These results clearly indicated a potential cooperative function between these three proteins during spermiogenesis. To gain further insight into this idea, the possibility of a direct interaction of SUN4 with SUN3 and/or Nesprin1 was tested.

2.3.1 SUN4 has the potential to interact with SUN3, Nesprin1 and itself

In accordance to previous approaches of SUN-KASH interaction studies (Stewart-Hutchinson et al., 2008; Göb et al., 2010), co-transfection/co-immunoprecipitation experiments were conducted using different combinations of EGFP- or Myc-tagged SUN4 with Myc-tagged SUN3 or EGFP-tagged Nesprin1 fusion constructs (Figure 2.17 A, B, C). These constructs were previously generated as described by Göb et al. (2010) and Pasch et al. (2015).

Selected Myc and EGFP fusion constructs were co-expressed in COS-7 cells and harvested after 24 hours incubation time. To verify successful co-transfection, a coverslip with the transfected cells was stained with respective antibodies against the used constructs. Microscopy images revealed that the different combinations of SUN4, SUN3 and Nesprin1 fusion constructs were expressed within the cells. The detected signals generally showed a complete overlap with localization at the NE, just as expected for SUN- and KASH-domain proteins (Figure 2.17 A', B', C'). Additionally the fluorescent signals also revealed co-localization within the cytoplasm of the transfected cells, probably due to overexpression of the constructs.

After transfection the cells were lysed and the protein complexes were immunoprecipitated using either anti-Myc or anti-EGFP antibodies. To test whether the potential interaction partner could be co-immunoprecipitated, the purified protein complexes were analyzed by SDS-PAGE and western blot. If the co-transfected putative protein partner was indeed present in the purified complex it should be able to be detected using either anti-EGFP or anti-Myc antibodies, respectively.

In a first experimental series, the potential interaction of SUN4 and SUN3 was tested. After co-transfecting Myc-tagged SUN3 and EGFP-tagged SUN4 fusion constructs, anti-Myc antibodies were used to immunoprecipitate the expressed Myc-

SUN3 fusion proteins. The subsequent western blot analysis using anti-EGFP antibodies revealed that EGFP-tagged SUN4 was indeed co-immunoprecipitated with the Myc-SUN3 protein (Figure 2.17 A’). To verify this result a reciprocal pulldown was also carried out: co-immunoprecipitating Myc-tagged SUN3 with EGFP-tagged SUN4, using anti-EGFP instead of anti-Myc antibodies for the pulldown. Consistent with the first result, this experiment revealed that Myc-tagged SUN3 could be co-immunoprecipitated when EGFP-tagged SUN4 was used as bait (data not shown). These experiments suggest that both proteins are indeed capable of interacting with each other.

To test whether the SUN-domain of SUN4 is able to interact with the KASH-domain of Nesprin1, Myc-tagged SUN4 and EGFP-tagged Nesprin1 were used in a similar approach. This time the Myc-tagged SUN4 fusion protein was used as bait by pulling down the protein complex with anti-Myc antibodies. The EGFP-tagged Nesprin1 was co-immunoprecipitated (Figure 2.17 B’). This demonstrates that SUN4 is not only able to bind to SUN3 but also to Nesprin1, which so far has only been described as a LINC complex partner of SUN3 in the posterior NE of the developing spermatid.

It was recently shown that somatic SUN proteins can form homotrimeric assemblies, which interact with three appropriate KASH-domain proteins (Sosa et al., 2012). Therefore, it was reasonable that SUN4 might interact with itself to form such homo- or, together with SUN3, even heterotrimeric SUN-domain protein assemblies. To test the potential of SUN4 to bind to itself, Myc- and EGFP-tagged SUN4 were co-expressed and a pulldown using anti-Myc antibodies was performed under the same experimental conditions as described above. As shown in Figure 2.17 C’ it was possible to co-immunoprecipitate both SUN4 fusion proteins, demonstrating that SUN4 indeed has the capability to interact not only with SUN3 but also with itself to form homo- or heterooligomeric assemblies. Taken together, the co-immunoprecipitation experiments revealed that ectopically expressed SUN4 has the intrinsic potential to interact with SUN3, Nesprin1 and furthermore also with itself.

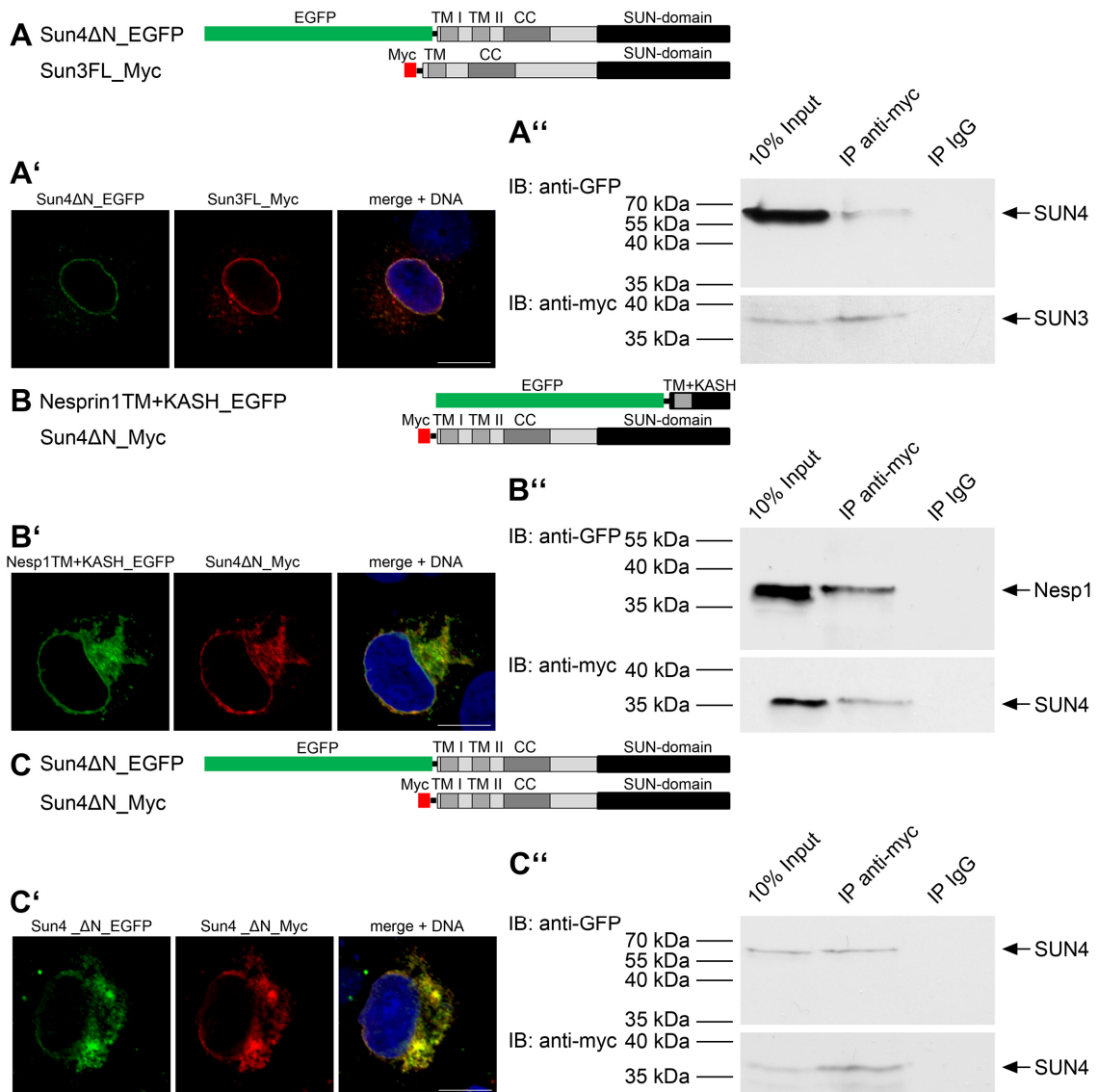


Figure 2.17: SUN4 is capable of interacting with SUN3, Nesprin1 and itself.

(A, B, C) Myc- and EGFP-tagged fusion constructs of either (A) Myc-SUN3 and EGFP-SUN4, or (B) Myc-SUN4 and EGFP-Nesprin1, or (C) Myc-SUN4 and EGFP-SUN4 were co-transfected in COS-7 cells and used for co-immunoprecipitation experiments. (A', B', C') Corresponding immunofluorescence images of the co-transfected COS-7 cells that were used as transfection control. The overlay of the respectively expressed fusion proteins is shown on the right, together with the DNA stained in blue. Scale bars: 10 μ m. (A'', B'', C'') After cell lysis in RIPA buffer (input control; left lane: 10% Input) the protein complexes were immunoprecipitated with anti-Myc antibodies. Using SDS-PAGE and western blot procedures the co-immunoprecipitated fusion proteins could be detected with either anti-Myc or anti-EGFP antibodies (middle lane: IP anti-myc). Unspecific rabbit IgG antibodies were used as control (right lane: IP IgG). Figure adapted from Pasch et al. (2015).

2.3.2 *In vivo* binding potential of SUN4

To investigate whether SUN4 forms heteromeric assemblies with SUN3 or homomeric assemblies with itself *in vivo* to interact in a potential LINC complex with Nesprin1, the localization pattern of SUN3 and SUN4 was analyzed in more detail. For this, cells from testis suspensions were double-stained with anti-SUN3 and anti-SUN4 antibodies and the immunofluorescence signals of the respective proteins analyzed with structured illumination microscopy (SIM). SIM has a greater resolution than confocal laser scanning microscope (CLSM), with which the general localization of SUN4 was analyzed. Scanning the posterior NE surface of different stages of developing spermatids to analyze the spatial distribution of SUN3 and SUN4, the fluorescent signals of these proteins showed mostly divergent patterns. Nonetheless, occasional co-localization of SUN3 and SUN4 could be observed as well (Figure 2.18), indicating that they may also form heteromeric assemblies or intermediates in addition to homomeric assemblies.

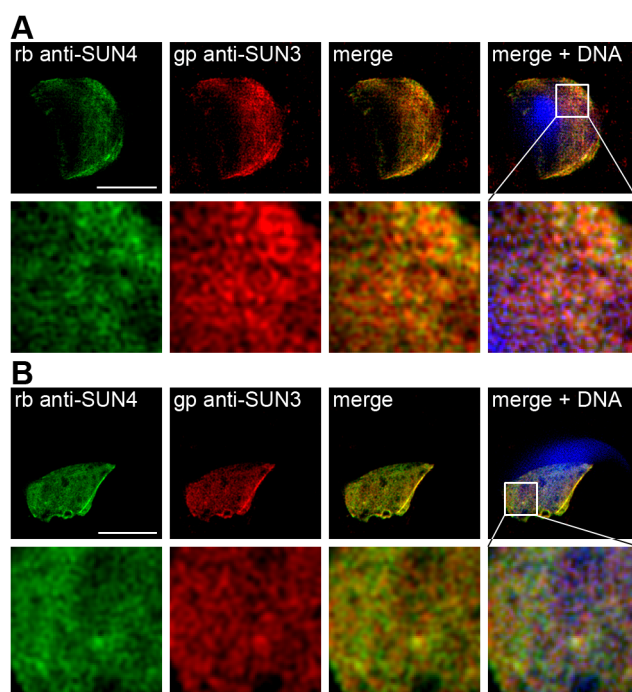


Figure 2.18: Structured illumination microscopy analysis of SUN4 and SUN3 localization patterns.

Co-immunofluorescence analysis of SUN4 and SUN3 co-stained testis cell suspension using structured illumination microscopy (SIM). The posterior NE of round (A) as well as of elongated (B) spermatids showed SUN4 (green) and SUN3 (red) signals mainly distinct from each other, but partly also co-localizing, as indicated by the yellow color in the merge. DNA is shown in blue. Scale bars: 5 µm. Figure from Pasch et al. (2015).

So far the current study revealed that SUN4 has the potential to bind to SUN3, Nesprin1 and additionally itself *in vitro*. According to the distribution patterns of SUN3 and SUN4 it seemed plausible that these proteins may form both homomeric and heteromeric assemblies or intermediates *in vivo*. To see whether SUN4 actually undergoes such interactions under natural conditions, co-immunoprecipitation experiments were conducted on testicular cell suspensions to precipitate endogenous SUN4 together with its interaction partners. For this approach fresh testicular cell suspensions were lysed and the pulldown of the proteins was performed using anti-SUN3, anti-SUN4 or anti-Nesprin1 antibodies. In all three different test series the directly pulled and purified protein could always be detected after SDS-PAGE and western blot procedures were conducted. However, none of the potential interaction partners of either of the other two potential LINC complex components could be visualized using this approach (data not shown). Variations of the protocol, e.g. extension of lysis or incubation times or increasing the amount of the probed material, could also not achieve any other results.

Nonetheless the potential of SUN4 to be able to interact with SUN3 as well as with Nesprin1 still remains due to the *in vitro* results and the localization patterns of these proteins.

3 Discussion

The generation of fertilization-competent spermatozoa is an important requirement for mammalian reproduction. During spermatogenesis, which comprises the developmental processes for production of the motile sperm, approximately 20% of the expressed genes in the mouse genome are expressed in male germ cells (Schultz et al., 2003). The tremendous amount of genes that is seemingly involved in male germ cell development gives a good impression of the high complexity and importance of these processes - germ cells must not only reduce their chromosomal content during meiosis, but also differentiate into motile spermatozoa with species-specific formed heads during spermiogenesis. Failures in nuclear sperm head formation are a frequent cause of male infertility, often resulting in nonfunctional sperm with structural abnormalities (Yan, 2009). Accordingly, there is a vast variety of candidate genes critical for fertility and many of these are not yet well characterized. This also includes many of the germ cell-specific ones that in total comprise approximately 4% of the mouse genome, of which most are presumably expressed during spermiogenesis (Schultz et al., 2003).

Despite the importance of sperm head formation for fertility only a general model has been suggested for how the sperm nuclei are shaped to achieve their species-specific elongated form. In this model the anterior positioned acrosome and the posterior positioned manchette are suggested to generate clutching forces to constrict the nucleus at opposing sides (Kierszenbaum et al., 2003; Kierszenbaum and Tres, 2004; Kierszenbaum et al., 2011). However, this model only includes the potential force generating structures on the nuclear exterior, but is missing any links or mechanisms for force transduction from the cytoskeletal elements to the nuclear interior. To date, several components of the NE have been detected that show a unique distribution and reorganization during sperm head formation (Alsheimer et al., 1998; Mylonis et al., 2004; Schütz et al., 2005a; Göb et al., 2010). Of major interest are the LINC complexes due to their core function of bridging the NE and thereby connecting nucleoplasmic structures to the cytoskeleton (Russell et al., 1991; Kierszenbaum and Tres, 2004; Göb et al., 2010; Kracklauer et al., 2010; Kierszenbaum et al., 2011; Kracklauer et al., 2013). Consistently, several spermiogenesis-specific LINC complexes or LINC complex components have been identified to localize at the anterior and/or posterior side of the elongating spermatid nucleus, and thus could be good candidates for the force transmission required to elongate and shape the nuclei.

In particular, the SUN1 η /Nesprin3 and the SUN3/Nesprin1 complexes have been found at the anterior pole and at the posterior side of late spermatids, respectively, and have therefore already been suggested to mediate opposing forces (Göb et al., 2010; Kracklauer et al., 2013). Furthermore, the potential LINC complex component SUN4 can be detected at the posterior nucleocytoplasmic junction (Shao et al., 1999), and might therefore also play a role in these processes.

At the beginning of the project the actual function of these LINC complex components during spermiogenesis remained unknown. To gain insight into the role of the LINC complex components during nuclear differentiation this study focused on SUN4. Here its specific properties, behavior and function were analyzed in more detail. Not only its exact localization and potential binding partners could be found, but in addition its role in sperm head formation and fertility was investigated. This represents a further step in the understanding of the nuclear remodeling during spermiogenesis and its importance for mammalian fertility.

3.1 SUN4 is critical for sperm head formation and male mice fertility

Correct elongation and shaping of the sperm head is a general requirement for the mammals to produce motile and fertilization-competent spermatozoa. Therefore the missing elongation step, which is paralleled by severe deformations of the nuclei, is not only the most prominent consequence of the SUN4 deficiency but evidently also the primary cause of male infertility in the *Sun4* knockout mice. While early round spermatids in the SUN4 deficient male mice appeared normal, demonstrating that early spermiogenesis was not affected, the nuclei of later stages were gravely misshaped with severe deformations and lobulations of the NE (Figure 2.12). The spermated spermatozoa that can be found in the epididymis consequently also exhibited profoundly misshaped heads and usually showed a tendency to become encircled by their tail, leading to immobility (Figure 2.13). Taken together this clearly demonstrates that SUN4 is essential for sperm head formation and male mice fertility.

Consistent with a role in shaping, Olins and colleagues (2009) have suggested the hypothesis that the lack of LINC complex components in granulocytic forms is an adaptation of the cells to facilitate cellular deformation. In this model, the lack of LINC complexes would result in a lack of connections between the nucleus and the surrounding cytoskeleton. Together with the low levels of certain lamins this could enhance NE flexibility and the malleability of the nuclear shape to generate a highly deformable granulocyte, which would then be able to migrate through tight tissue spaces (Olins et al., 2009). In *Arabidopsis thaliana* AtSUNs and AtWIPs (*Arabidopsis thaliana*-specific SUN and KASH proteins, respectively) have recently been found necessary, as LINC complex components, for maintaining the elongated nuclear shape of epidermal cells (Oda and Fukuda, 2011; Zhou et al., 2012a). The results published by Oda and Fukuda (2011) show that compared to wild type plants, where the mature root hairs contain a highly elongated nucleus, the nuclei of double knockdown plants for AtSUN1 and AtSUN2 are nearly round. Since the single knockdowns of neither AtSUN1 nor AtSUN2 revealed a change in the phenotype, the results indicate furthermore that the SUN proteins function in maintaining the nuclear shape within the root hairs is redundant (Oda and Fukuda, 2011). In a more recent study by Zhou et al. (2012a), the interaction partners of the plant SUN proteins were identified: AtWIP1, AtWIP2, and AtWIP3. In this study the authors were not only able to show that AtWIPs are required to maintain the elongated nuclear shape as AtSUNs, but also revealed that this is the case for at least three different types of epidermal cells. Finding AtWIPs as the first identified KASH proteins in plants, Zhou and colleagues (2012a) suggested

that the SUN-KASH interactions are conserved beyond the opisthokonts, but have diverged in their function. Taking the severely deformed sperm cell nuclei under SUN4 deficiency into account, the results presented here suggest that the LINC complexes have rather specialized in their function, but not necessarily diverged, because the SUN protein SUN4 evidently also plays a role in nuclear shaping in mammals. The findings of this study do not simply indicate a role of SUN4 in maintaining the spermatid nuclear shape - they actually demonstrate that LINC complex components are crucial for directed nuclear shaping in mammals. SUN4 and/or SUN4 dependent LINC complexes are especially required in the posterior NE to shape the spermatid nucleus, most likely by anchoring the manchette to the NE and thereby mediating force transmission.

Interestingly, about 25 years ago Russel et al. (1991) reported on linkers between the NE and the microtubules of the spermatid-specific manchette. In particular, they described rod-like elements connecting the innermost manchette microtubules to the outer leaflet of the NE. Furthermore, these elements pass through the PNS to the nuclear interior. The filaments were proposed to serve as a basis for the transmission of forces, enabling the directed deformation of the round nucleus to elongate the sperm head during spermiogenesis (Russell et al., 1991). The ultrastructural analysis presented in this study revealed that, while such filaments can easily be found connecting the NE and the manchette microtubules in the wild type, they are missing in SUN4 deficient spermatids (Figure 2.16). Therefore, the data presented here support the idea that these rod-like filaments may be formed by SUN4 dependent LINC complexes. These could also include SUN3 and Nesprin1, as these LINC complex components were missing in the posterior NE in the absence of SUN4. The disruption of the connection between the manchette microtubules and the NE in the *Sun4^{-/-}* spermatids leads to a severely disorganized manchette. While in the wild type a microtubule mantle around the posterior spermatid nucleus can be seen, in the *Sun4* knockout spermatids only abnormal microtubule arrays can be found, which appears to correlate with the deformed nuclei.

The exact connection between the posterior LINC complexes and the manchette microtubules has not been investigated so far. Generally it seems rather unlikely that Nesprin1 would bind to the microtubules directly, but this connection could be realized via the binding to a microtubule motor protein (Russell et al., 1991; Göb et al., 2010; Kracklauer et al., 2013; Cartwright and Karakesisoglu, 2014). A number of previous studies reported on a high abundance of motor (and associated non-motor) proteins in particular in the spermatid-specific microtubule systems (reviewed in

Kierszenbaum et al., 2011). Motor proteins are known to be crucial for vesicle transport and might therefore play a role in sperm head shaping and male fertility (Wang et al., 2010; Kierszenbaum et al., 2011). For instance, KIFC1 and related motor proteins have been found tightly associated with the NE and the manchette or manchette-like microtubules in the rat and *Octopus*, respectively (Yang and Sperry, 2003; Yang et al., 2006; Wang et al., 2010). In the rat, the manchette-binding motor protein KIFC1 has been shown to associate with nucleoporin-containing complexes at the nuclear membrane, and proposed to mediate cargo transport along the nuclear membrane (Yang et al., 2006). In *Octopus tankahkeei* the KIFC1-like motor protein has not only been implicated in assisting nucleocytoplasmic cargo trafficking, but additionally seems to play an active role in nuclear head shaping by linking the manchette-like perinuclear microtubules to the nucleus (Wang et al., 2010). Interestingly, in mammals Nesprin1 has been found functioning together with Kif3B, a subunit of the kinesin-2 motor protein (Fan and Beck, 2004). Apparently a Kif3B-like kinesin in other species is highly expressed during spermiogenesis, where it is suggested to contribute to structural changes, most likely by transferring forces to the NE (Dang et al., 2012). Therefore it seems reasonable that the posterior LINC complexes may connect to kinesin motor proteins, which interact with the manchette microtubules in mammals.

SUN4 deficiency ultimately culminates in the production of malformed spermatozoa with severely deformed sperm heads. These *Sun4*^{-/-} spermatozoa are still delivered to the epididymis, where due to their abnormal roundish heads and the detachment of the acrosome they display a globozoospermia-like phenotype (Figure 2.13) (Dam et al., 2007; Dam et al., 2011). Consistent with other spermiogenesis-specific knockout mouse lines, which demonstrate a globozoospermia(-like) phenotype as well (for reviews see: Yan, 2009; de Boer et al., 2014), the *Sun4* knockout male mice are infertile due to their non-functional spermatozoa.

Interestingly, while SUN4 is a component of the posterior NE, the affected genes in most of the other globozoospermia(-like) mouse models encode cytoplasmic proteins, which are usually involved in acrosome attachment and/or formation (Yan, 2009; Kierszenbaum et al., 2011). Although these proteins function in a very different manner, the inactivation of their genes leads to remarkably similar phenotypes. In general it appears plausible that such a phenotype is the result of a generally perturbed sperm head formation. This could be explained by the model of sperm head shaping developed by Kierszenbaum and Tres (2004), in which the anterior acrosome-acroplaxome complex with its marginal ring and the posterior manchette with its perinuclear ring take important roles as opposing constrictors in a sleeve-like manner

to elongate the spermatid nucleus. In accordance with this model it was shown that the interconnection of these structures to the NE as a basis to transfer the cytoplasmic forces onto the nucleus is of utmost importance. In this context, it seems conceivable that the absence of SUN4 as a crucial posterior NE component, evidently involved in anchoring the manchette to the nucleus, evokes a similar sperm head phenotype as the functional inactivation of proteins that are essential for the correct acrosome formation and or attachment. This would imply that for the correct shaping of the sperm head the anterior acrosome/acroplaxome and the posterior manchette are required in roughly equal proportions to contribute opposing forces, and that correct sperm head formation can only be accomplished if the whole acrosome-acroplaxome-manchette complex is functional. It should however be noted that for the correct sperm head shaping the close association of the spermatid nucleus to the Sertoli cell is also of utmost importance. According to the spermatid head shaping model by Kierszenbaum and Tres (2004) the Sertoli cell also contributes to the head shaping by providing exogenous contractile forces in form of F-actin-containing hoops that contact the anterior part of the spermatid nucleus.

Nonetheless, the absence of SUN4 seriously interferes with the general NE integrity. In SUN4 deficient spermatids the cell nuclei not only fail to elongate, they actually show substantial nuclear deformations and often also nuclear membrane protrusions (Figure 2.12). These malformations might argue for a general destabilized membrane system, but they could also be a catastrophic result of the disturbed nucleocytoplasmic force transmission from the manchette over the NE to the nuclear interior. Interestingly, only recently Cain and colleagues (2014) were able to show that LINC complexes are required to maintain the NE spacing in cells that are exposed to increased mechanical stress. This clearly demonstrates that LINC complexes are essential to bear forces in order to keep the NE intact, at least in *C. elegans*. Together these findings suggest that LINC complexes not only bridge the NE, they also stabilize it and might function in NE integrity to either maintain or determine the nuclear shape by bearing and/or transmitting mechanical forces (Zhou et al., 2012a; Cain et al., 2014, this study).

3.2 *Sun4^{-/-}* spermatozoa become encircled by their tail

Another prominent change that can be observed in the spermatozoa of SUN4 deficient mice is a so-called tail coiling. Ultrastructural analysis revealed that during the epididymal maturation not only the acrosomes become detached, but the tails

somewhat appear to encircle the sperm heads (Figure 2.13). Similar phenotypes were previously also described for other mouse lines carrying mutations in testis expressed genes, e.g. *Azh*^{-/-}, *Gopc*^{-/-} and *Hrb*^{-/-} mice (Mochida et al., 1999; Suzuki-Toyota et al., 2004; Juneja and van Deursen, 2005; Suzuki-Toyota et al., 2007). Similar to the *Gopc*^{-/-} mice, where this process has been analyzed in more detail, the coiling of the tail in the *Sun4*^{-/-} spermatozoa also starts during epididymal passage. Thereby the general timing of the process seems to be analogous (Suzuki-Toyota et al., 2007): normal tails are maintained until spermatozoa reach the proximal caput region of the epididymis, whereas most spermatozoa in the cauda region show coiled tails. But unlike the *Gopc*^{-/-} globozoospermia mouse model, where tail coiling appears together with a gathering of the mitochondria at the proximal part of the mid piece in a stratified sheath, the tails of the *Sun4*^{-/-} spermatozoa seem to maintain a single layered mitochondrial sheath during epididymal passage. Taking this into account, it appears implausible that tail coiling is a direct effect of (or for a weak adhesion between) the mitochondria and the ODFs as suggested by Suzuki-Toyota and colleagues (Suzuki-Toyota et al., 2007). It also does not favor an interaction of SUN4 with ODF1 within the flagellum, which was postulated by Shao et al. (1999), since the organization of the axonemal microtubules, the ODFs and consequently the mitochondria are overtly intact in the *Sun4*^{-/-} spermatozoa. Just recently de Boer and colleagues (2014) reported that mutations that are functionally related to sperm head formation in general show affected sperm motility. They found that a functioning tail, and with this regular sperm motility, is dependent on proper sperm head development. This suggests some kind of feedback mechanism as an evolutionary benefit to protect multi-generation fitness (de Boer et al., 2014). This could explain the general occurrence and close temporal correlation of tail coiling in different mutant mouse lines that show impaired sperm head development.

3.3 SUN4 is a posterior LINC complex component

The results of this study clearly demonstrate that SUN4 is a spermiogenesis-specific protein, which localizes exclusively to the posterior NE of round and elongating spermatids. In addition to the obvious co-localization of SUN4 with SUN3 and Nesprin1, it could also be shown that these proteins have the potential to interact with one another when expressed ectopically. Accordingly the investigation of the *Sun4*^{-/-} spermatids revealed that the absence of SUN4 leads to a reorganization of its potential interaction partners, which reveals their absence from the posterior NE as well.

The expression analyses of *Sun4* that were conducted on the mRNA and protein levels independently revealed that SUN4 is a testis-specific protein, which is solely expressed in haploid sperm cell stages correlating with nuclear elongation and sperm differentiation. This finding is consistent with the results of the previous study by Shao et al. (1999), who detected a spermatid-specific expression pattern of SUN4 as well. In contrast to the expression profile, the localization pattern described by the previous study was not as consistent with the results demonstrated here. Shao et al. (1999) described SUN4 in the posterior region of the elongating nucleus during spermiogenesis; more precisely, they found it to be located at the spermatid-specific manchette in the posterior nucleocytoplasmic junction. Though the results presented in this study also suggest SUN4 to be part of the nucleocytoplasmic junction, it was clearly detected within the posterior NE and not within the manchette. The localization of SUN4 within the posterior NE of differentiating spermatids is consistent with the localization of Spag4, the presumed *Drosophila* ortholog of the mammalian SUN4, which has been described in this region as well (Kracklauer et al., 2010). Within the posterior NE SUN4 was found closely associated with the manchette, as it always aligned to the nuclear side of the regions decorated by the microtubules (Figure 2.6 C). This localization pattern not only resembled that of SUN3 and its binding partner Nesprin1, which were previously investigated (Göb et al., 2010); SUN4 also co-localized with these LINC complex components (Figure 2.17), further confirming its presence within the posterior NE of round and elongating spermatids. In fact, recent EM analysis confirmed the presence of SUN4 within the posterior NE of differentiating spermatids and furthermore indicated SUN4 to be integrated within the INM of the NE (Grünwald, L.: Master Thesis).

Shao et al. (1999) furthermore described SUN4 as a component of the ODF of the axoneme. This localization could also not be confirmed in this study. Although three different antibodies, raised against two different SUN4 epitopes and in two different host species, were used for the localization analyses, SUN4 could never be detected within the flagellum (Figure 2.5). Interestingly, SUN4 was also described to be interacting with ODF1, a main component of the ODF within the sperm flagellum (Petersen et al., 1999; Shao et al., 1999). Although SUN4 is not detectable by immunofluorescence analysis to be present in the sperm tail, such an interaction might still be present, even though this would then need to be confined to the posterior NE region where SUN4 is localized.

The remarkable congruency between SUN4 and the proposed SUN3/Nesprin1 LINC complex points to a cooperative function among each other, and even further with

the manchette in the posterior nucleocytoplasmic intersection due to its close association. In line with this, *Sun4^{-/-}* spermatids not only show a disorganized manchette, they also reveal a relocalization of SUN3 and the absence of Nesprin1 from the posterior NE. This indicates that SUN4 is crucial for the correct localization of SUN3 and Nesprin1. After ectopic expression of SUN4 and SUN3 or SUN4 and Nesprin1 fusion constructs the interaction potential of these potential LINC complex components was affirmed in this study. However, such binding potential could not be confirmed in co-immunoprecipitation experiments using extracts from testicular cell suspensions. Assuming that SUN4, SUN3 and Nesprin1 cooperate in the NE-manchette-intersection, they would be integrated in a very strong and highly complex multiprotein network capable of transferring forces. The big technical challenge here was to be able to solubilize the target proteins with a buffer strong enough to break the nucleocytoskeletal multiprotein network system down, but at the same time leaving the protein-protein interactions intact, which is a clearly contradictory goal. Therefore it is not surprising that this experiment, despite using different protocols for the co-immunoprecipitation approach, has not worked.

High resolution SIM analysis further supported the proposed SUN3/SUN4 interactions by revealing frequent co-localization of these proteins within the posterior NE of early and late spermatid stages (Figure 2.18). Although SUN3 and SUN4 preferentially seem to form homotrimers to interact with appropriate KASH-domain partners, as evident from the mostly distinct localization patterns of SUN3 and SUN4, this indicates that it is likely that they also form heterotrimeric assemblies. Notably, the absence of SUN4 severely alters the localization of SUN3. In *Sun4^{-/-}* spermatids SUN3 disappears from the posterior NE and relocates to the cytoplasm, where it tends to form aggregates. Therefore a direct or at least indirect interaction with SUN4 seems to be a prerequisite for the correct targeting and localization of SUN3 in the posterior NE. According to bioinformatic predictions, the putative nucleoplasmic domain of SUN3 consists of only seven amino acids (Göb et al., 2010), presumably too few to efficiently anchor the protein within the lamina or to other nucleoplasmic components. This could explain why SUN3 was found to be retained in the ER when ectopically expressed in somatic cells in a previous study (Crisp et al., 2006). In its natural environment, i.e. spermatids, it may therefore be targeted and anchored in the posterior NE by binding to the INM component SUN4 (Göb et al., 2010; this study). The results presented here clearly demonstrate that the localization of SUN3 depends on the presence of SUN4. Besides forming heterotrimeric SUN-domain assemblies as a basis for posterior LINC complexes, SUN3 and SUN4 might also form heteromeric intermediates, which might be replaced by homotypic interactions when SUN3 has reached a certain destination. It

may also be conceivable that SUN3 and SUN4 interact only indirectly with each other due to their interactions with their potential KASH-domain counterpart Nesprin1, to which both are able to bind.

From the literature it is known that the ONM localization of several KASH proteins depends on the presence of their SUN protein interaction partners within the INM (Padmakumar et al., 2005; Crisp et al., 2006; Ketema et al., 2007; Stewart-Hutchinson et al., 2008; Zhou et al., 2012a). This SUN-domain dependent mechanism to retain the KASH proteins within the NE is extremely conserved over different organisms. The interaction of SUN4 and Nesprin1 is supported by the fact that Nesprin1 is missing from the NE in the absence of SUN4, because it is obviously missing its interaction partner in order to be retained within the ONM. Recent crystallization studies of the LINC complex revealed that this complex consists of a SUN trimer which binds to three appropriate KASH protein partners (Sosa et al., 2012). Considering this oligomeric structure and the competence of SUN4 to bind to SUN3 and Nesprin1 as well as to itself, it seems reasonable that SUN4 might form a LINC complex together with SUN3 and Nesprin1. Thereby SUN4 and SUN3 may form hetero- or homotrimers within the INM that bind within the PNS to three Nesprin1 molecules, which span the ONM and interact with the microtubules of the spermatid manchette, likely via microtubule motor proteins (Figure 3.1). The connection between SUN4 and Nesprin1 would therefore enable the formation of a SUN4-containing posterior LINC complex, which enables SUN4 to function directly in nucleocytoskeletal linkage and contribute to a potential role in sperm head formation. The small rod-like elements on the posterior nuclear surface of wild type spermatids discovered by Russell and colleagues (1991) represent exactly such interconnections between the NE and the manchette microtubules. The ultrastructural analysis in this study also revealed that in SUN4 deficient spermatids these numerous linkers could not be found anymore (Figure 2.16). This clearly indicates that the rod-like elements in the wild type may represent the SUN4-containing (or SUN4 dependent) posterior LINC complexes described here that are consequently missing in the *Sun4^{-/-}* spermatids as well. The results presented so far support a model of these LINC complexes as components of the posterior nucleocytoplasmic interconnection capable of transferring forces from the cytoskeleton onto the nucleus (Figure 3.1).

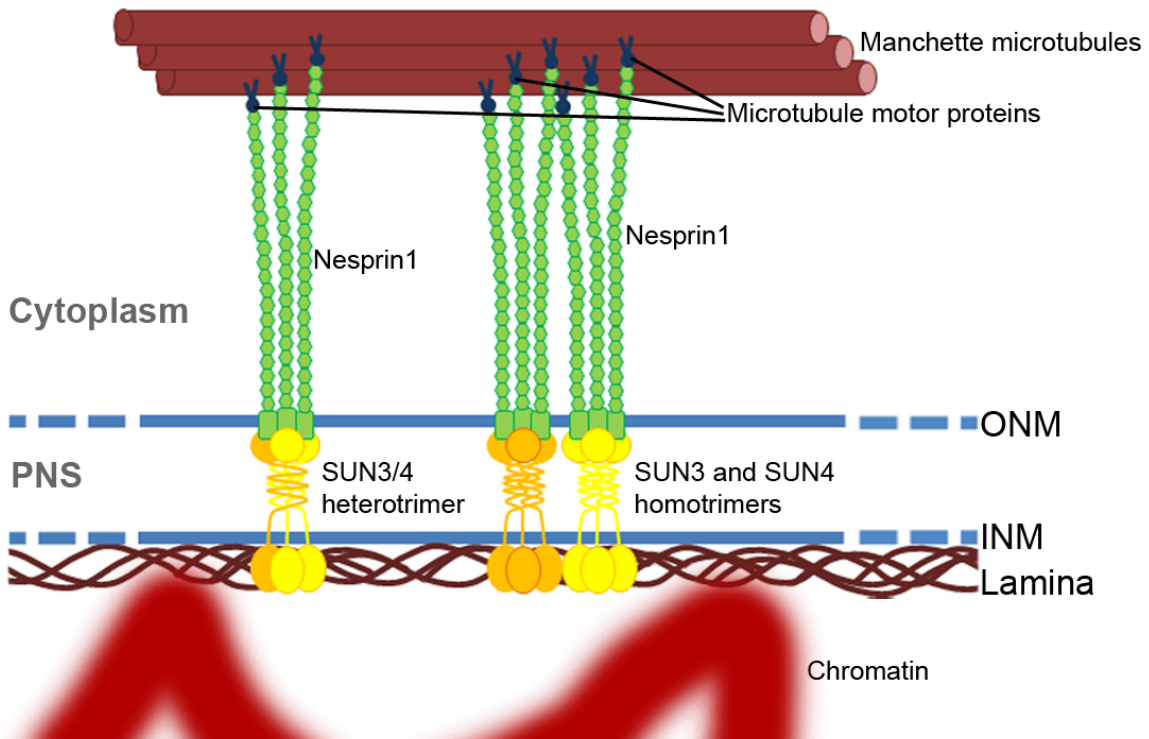


Figure 3.1: Theoretical model of the SUN4 dependent posterior LINC complexes during nuclear remodeling in spermatogenesis.

Schematic drawing representing the posterior nuclear envelope (NE) of an elongating spermatid with its outer nuclear membrane (ONM) and inner nuclear membrane (INM), and the underlying lamina. Embedded in the NE are the spermatid-specific LINC complexes composed of either a SUN3/SUN4 heterotrimer or a SUN3 or SUN4 homotrimer, which are connected in the perinuclear space (PNS) to three Nesprin1. To function as components in the interconnection between the nucleoplasm and the cytoplasm to transfer forces from the cytoskeleton onto the posterior nucleus the Nesprins are connected to the manchette, supposedly via binding to microtubule motor proteins.

3.4 SUN4 deficiency influences the distribution of other NE components

The reorganization and/or absence of the putative interaction partners of SUN4 (SUN3 and Nesprin1) are not the only significant changes in the NE of SUN4 deficient germ cells. The additional results presented in this chapter clearly demonstrate that other components of the posterior NE are reorganized in the absence of SUN4. In particular a change in the distribution pattern of the posterior SUN1/SUN1 η and Nesprin3 complexes can be observed.

Proteins within the NE of differentiating spermatids are not commonly found homogeneously distributed as in somatic cells; rather, they are polarized to certain areas, most likely according to their specific function (Göb et al., 2010; Frohnert et al.,

2011; Yassine et al., 2015; this study). In the current study it could be demonstrated that the dual localization of the SUN1 η /Nesprin3 LINC complexes in SUN4 deficient spermatids in principle remains the same as in the wild type. However, closer immunofluorescence analyses revealed that the posterior SUN1 η and Nesprin3 signals could be found distributed throughout the entire posterior half of the NE instead of relocating towards the posterior pole of the nucleus during differentiation. This changed localization pattern of the posterior SUN1 η /Nesprin3 LINC complexes displayed a more or less homogenous distribution of the LINC components (Figure 2.14 B', D'). These results demonstrate that in the absence of SUN4 the strict territoriality of the posterior SUN1 η /Nesprin3 LINC complexes is impaired, in turn suggesting a role of the SUN4-containing LINC complexes in the maintenance of this territoriality. Therefore it seems plausible that the LINC complexes consisting of SUN3 and/or SUN4 and Nesprin1 are either directly regulating the posterior NE partitioning, or indirectly providing some kind of barrier for the SUN1 η /Nesprin3 LINC complexes.

An alternative explanation for the changed distribution of SUN1 in the posterior region of the *Sun4* $^{/-}$ spermatids is based upon the intimate association of SUN1 with the NPCs that has been described by Liu et al. (2007). According to this study SUN1 is needed for the uniform distribution of NPCs and therefore functionally associated with them. Conversely, it is known from the literature that NPCs redistribute during spermatid nuclear differentiation. Specifically, they alter from a homogenous distribution towards an exclusive localization within the RNE, the excess NE that remains after the nuclear volume reduction (Rattner and Brinkley, 1971; Ho, 2010). As such, the NPCs redistribute towards the posterior part of the nucleus during the formation and enlargement of the acrosome. They are suggested to become excluded from the posterior NE due to the formation of the manchette, which assembles closely associated with the underlying NE as well. In late spermatid stages the NPCs can be found highly concentrated at the posterior pole of the nucleus surrounding the implantation fossa, the site where the RNE will be formed (Ho, 2010). In accordance with the redistribution of the NPCs, the fluorescent signal of SUN1 in the posterior part of the elongating spermatid nucleus also retracts towards the posterior pole in the wild type. Therefore, the missing or disorganized manchette in the *Sun4* $^{/-}$ spermatids would be an explanation for the more or less homogenous distribution of the SUN1 signal that remains in the entire posterior part, as NPCs probably remain in the posterior NE as well (due to the absence of a functioning manchette that would exclude them from this region). This would however not explain why the Nesprin3 distribution is changed in the SUN4 deficient spermatids as well, because SUN1 has been suggested to function independently of Nesprin in its role of maintaining the uniform NPC distribution (Liu et

al., 2007). The SUN1 localized in the posterior part of the spermatid nucleus clearly has a KASH binding partner, as evidenced from the interaction studies and the identical pattern change in the localizations within the posterior NE of *Sun4*^{-/-} spermatids (Göb et al., 2010; this study). Whether SUN1 is associated with NPCs during the spermatid differentiation has not been investigated so far and therefore remains an important task for the future. The NPC distribution in the mutant spermatids also needs to be studied in order to answer the question why the distribution of SUN1 and Nesprin3 is changed under SUN4 deficiency, and if this is dependent on a possibly changed NPC distribution.

3.5 SUN5 reveals a unique localization pattern in developing spermatids

Until recently, SUN5 has been described as a spermatid-specific protein exclusively localizing to the anterior NE of round spermatids facing the acrosome (Frohnert et al., 2011). In this study the potential LINC complex component SUN5 was detected by a newly-generated polyclonal antibody, and showed a co-localization with the Golgi marker GM130 and a NE localization at the posterior side in early spermatid stages (Figure 2.7 A). This unexpected localization pattern has recently been confirmed by a study from Yassine et al. (2015), who were able to show that SUN5 transits the Golgi apparatus for posttranslational modifications and is otherwise evenly distributed at the posterior side of elongating spermatid nuclei. The rather cytoplasmic localization of SUN5 could also be seen, although the SUN5 antibody from our lab showed such a staining exclusively within the very early spermatid stages and not within spermatocytes as noted by Yassine and colleagues as well (2015). Therefore it seems that the expression of SUN5 starts in haploid germ cell stages as suggested by the former study from Frohnert et al. (2011). But in contrast to this study, SUN5 could never be found at the anterior side of the nuclei facing the acrosomic vesicle (Frohnert et al., 2011); this apical region was always free of SUN5-specific staining, consistent with the more recent study (Yassine et al., 2015).

After evaluating the anti-SUN5 antibody and the finding that SUN5 indeed is a component of the posterior NE, its distribution pattern could be analyzed regarding changes in the SUN4 deficient mice. Interestingly, the distribution of SUN5 is only influenced in its localization pattern by the absence of SUN4 during late spermatid stages. In early stages of *Sun4*^{-/-} spermatids SUN5 can still be found in the posterior NE, probably exactly where it would be localized within the wild type spermatid nuclei

as well. As shown in Figure 2.7 B, in the wild type spermatids SUN5 seems to be integrated into the posterior NE slightly before SUN4 and might therefore not be influenced by the absence of SUN4 at this timepoint. However, although early stages of SUN4 deficient spermatids show an apparently normal SUN5 signal, the signal of later spermatid stages was always abnormal. Here in most cases no signal could be found within the NE of the differentiating nucleus at all. In several cases however the cells revealed a patchy SUN5 signal pattern, instead of forming a circular structure around the center of the nucleus as seen in the wild type (Figure 2.15). This indicates that the presence of SUN4 is essential for the correct SUN5 localization to a certain structure (presumably the perinuclear ring; see below 3.6) during nuclear elongation of the spermatids.

3.6 SUN4 is crucial for the correct localization and assembly of the spermatid-specific manchette

Besides the altered distribution of LINC complexes and LINC complex components within the posterior nucleocytoplasmic junction and the obvious malformations of the nucleus, the SUN4 deficient germ cells display impairment of both assembly and organization of the spermatid-specific manchette (Figure 2.12, 2.14, 2.15, 2.16). A typical manchette consists of a perinuclear ring around the center of the developing spermatid nucleus and a microtubule mantle that is radiating from it along the anterior-posterior axis of the nucleus as described in the literature (Fawcett et al., 1971; Rattner and Brinkley, 1972; MacKinnon and Abraham, 1972; Rattner and Olsen, 1973; Dooher and Bennett, 1973; Wolosewick and Bryan, 1977). In *Sun4^{-/-}* spermatids, instead of a highly-organized microtubule mantle surrounding the posterior nucleus, only aberrant microtubule arrays could be found.

Interestingly, these disorganized microtubule bundles are usually completely dissociated from the NE. Whether the dissociation of the microtubules from the NE is the reason why usually no microtubule structures could be found in proximity of the nucleus, or whether it is a general impairment of the manchette tubulin polymerization in the SUN4 deficient spermatids could not be conclusively clarified. A similar manchette phenotype displaying microtubule arrays in various sizes formed at some distance from the NE was also described for *Gopc^{-/-}* spermatids. In these mutant spermatids the microtubules were still attached to the residues of a perinuclear ring, but were running in various directions (Ito et al., 2004). In contrast to *Sun4^{-/-}* spermatids the *Gopc^{-/-}* spermatids display nuclear invaginations, which contain manchette

microtubules, a phenotype that can also be observed in the *Hrb* mutant mice (Ito et al., 2004; Kierszenbaum et al., 2004). Unlike the *Sun4* mutant spermatids, which develop their phenotype due to the absence of a component of the posterior NE, the manchette phenotypes of the *Gopc* and *Hrb* mutant spermatids are primarily caused by the absence of the acrosome due to a vesicle fusion defect. This suggests that SUN4, whether directly or indirectly, is involved in the anchorage of the manchette, presumably by linking the manchette microtubules to the NE within the posterior spermatid nucleus. The acrosome, on the other hand, has also been suggested to be involved in anchoring the manchette to the nucleus (Mochida et al., 1998; Ito et al., 2004; Kierszenbaum et al., 2004). Similar manchette phenotypes can furthermore be found in mutant mice of genes associated with manchette formation, like *Azh* and *Clip-170* knockout mice, which also show a completely perturbed manchette formation (Cole et al., 1988; Meistrich et al., 1990; Akhmanova et al., 2005).

Interestingly, in late spermatids the distribution pattern of the spermiogenesis-specific SUN5 closely mirrors that of CLIP-50, resembling a circular structure around the center of the elongating spermatid nucleus. CLIP-50 has been characterized as a member of the microtubule binding protein family CLIP-170/restin and is abundant in the testis (Pierre et al., 1992; Tarsounas et al., 2001). It was described to localize to the centriolar region and the perinuclear ring, where it appears to directly interact with tubulin and assist in the nucleation of microtubular structures (Tarsounas et al., 2001). In the absence of SUN4, CLIP-50 and SUN5 can still be found in close proximity, but both signals are aberrant in that they form rather small patchy structures instead of a circular ring in late spermatids (Figure 2.15). This localization is not only consistent with the destruction of the perinuclear ring in the SUN4 deficient germ cells, it further suggests an interaction of CLIP-50 and SUN5 in the elongating spermatid. The finding that SUN5 localizes close to the anterior side of the perinuclear ring actually suggests that it might function in anchoring the manchette structure to the NE- and/or acrosome-associated structures (see above). Considering the perinuclear ring as a MTOC, the attachment of it by the LINC complex component SUN5 would also be consistent with the conserved function of LINC complexes in anchoring such organizing centers (Razafsky and Hodzic, 2009; Graumann et al., 2010; Starr and Fridolfsson, 2010; Yamamoto, 2014). Although the origin of the manchette microtubules is still controversial, the finding that manchette microtubule structures are only assembled at sites where the perinuclear ring still remains in fragments supports the hypothesis of the perinuclear ring as the major MTOC of the manchette (O'Donnell and O'Bryan, 2014). The main argument against the perinuclear ring as the organizing center is the fact that it does not contain γ -tubulin, which is known for other cellular MTOCs as the

essential nucleator. This might be compensated by δ -tubulin, which is a component of the perinuclear ring and supposed to play a critical role in organizing microtubules, even though its ability to nucleate tubulin currently lacks direct evidence (Kato et al., 2004; O'Donnell and O'Bryan, 2014).

Together these results clearly support the idea of a functional interaction between different components of the NE and the substructures of the manchette, i.e. the perinuclear ring and the microtubule mantle (Göb et al., 2010; Kierszenbaum et al., 2011; Kracklauer et al., 2013; this study). Consistent with this, the severely impaired manchette closely correlates with the missing elongation of the spermatid nucleus and the profound nuclear deformations that can be observed in the homozygous *Sun4* knockout mice. These findings clearly support the notion that SUN4 dependent LINC complexes are not only essential for the anchorage of the manchette microtubules, but also for the correct assembly of the spermatid-specific manchette as a whole. It therefore seems likely that SUN5 is involved in anchoring the manchette perinuclear ring to the nucleus, and the LINC complexes consisting of SUN3 and/or SUN4 and Nesprin1 attach the manchette microtubules along their axis to the nuclear interior, a connection competent for transferring forces.

3.7 Localization of the basal body is not affected by the absence of SUN4

The centriole/basal body, which initiates the formation of the sperm axoneme, represents another MTOC within the differentiating germ cell (Hermo et al., 2010c). In the *Sun4*^{-/-} spermatids this apparatus seems to be unaffected by the absence of the posterior LINC complex component, as the results of this study show a normal appearing positioning and initiation of the axoneme and flagellum.

Interestingly, a previous study on *Drosophila* sperm differentiation has shown that Spag4, the postulated ortholog of mammalian SUN4, is crucial for the anchorage of the basal body to the NE (Kracklauer et al., 2010). In their study, Kracklauer and colleagues (2010) demonstrated that the basal body is detached from the condensing nuclei and is frequently shifted sideways in the spermatids of the *Spag4* knockout fly. In mammals, however, absence of SUN4 does not seem to interfere with positioning and attachment of the basal body. In *Sun4*^{-/-} spermatids centrioles were always located closely associated with the implantation fossa/posterior pole (Figure 2.14 D').

In contrast to the mammalian NE, in *Drosophila* Spag4 is the only SUN-domain protein expressed during sperm differentiation, and therefore the only possible SUN-domain protein involved in anchoring the basal body to the nucleus. Mammalian spermatids express at least four different SUN-domain proteins, which accordingly distribute the different tasks to be achieved during spermiogenic development among them. In this way the spermiogenesis-specific SUN-domain proteins represented by SUN1 η , SUN3, SUN4 and SUN5 could not only specialize for individual functions, but might also compensate for the loss of a particular family member. Such a redundancy of SUN-domain proteins has been described for SUN1 and SUN2 in somatic and to a certain degree in meiotic cells as well (Ding et al., 2007; Lei et al., 2009; Link et al., 2014). Thus it seems reasonable, given that SUN4 indeed comprises a role in attaching the basal body to the posterior pole of the NE, that one of the other spermiogenesis-specific SUN proteins may compensate for a SUN4 deficiency. A good candidate for such compensation would be SUN1, as it remains at the posterior NE in SUN4 deficient spermatids.

A different possibility for anchoring the basal body to the NE in differentiating spermatids in general is represented by SUN5, which seems to play a role in anchoring the perinuclear ring as a potential MTOC as well. Therefore it is conceivable that this SUN-domain protein may have specialized in the attachment of MTOCs to the NE in mammalian spermatids. Preliminary data indeed demonstrated a punctate SUN5 signal, which was found at the posterior pole in some of the fluorescent images (data not shown). Therefore analysis of whether SUN5 not only functions in attaching the perinuclear ring but also in attaching the basal body to the NE remains an interesting question which needs to be clarified in the future.

The results of this study clearly indicate that the basal body is still correctly positioned and anchored to the posterior pole close to the implantation fossa of the *Sun4* $^{-/-}$ spermatid nucleus. Together with the unaffected localization of the anterior positioned acrosome this suggests that the polarity of the developing sperm is not affected by the absence of SUN4 during the initiation of the flagellum. Although SUN4 deficiency alters the distribution of different NE components and associated structures and interferes with general NE integrity (as nuclei of *Sun4* $^{-/-}$ spermatids are gravely misshaped and reveal membrane protrusions), it seems that SUN4 is not required to establish and maintain the general nuclear polarity in spermatids.

3.8 Future perspectives

Taken together, the results presented here support a role for LINC complexes in nuclear shaping during sperm head formation in mammals. SUN4 localizes to the posterior NE, where it interacts with SUN3 and Nesprin1, likely by forming functional LINC complexes that bridge the nuclear membranes to anchor the spermatid-specific manchette microtubules at the lateral periphery of the nucleus. Surprisingly, SUN4-containing LINC complexes are not only crucial in anchoring the manchette, but also determine and coordinate the localization of other NE components. This also includes SUN5, which according to the hypothesis presented in this study might play a role in the correct assembly and positioning of the manchette perinuclear ring from which the manchette microtubules radiate. In *Sun4^{-/-}* spermatids the missing links between the nuclear interior and the cytoskeletal elements (manchette microtubules), which are presumably represented by the SUN4-containing LINC complexes, not only account for the disorganization of the manchette but also for the grave malformations and NE protrusions of the spermatid nuclei. The diverse failures due to the absence of SUN4 finally culminate in spermatozoa displaying a globozoospermia-like phenotype and infertility of male mice. In accordance with the results presented here Calvi et al. (2015) recently presented a study confirming the essential function of SUN4 in anchoring the spermatid-specific manchette as well as a role in sperm head formation.

The proposed model of the LINC complexes consisting of SUN3 and/or SUN4 and Nesprin1 in the posterior NE linking the nucleus with the spermatid-specific manchette (Figure 3.1) is an outstanding example of directed nuclear shaping. This study not only emphasizes the significance of SUN-domain proteins and LINC complexes during spermiogenesis, it actually demonstrates their requirement within the NE for the correct differentiation and maturation of the male germ cell.

Although SUN4 could be assigned a critical role in sperm head formation, most likely by anchoring the manchette to transmit forces to the nucleus, many questions still remain unanswered. In cell culture systems it could be shown that SUN4 is able to bind to SUN3 and SIM analysis revealed that they also co-localize within the posterior NE. However, whether SUN3 and SUN4 only build intermediates or whether they interact directly to form SUN heterotrimers that further interact with three KASH-domain proteins to form spermatid-specific LINC complexes is not clear. Proximity labeling or crystallization of SUN3 and SUN4 proteins might be of help to elucidate this potential

interaction. Furthermore crystallization would also be able to define the stoichiometry of these proteins within an oligomeric complex.

Given that SUN3 and/or SUN4 and Nesprin1 form a LINC complex in the posterior NE connecting the nucleus with the manchette to transfer the cytoplasmic forces and enable nuclear shaping, the mechanisms for how these LINC complexes are anchored in their surroundings still remain unknown. In comparison to the short nucleoplasmic domain of SUN3, the one of SUN4 is large enough to anchor the protein within the nuclear lamina. Though it could therefore be expected that SUN4 would anchor a heterooligomeric complex of SUN3 and SUN4, if existing, within the lamina, the exact counterpart and mechanism remain elusive. For Nesprin1 on the cytoplasmic side, it seems plausible that it would interact with microtubule-binding motor proteins to connect it to the manchette microtubules in the spermatid, yet this mediator needs to be uncovered as well. To investigate the missing link between the ONM integrated KASH protein and the manchette microtubules biochemical approaches including protein interaction assays should be performed.

Above all, the relevance of LINC complexes for nuclear shaping during sperm differentiation and of SUN4 dependent LINC complex components in particular is clearly evidenced by the resulting infertility of SUN4 deficient male mice. Elucidating the role of LINC complex components in sperm head formation brings us closer to understanding the mechanisms of germ cell development. This is highly important for future medical treatments and might help to address idiopathic infertility in men. Characterizing genes that are essential for the correct differentiation of mammalian sperm is of clear benefit for the diagnostic workup in male infertility, as involved genes can be tested for their correct expression and/or functionality.

4 Materials

4.1 Biological material

4.1.1 Bacteria

StrataClone SoloPack Competent Cells

StrataClone SoloPack Competent Cells from the StrataClone Blunt PCR Cloning Kit (Agilent Technologies, Böblingen) were used for transformation together with the StrataClone PCR Cloning Vector pSC-B-amp/kan (4.2.1). Transformation of bacteria was performed according to manufacturer's instructions.

E. coli XL1 blue

Competent *E.coli* XL1 blue (Agilent Technologies, Böblingen) were transformed with the pET21a(+) vector (4.2.1) and used for amplification of the cloned plasmid DNA.

E. coli Rosetta™(DE3)

Competent *E. coli* Rosetta™ (Novagen, Darmstadt) were used for expression of recombinant proteins. These bacteria contain an additional chloramphenicol-resistant plasmid designed to enhance expression of eukaryotic proteins that contain codons which are rarely used in bacteria. The additional DE3 designation states that this vector contains an IPTG-inducible T7 RNA polymerase suitable for protein expression of T7-driven expression vectors as pET vectors.

4.1.2 Cell lines

COS-7

The COS-7 is an adherent fibroblast-like cell line derived from African green monkey kidney tissue. It was used for transfection (5.2.2) and co-immunoprecipitation experiments (5.6.4).

4.1.3 Animals

The animals used in this study were mice from the *Spag4^{tm1(KOMP)Mbp}* mouse strain, which were bred in the animal facility of the Biocenter at the University of Würzburg. The mouse strain was generated from targeted ES cells obtained from the KOMP Repository (www.komp.org; Spag4 targeting project: 24921, design ID: 234716), a NCRR-NIH-supported mouse strain repository (U42-RR024244). ES cells used for generation were created by the CSD consortium, funded by the trans-NIH Knock-Out Mouse Project (KOMP) (Grant # 5U01HG004080).

4.1.4 Antibodies

All antibodies used in this study are listed in Table 4.1 and Table 4.2. Primary antibodies were ordered from commercial sources or produced for our lab by Bioscience (Göttingen). Before use, the antibodies were affinity-purified (5.6.9) and tested for their specificity.

Table 4.1: Primary antibodies used in this study. Gp, guinea pig; m, mouse; rb, rabbit; IF, immunofluorescence; WB, western blot; RT, room temperature; o/n, overnight.

Antibody	Host animal	Antibody epitope	Manufacturer/ reference	Dilution and Incubation time		
				IF cells	IF paraffin	WB /frozen
actin	m	C-terminal (mouse)	Sigma-Aldrich, Steinheim (A4700)			1:500
β-tubulin	m	β1-β5 (rat)	Sigma-Aldrich, Steinheim (T4026)		1:200 1h RT	
γ-tubulin	rb	C-terminal AA 437-451 (Xenopus)	Sigma-Aldrich, Steinheim (T3320)		1:300 1h RT	
CAGE1	rb	C-terminal (mouse)	own synthesis; Bioscience, Göttingen		1:200 1h RT	
CLIP1	rb	CLIP170 (human)	Sigma-Aldrich, Steinheim (HPA026678)		1:200 1h RT	
DCTN1	rb	AA 140-210 (human)	Abcam (ab75034)		1:600 o/n 4°C	
GFP (B-2)	m	GFP-tag	Santa Cruz (sc-9996)			1:200 1,5h RT
GM130	m	AA 869-982 (rat)	BD Biosciences, Erembodegem (#610822)		1:400 1h RT	

Materials

Myc	m	Myc-tag	Invitrogen (9E10)	1:200 1h RT		1:1000 1,5h RT
Myc	rb	Myc-tag	Upstate Millipore (06-549)			
SUN1	gp	AA 427-722 (mouse)	own synthesis; Bioscience, Göttingen		1:800 o/n 4°C	
SUN3	gp	AA 31-148 (mouse)	own synthesis; Bioscience, Göttingen		1:300 1h RT	1:5000 1,5h RT
SUN4	rb	AA 246-260 (mouse)	Bioscience, Göttingen	1:300 1h RT	1:300 1h RT	
SUN4	rb	N-terminal: AA 11-127 (mouse)	own synthesis; Bioscience, Göttingen		1:800 1h RT	
SUN4	gp	N-terminal: AA 11-127 (mouse)	own synthesis; Bioscience, Göttingen		1:800 1h RT	1:5000 1,5h RT
SUN5	gp	AA 95-170 (mouse)	own synthesis; Bioscience, Göttingen		1:200 o/n 4°C	
SYNE1	rb	(human)	Atlas antibodies, Stockholm (HPA019113)	1:100 1h RT	1:20 1h RT	1:1000 1,5h RT
Nesprin3	rb		Wilhelmsen et al., 2005		1:500 o/n 4°C	
IgG	gp	unspecific	Dianova, Hamburg (006-000-003)			
IgG	m	unspecific	Dianova, Hamburg (015-000-003)			
IgG	rb	unspecific	Dianova, Hamburg (011-000-003)			

Table 4.2: Secondary antibodies used in this study. Gt, goat; IF, Immunofluorescence; HRP, horseradish peroxidase; WB, western blot.

Antibody	Antigen	Host animal	Manufacturer	Dilution	
				IF	WB
Alexa 488	IgG guinea pig	gt	Life Technologies, Darmstadt	1:200	
Alexa 488	IgG rabbit	gt	Life Technologies, Darmstadt	1:200	
Alexa 594	IgG rabbit	gt	Life Technologies, Darmstadt	1:200	
Cy2	IgG guinea pig	gt	Dianova, Hamburg	1:50	
Cy2	IgG mouse	gt	Dianova, Hamburg	1:50	
Texas Red	IgG guinea pig	gt	Dianova, Hamburg	1:100	
Texas Red	IgG mouse	gt	Dianova, Hamburg	1:50	
Texas Red	IgG rabbit	gt	Dianova, Hamburg	1:50	
HRP	IgG guinea pig	gt	Dianova, Hamburg		1:10000
HRP	IgG mouse	gt	Dianova, Hamburg		1:10000
HRP	IgG rabbit	gt	Dianova, Hamburg		1:10000

4.2 Molecular material

4.2.1 Plasmids

StrataClone pSC-B-amp/kan

The StrataClone PCR cloning vector pSC-B-amp/kan is part of the StrataClone Blunt PCR Cloning Kit (Agilent Technologies, Böblingen) and was used to clone blunt-ended PCR products. For positive selection the plasmid contains kanamycin- and ampicillin-resistance and a *lacZ'* α-complementation cassette for blue-white screening. To ensure correct insertion of recombinant DNA the standard T3 and T7 primers were used for colony PCR (5.5.5.3) and/or sequencing (5.5.9).

pET21a(+)

The expression vector pET21a(+) (Novagen, Darmstadt) was used to generate recombinant fusion proteins with a C-terminal (His)₆-tag. For positive selection the plasmid contains ampicillin-resistance. The pET21a(+) is a T7 promotor-driven plasmid and therefore compatible with the RosettaTM(DE3) *E. coli* bacteria for protein expression.

4.2.2 Oligonucleotides

The primers used in this study (Table 4.3) were designed for PCR genotyping of the *Spag4^{tm1(KOMP)Mbp}* mouse strain, cDNA cloning or RT-PCR analysis. Synthesis of the selected oligonucleotides was performed by Sigma-Aldrich (Steinheim).

Table 4.3: Oligonucleotides used in this study. P, *Phusion™* DNA Polymerase; T, Taq DNA Polymerase.

Primer	Sequence (5' to 3')	Annealing temperature (polymerase)	Application
S4_CSD_vec5'ko	CACACCTCCCCCTGAACCTGA		Amplification of wildtype and knockout Spag4
SD_Spag4_SRI_3'	GGTGGCTCACAACTGTTCTTAACTCC	64°C (P)	
S4_Ex10_5'wt	CCAGATGTGTTCCCTGGAAATTG		allele
S4_Nterm_5'_Nde	CATATGGCATCCTCTCATAATCA		Amplification of mouse <i>Sun4</i> N-terminal cDNA
S4_Nterm_3'_Sal	GTCGACCTCCTGCCTCAGATC	61°C (P)	for antibody generation
Sun4_cc_5'	CCTTGAGAACGAAACCTACG		RT-PCR amplification for <i>Sun4</i> mRNA expression analysis
Sun4_cc_3'	GTCAGGTTGCGCACGAAGT	54°C (T)	

4.2.3 Recombinant DNA constructs

Recombinant DNA constructs used for expression in COS-7 cells and subsequent co-immunoprecipitation experiments were cloned as previously described (Göb et al., 2010: Sun3FL_Myc and Nesprin1TM+KASH_EGFP; Pasch et al., 2015: Sun4ΔN_Myc and Sun4ΔN_EGFP).

To generate the “SUN4 N-term 6xHIS” protein for antibody synthesis a part of the N-terminal SUN4 domain of murine SUN4 (AA11-127) was amplified from the full length *Sun4* cDNA construct “Sun4_ganz_Strata_KoI5” (Beck, C.: Master-Thesis) using the S4_Nterm_5'_Nde/ S4_Nterm_3'_Sal primer pair (see 4.2.2, Table 4.3). The amplified cDNA was ligated into the pET21a(+) vector using NdeI and SalI restriction sites, and used for protein expression in *E. coli* Rosetta™(DE3) bacteria.

4.3 Chemicals

If not stated otherwise, all chemicals used in this study were purchased from AppliChem (Darmstadt), Merck (Darmstadt), Roth (Karlsruhe), Serva (Heidelberg) or Sigma-Aldrich (Steinheim).

4.4 Equipment and Software

Special equipment and software used in this study are listed in Table 4.4 and Table 4.5, respectively.

Table 4.4: Special equipment used in this study.

Camera AxioCamm MRM	Zeiss, Oberkochen
Centrifuge 6-16K	Sigma, Osterode
Centrifuge MIKRO 200/ MIKRO 200R	Hettich, Tuttlingen
CertoClav autoclave (CV-EL 10L/12L)	CertoClav, Traun
Confocal laser scanning microscope TCS-SP2 AOBS	Leica, Wetzlar
Cryomicrotome 2800 Frigocut E	Reichert-Jung, Depew NY
CX41 upright microscope	Olympus, Hamburg
EC3 camera	Leica, Wetzlar
Electrophoresis Power Supply	Peqlab, Erlangen
ELYRA S.1	Carl Zeiss Microscopy GmbH, Jena
Epifluorescence microscope Axiophot Stereo HB050	Zeiss, Oberkochen
Gradient Thermocycler T100	Bio-Rad, Munich
Graphite blotting chamber	LMS (Hartenstein, Würzburg)
Heating block	Liebisch (Hartenstein, Würzburg)
Hybridisation Oven MINI 10	MWG Biotech, Ebersberg
Hybridisation Oven/ Incubator	Memmert, Schwabach
Infinite M200	Tecan, Männedorf
JEM-2100 transmission electron microscope	Jeol, Eching bei München
Odyssey infrared imager	LI-COR®, Bad Homburg
Paraffin microtome	Leitz, Wetzlar
Peel-a-way® tissue embedding moulds	Plano, Wetzlar

Protein gel electrophoresis chamber	LMS Labortechnik, Dossenheim
TemCam F416 camera	TVIPS, Gauting
Thermocycler Primus 25 advanced	Peqlab, Erlangen
Ultramicrotome Leica EM UC7	Leica, Wetzlar

Table 4.5: Software used in this study.

Software	Application
EMMENU Version 4.0.9.31 (TVIPS)	Image acquisition
Image Studio Version 3.1 (LI-COR)	Image acquisition
Leica LCS Lite (confocal software TCS-SP2)	Image acquisition
Leica LAS EZ	Image acquisition
ZEN 2012 (Zeiss)	Image acquisition
CLC DNA Workbench 6	DNA sequence analysis
ImageJ	Image analysis
Adobe Photoshop CS5	Image analysis and processing
R statistical Project	Statistical analysis
Microsoft Excel	Statistical analysis and data management

5 Methods

5.1 Microbiological methods

5.1.1 Culturing of bacteria

5.1.1.1 Liquid culture

- LB medium:

10g/l bacto-trypton
5g/l yeast-extract
10g/l NaCl
adjust to pH 7.4; sterilize by autoclaving
- Antibiotic stock solutions:

Ampicillin	100 mg/ml in ddH ₂ O
Kanamycin	50 mg/ml in ddH ₂ O
Chloramphenicol	34 mg/ml in ethanol

Bacteria were cultured in 10 ml of sterile LB-medium and the appropriate antibiotic (working concentration: ampicillin 100 µg/ml, kanamycin 50 µg/ml and/or chloramphenicol 34 µg/ml) in a 50 ml tube. The medium was inoculated with a bacterial colony from either a glycerol stock (5.1.1.2) or an agar plate (5.1.1.3). Subsequently the liquid culture was incubated overnight at 37°C under continuous agitation.

5.1.1.2 Preparation of a glycerol stock

For stable long-term storage of bacterial colonies glycerol stocks were prepared. For this 150 µl of sterile glycerol and 850 µl of liquid culture were gently mixed in a 1.5 ml tube by pipetting and stored at -80°C.

5.1.1.3 Culturing bacteria on agar plates

- 1.5% (w/v) agar in LB medium (5.1.1.1)
- Antibiotic stock solutions (5.1.1.1)

To prepare agar plates, agar was dissolved in LB medium, autoclaved, and after cooling down the solution to approximately 50°C the desired antibiotic was added in the appropriate working concentration. Subsequently, the liquid medium was poured into sterile petri dishes, and left at room temperature (RT) for setting. Plates were stored upside down at 4°C until usage (for up to 6 weeks). To culture bacteria on an

agar plate 100 – 200 µl of a liquid culture was spread on a preheated plate and incubated at 37°C overnight.

5.1.2 Production of competent bacteria

- LB medium (5.1.1.1)
- Antibiotic stock solutions (5.1.1.1)
- Liquid nitrogen
- Transforming and Storage Solution (TSS):
LB medium
10% (w/v) PEG 3350 or 8000
5% (v/v) DMSO
50-70 mM Mg²⁺ (MgCl₂)
adjust to pH 6.5, sterile filtration
(storage at -20°C)

To generate competent bacteria for efficient transformation, the appropriate amount of required selection antibiotics according to the bacterial strain was added to 200 ml of LB medium. Then 3 ml of an overnight liquid culture (*E. coli* XL1 blue or *E. coli* RosettaTM(DE3)) was added, and the inoculated culture was incubated on a shaker at 37°C until the exponential growth phase (OD₆₀₀ = 0.4 – 0.8) was reached. Afterwards the culture was centrifuged at 900 × g for 10 minutes at 4°C. Subsequently, the supernatant was discarded and the bacterial pellet gently resuspended in 1/40 of the initial volume ice-cold TSS. The bacterial suspension was aliquoted (100 µl in 1.5 ml *Eppendorf* tubes), which were flash-frozen in liquid nitrogen before transfer for long-term storage into a -80°C freezer.

5.1.3 Transformation of bacteria with plasmid DNA

- LB medium (5.1.1.1)

To transform competent bacteria with circular plasmid DNA, which includes its own replication origin and antibiotic resistance, an aliquot of competent bacteria (5.1.2) was thawed on ice and gently mixed with 50-150 ng of purified plasmid DNA or a complete ligation mix (for ligation see 5.5.8.3). Afterwards the mixture was incubated on ice for one hour. The mixture was then exposed to heat shock (60 seconds at 42°C), after which the bacteria were cooled down for 3 minutes on ice and 900 µl of pre-warmed (37°C) LB medium was added. To give the bacteria time to establish resistance, they were cultured for one hour at 37°C under continuous agitation. Finally, 100 µl of the solution with the transformed bacteria was streaked onto an agar plate

with the required resistance. The rest of the solution was centrifuged at approximately 700 x g for 3 minutes, so the supernatant except for the last 150-200 µl could be removed. Subsequently, the pellet was gently mixed with the remaining medium and streaked onto an agar plate containing the matching resistance antibiotics. The bacteria were cultured on the agar plates at 37°C overnight.

The transformation with the *StrataClone* SoloPack Competent Cells was performed according to the manufacturer's instructions.

5.1.3.1 Determination of the transformation efficiency

To determine the transformation efficiency of chemically competent bacteria, selected aliquots were transformed with 1, 10 and 100 pg of the standard pUC19-vector DNA and streaked out on respective agar plates. After overnight incubation the colonies were counted. The transformation efficiency is defined as the amount of colonies per µg DNA. The calculated value should be at least at about 1x10⁷ transformants for an efficient competence.

5.2 Cell culture

5.2.1 Culturing of COS-7 cells

- Culture medium: DMEM(1X)+GlutaMAX™-I (Gibco by Life Technologies, Darmstadt)
10% fetal calf serum (FCS; PAA, Cölbe)
1% penicillin/streptomycin
- Trypsin: 0.06% (w/v) trypsin
0.02% (w/v) EDTA
in PBS
- PBS: 140 mM NaCl
2.6 mM KCl
6.4 mM Na₂HPO₄
1.4 mM KH₂PO₄
adjust to pH 7.4

COS-7 cells were grown in culture medium in 60mm petri dishes at 37°C and 5% CO₂. To maintain a stable cell line, cells were split twice a week. During splitting the old medium was aspirated and subsequently the cells were gently rinsed with 2 ml of pre-warmed PBS (37°C). After aspirating the PBS the cells were incubated in 1 ml of pre-warmed Trypsin (37°C) for at least 5 minutes until the cells detached from the bottom of the petri dish. The cells were then mixed with 5 ml of fresh culture medium. Finally, approximately 1.5x10⁵ cells were seeded into a new 60mm petri dish supplied with 5 ml of fresh culture medium. For transfection, 8-10x10⁴ cells were seeded into a 35mm petri dish supplied with 2.5ml of fresh culture medium and a sterile 12mm coverslip used for fluorescent transfection control. The cells were incubated at 37°C and 5% CO₂ for approximately 24 hours to reach a 40-80% confluence for efficient transfection.

5.2.2 Transfection of COS-7 cells

- Effectene® Transfection Reagent (Qiagen, Hilden)

The process of introducing plasmid DNA into a eukaryotic cell is called transfection. In this study the Effectene® Transfection System was used according to the manufacturer's instructions to transfet COS-7 cells. By use of this transfection reagent the DNA to be transfected condenses and forms Effectene-DNA complexes, which are mixed with medium and added to the cells. The spontaneously formed micelle structures can then easily pass through the cell plasma membrane. The transfected cells were further incubated at 37°C and 5% CO₂ for 24 hours until they were used for immunofluorescence studies or co-immunoprecipitation analysis.

5.3 Mouse husbandry

Laboratory mice of the species *Mus musculus* are the most commonly-used mammalian research model. Due to their close relatedness to humans, their high reproductive rate with reasonable space requirements, and their easy maintenance and handling they make a suitable model organism for basic and human-related research. Furthermore, the mouse genome has been sequenced and therefore biological data accessibility and data comparison are relatively easy.

The *Spag4^{tm1(KOMP)Mbp}* mice used in this study were bred and raised in the animal facility of the Biocenter at the University of Würzburg. The animals were maintained under strict guidelines to ensure careful, consistent and ethical handling of mice according to the German Animal Welfare Act (German Ministry of Agriculture, Health and Economic Cooperation). The mice were kept under stable conditions of approximately 22°C room temperature, a humidity of 65% and a 12h/12h day/night cycle. Heterozygous Spag4 males and females were used for breeding to produce heterozygous as well as homozygous control (wild type) and knockout mice, which were used for tissue preparations. To verify gene targeting and differentiate between the different genotypes, genetic material was taken from the mice at the age of three weeks, when the male and female pups were separated and marked with a serial number for identification. After proteinase K digestion of the genetic material the DNA was purified (5.5.1) and used for genotyping of the *Spag4^{tm1(KOMP)Mbp}* offspring (5.5.5.2).

5.4 Tissue and organ isolation

Somatic and testis tissue samples were obtained from wild type, heterozygous and knockout *Spag4^{tm1(KOMP)Mbp}* littermates. The mice were sacrificed by CO₂ euthanization and cervical dislocation. Subsequently, the required tissues or organs were removed and further processed depending on the type of analysis.

5.4.1 Testis tissue dissection

- PBS (5.2.1)

Testes were isolated by a cut across the lower abdomen of a mouse. The testes were then exposed by pulling out the fatty tissue. After separation from the fatty tissue and cutting off the epididymis, the testes were quickly rinsed in ice-cold PBS and further processed as needed.

5.4.1.1 Preparation of testicular cell suspension

- PBS (5.2.1)
- 2x SDS sample buffer:
 - 120 mM Tris-HCl, pH 6.8
 - 10% (w/v) SDS
 - 20% (v/v) glycerol
 - 20% (v/v) 2-mercaptoethanol
 - bromophenol blue

The PBS-rinsed testis was placed into an ice-cold petri dish. There the tunica albuginea and the rete testis were removed and the remaining tissue, mainly the seminiferous tubules, was mechanically chopped using two razor blades. To isolate the germ cells from the small chopped up tubules about 2 ml of PBS were added and the tissue was resuspended several times with a pipette. Subsequently, the cell suspension was filtered through a polyamide filter cloth with a mesh width of 30 µm and collected in a 50 ml tube. The cells were centrifuged at 500 x g for 10 minutes at 4°C and after removal of the supernatant the cell pellet was resuspended in 1 ml of cold PBS.

Afterwards the cells could be counted using a hemocytometer slide (Neubauer). To calculate the total cell number the following formula was used:

$$\text{total cell count} = 16 \times \text{average cells per small square} \times 10^4 \times \text{dilution factor} \times \text{total volume}$$

Cell suspensions were further used for RNA extraction (5.5.3), EM analysis (5.7.4.1) or protein analysis. For protein analysis the cells were again pelleted by centrifugation at 500 x g for 10 minutes at 4°C and the cell sediment resuspended in 10 µl of 2x SDS sample buffer per 1 x 10⁶ cells. Then the protein suspension was vortexed and heated to 95°C for 5-10 minutes and stored at -20°C until use.

5.4.1.2 Preparation of whole protein tissue samples

- 2x SDS sample buffer (5.4.1.1)

A small piece of the tissue of interest was collected and placed into an ice-cold petri dish. There the tissue piece was mechanically chopped using two razor blades and transferred into a small tube for homogenization with a pestle. After and/or during homogenization an adequate amount of 2x SDS sample buffer was added, then the tissue sample was vortexed and heated to 95°C for approximately 15 minutes, before being stored at -20°C.

If different tissue samples needed to be compared and/or used for protein analysis, the relative amount of protein within a sample was measured using the LI-COR Odyssey infrared imager. The amounts of the required samples were accordingly adjusted so that equal amounts of total protein could be used for SDS-PAGE (5.6.1) and western blot experiments (5.6.3).

5.5 Molecular methods

5.5.1 Purification of genomic DNA

- SDS-mix (pH 7,5):
17 mM Tris-HCl
17 mM EDTA
170 mM NaCl
0.85% (w/v) SDS
- proteinase K solution:
20 mg/ml proteinase K (Serva, Heidelberg)
in 10 mM CaCl₂
(stored at -20°C in aliquots à 200 µl)
- saturated NaCl:
6 M NaCl

In order to verify gene targeting or to differentiate between the different genotypes of the *Spag4^{tm1(KOMP)Mbp}* offspring the genetic material taken from the mice was purified. The first step was an overnight proteinase K digestion. For this 500 µl SDS-mix and 50 µl of the proteinase K solution was added to the isolated tissue material and incubated at 56°C under continuous agitation overnight. Thereafter, 250 µl of saturated NaCl was added and incubated under continuous agitation at RT for 10 minutes and on ice for another 15 minutes. Subsequently, the solution was centrifuged at 8000 x g for 8 minutes at 4°C to precipitate insoluble material. 500 µl of the DNA containing supernatant was transferred into a new 1.5 ml reaction tube and DNA was precipitated by adding 1 ml of 100% EtOH (ice cold by storage at -20°C) and inverting or gently shaking the tube. The DNA was pelleted by centrifugation at 18000 x g for 10 minutes at RT and washed twice with 80% EtOH. After drying the DNA for 2h at RT and an additional 10 minutes at 60°C the DNA was resolubilized in an adequate amount of ddH₂O (volume depending on pellet size) and left overnight at 4°C. The DNA concentration was measured using the *Infinite M200* from Tecan (Männedorf, Switzerland). The isolated genomic DNA was stored at 4°C until use in PCR analyses.

5.5.2 Purification of plasmid DNA

- *NucleoSpin® Plasmid* (Macherey-Nagel, Düren)

Plasmid DNA was obtained from a 10 ml overnight culture of a respective bacterial transformant. To purify the DNA a *NucleoSpin® Plasmid* kit was used according to the manufacturer's instructions. In the final step plasmid DNA was eluted with 50 µl ddH₂O and the concentration measured using an *Infinite M200* from Tecan (Männedorf, Switzerland).

5.5.3 RNA extraction

- *peqGOLD TrifastTM* (PEQLAB, Erlangen)

To extract total RNA, 1/3 testis or an equally small piece of the required tissue, dissected from the mouse, was placed into a small petri dish on ice. The tissue was chopped with two razor blades and transferred into a small 1.5 ml reaction tube for further homogenization with a pestle. Subsequently, 500 µl of the *peqGOLD TrifastTM* was added and the mRNA was extracted following the instructions of the manufacturer of the *peqGOLD TrifastTM* kit.

5.5.4 Generation of cDNA by reverse transcription

- *RiboLockTM* ribonuclease inhibitor (Fermentas, St. Leon Roth)
- *M-MLV reverse transcriptase* and *M-MLV RT 5x buffer* (Promega, Mannheim)
- dNTPs (Fermentas, St. Leon Roth)
- Oligo(dT)₁₈ primer (Fermentas, St. Leon Roth)

Conversion of extracted mRNA into complementary DNA (cDNA), which contains only coding regions and no introns or regulatory DNA sequences, was accomplished by reverse transcription. For this Oligo(dT)₁₈, which is complementary to the poly(A)-tail of every processed mRNA, was used as primer to generate cDNA with the *M-MLV reverse transcriptase*.

Protocol for M-MLV reverse transcription (20 µl preparation):

1 µg mRNA
1 µl *RiboLockTM* ribonuclease inhibitor (40 units/µl)
4 µl *M-MLV RT 5x buffer*
1 µl dNTPs
1 µl Oligo(dT)₁₈ primer (500 µg/ml)
1 µl *M-MLV reverse transcriptase* (200 units/µl)
→add ddH₂O to 20 µl

This reaction mix was incubated in a thermocycler at 37°C for one hour and subsequently at 95°C for 5 minutes to inactivate the enzymatic reaction. The resulting cDNA was stored at -20°C until use for cloning attempts or specific gene expression analyses.

5.5.5 Polymerase chain reaction (PCR)

The polymerase chain reaction (PCR) is a method used to amplify small amounts of DNA *in vitro*. It is based on the principle of natural DNA replication and is a

cyclic repetition of the reaction steps to reach an exponential amplification. One cycle consists out of three major steps, which are repeated 25-35 times:

1. The first step is the **denaturation**; here the double-stranded DNA opens up at 95-98°C.
2. In the **annealing** step, short single-stranded DNA oligonucleotides bind to the denatured DNA template. These so called primers (listed in Table 4.3. under 4.2.2), which are designed as complementary starter molecules, define the 5' start and 3' end of the desired DNA fragment and initiate new synthesis. The annealing temperature depends on the specific sequence and the length of the primers. It should be nearly equal for the two chosen primers used in one reaction. Usually the temperature is between 50 and 65°C, which furthermore depends on the used enzyme during DNA catalysis.
3. In the last step, the **elongation**, the complementary DNA fragment is assembled by use of a thermostable DNA polymerase, which binds to the 3' end of the primers and synthesizes the new DNA strand at 72°C. Thereby the length of the desired DNA fragment and the enzyme determine the elongation time.

5.5.5.1 Amplification of cDNA with *Phusion™* DNA polymerase

- *Phusion™* DNA polymerase and 5x *Phusion HF buffer* (Thermo Scientific, Schwerte)
- dNTPs (Fermentas, St. Leon Roth)
- specific primer pairs (see 4.2.2, Table 4.3)
- DMSO

For cloning attempts, DNA was amplified using the *Phusion™* DNA polymerase. This is a high fidelity DNA polymerase with a proofreading activity, which produces non-phosphorylated blunt ends.

Protocol for *Phusion™* DNA polymerase (50 µl PCR preparation):

5-10 ng template DNA or 1µl cDNA
1 µl 5' primer (10 pmol/µl)
1 µl 3' primer (10 pmol/µl)
1 µl dNTPs (10 mM/nucleotide)
1.5 µl DMSO
10 µl 5x HF reaction buffer
0.3 µl *Phusion™* DNA polymerase (2 units/µl)
→add ddH₂O to 50 µl

The reaction was mixed on ice. First, the calculated amount of ddH₂O was provided. As the last substance the *Phusion™* DNA polymerase was added and the

reaction was subsequently placed into a thermocycler with the program adjusted for the used primers.

Cycling protocol:

initial denaturation	2 min at 98°C	
denaturation	20 sec at 98°C	
primer annealing	30 sec at X°C (see Table 4.3)	} 25x
elongation	1 kb/15 sec at 72°C	
final elongation	10 min at 72°C	
cooling down to 8°C		

The PCR products were analyzed with a UV-Transilluminator after DNA electrophoresis (5.5.6) in a 1 % agarose gel.

5.5.5.2 Amplification of genomic DNA/ genotyping

- *Phusion™* DNA polymerase and 5x *Phusion HF buffer* (Thermo Scientific, Schwerte)
- dNTPs (Fermentas, St. Leon Roth)
- specific primers S4_CSD_vec5'ko, S4_Ex10_5'wt, SD_Spag4_SRI_3'
- DMSO

For the amplification of genomic DNA to verify gene targeting and for general genotyping of the *Spag4*^{tm1(KOMP)Mbp} offspring, approximately the same method was used as described for cDNA amplification (5.5.5.1). Because the content of the desired target genomic DNA fragment within the total DNA content is much lower than in cDNA or plasmid DNA, at least 300 ng of genomic DNA was used as template for PCR amplification. Primers were selected according to the specification by the KOMP Repository. To co-detect the wild type and the targeted alleles at the same time, both 5'-oligonucleotides and the 3'-oligonucleotide were used in the same PCR preparation. The 5'-oligonucleotide S4_CSD_vec5'ko and the 3'-oligonucleotide SD_Spag4_SRI_3' are expected to amplify a 593 bp fragment for the knockout allele. The 5'-primer S4_Ex10_5'wt, which is corresponding to a sequence in exon 10 that is missing in the KO allele (see 4.2.2, Table 4.3), together with the SD_Spag4_SRI_3' are anticipated to amplify a 446 bp fragment for the wild type allele. While in the homozygous situation only the 593 bp fragment for the knockout or the 446 bp fragment for the wild type were amplified, in the heterozygous situation, both fragments were amplified. For genotyping reactions a master-mix of an x-fold enlargement, according to the number of genomic DNA samples, was prepared following the adjusted protocol for genotyping.

Protocol for genotyping of the *Spag4*^{tm1(KOMP)Mbp} offspring (25 µl PCR preparation):

300 ng purified genomic DNA
 0.25 µl 5' KO primer (S4_CSD_vec5'ko; 10 pmol/µl)
 0.5 µl 5' WT primer (S4_Ex10_5'wt; 10 pmol/µl)
 0.75 µl 3' primer (SD_Spag4_SRI_3'; 10 pmol/µl)
 0.5 µl dNTPs (10 mM/nucleotide)
 0.75 µl DMSO
 5 µl 5x HF reaction buffer
 0.15 µl *Phusion*TM DNA polymerase (2 units/µl)
 →add ddH₂O to 25 µl

After the master-mix without the DNA was prepared on ice, it was aliquoted into the provided PCR tubes. These were labeled according to the different samples to be genotyped. As final step approximately 300 ng genomic DNA of the different samples was added to the appropriate tubes and gently mixed before the tubes were placed into a thermocycler with the program adjusted for the genotyping.

Cycling protocol:

initial denaturation	2 min at 98°C	
denaturation	25 sec at 98°C	
primer annealing	20 sec at 64°C	35x
elongation	10 sec at 72°C	
final elongation	7 min at 72°C	
cooling down to 8°C		

The PCR products were analyzed with a UV-Transilluminator after DNA electrophoresis (5.5.6) in a 1.5 % agarose gel. This higher percentage of the gel was used to differentiate more precisely between the wild type and the knockout alleles, to be able to visualize the expected short fragments as separate signals.

5.5.5.3 Colony PCR

- Taq DNA polymerase and 10x Taq buffer (own synthesis at the department)
- dNTPs (Fermentas, St. Leon Roth)
- specific primer pairs (see 4.2.2, Table 4.3)
- MgCl₂ (25 mM)

To verify a successful transformation and to check whether a cloned DNA fragment was inserted correctly into a certain plasmid a colony PCR was conducted using Taq DNA polymerase. Taq DNA polymerase produces 5'-overhangs and has no proofreading activity. In this study it was used to screen larger amounts of positive bacterial colonies for the right vector insert, as mutations that might occur during the PCR do not matter. For a colony PCR a master-mix of an x-fold enlargement,

according to the number of colonies to be tested, was prepared following the protocol for Taq DNA polymerase.

Protocol for Taq DNA polymerase (25 µl PCR preparation):

bacteria colony

0.25 µl 5' primer (10 pmol/µl)
 0.25 µl 3' primer (10 pmol/µl)
 0.5 µl dNTPs (10 mM/nucleotide)
 1.5 µl MgCl₂ (25 mM)
 2.5 µl 10x Taq buffer
 0.5 µl Taq DNA polymerase (5 units/µl; own synthesis)
 →add ddH₂O to 25 µl

The master-mix was portioned into PCR tubes (25 µl/tube) on ice. Subsequently, each PCR reaction mix was resuspended with the bacteria of a single colony that was picked from the agar plate using a pipette tip before placing the tubes into a thermocycler. To save the colonies a copy plate for the ones used in the PCR analysis was generated by tipping the pipette tips in a numbered order onto a new agar plate before resuspension within the PCR preparation.

Cycling protocol:

initial denaturation	2 min at 98°C	
denaturation	20 sec at 98°C	
primer annealing	30 sec at X°C (see Table 4.3)	} 25x
elongation	1 kb/1 min at 72°C	
final elongation	10 min at 72°C	
cooling down to 8°C		

The PCR products were analyzed with an UV-Transilluminator after DNA electrophoresis (5.5.6) in a 1 % agarose gel.

5.5.6 DNA electrophoresis

- 20x SB buffer: 200 mM NaOH
adjust to pH 8.0 with saturated boric acid
- 6x DNA loading buffer: 60% (v/v) glycerol
30% (v/v) 0.2 M EDTA
10% (v/v) ddH₂O
+ 4% orange G
+ 2% xylene cyanol
- λ DNA EcoRI+HindIII DNA marker (Fermentas, St. Leon Roth)
- agarose (peqGOLD Universal Agarose from PeqLab, Erlangen) in 1x SB buffer
- ethidium bromide

DNA fragments were separated according to their size on agarose gel using standard procedures. 1% agarose was heated in 40 ml 1x SB buffer until it was dissolved completely. For visualizing the DNA within the gel, 0.5 µl ethidium bromide was added into the solution before pouring it into a cast, which was equipped with an appropriate comb. After the agarose gel had cooled down, the gel was placed into the electrophoresis chamber, filled with 1x SB buffer until slightly atop of the gel. Once the comb was removed, the gel was loaded with the DNA samples that were mixed with 6x loading buffer in advance. As reference a λ DNA EcoRI+HindIII DNA marker was loaded in parallel. The gel was run for 10-15 minutes at approximately 190V to separate the fragments. During this time, the negatively charged DNA moves towards the positively charged anode of the electrophoresis chamber, and small fragments migrate faster than bigger fragments. The ethidium bromide-stained DNA could then be visualized by UV light using a UV-Transilluminator equipped with a documentation system.

5.5.7 Preparative DNA electrophoresis and gel extraction

- *NucleoSpin® Gel and PCR Clean up* (Macherey-Nagel, Düren)

When the amplified DNA fragment was needed for further usage it could be isolated and extracted from the gel. For this the fragment was cut out of the gel under UV light using a sterile scalpel. For extraction and purification of the DNA from the gel the *NucleoSpin® Gel and PCR Clean up* kit was used following the manufacturer's instructions.

5.5.8 DNA cloning

DNA cloning refers to an experimental method in which recombinant DNA is assembled and its replication is directed within a certain host organism. As host organisms different strains of *Escherichia coli* were used, in which the plasmid, including the desired recombinant DNA, was introduced. After successful replication the plasmid may also be isolated again (5.5.2).

5.5.8.1 StrataClone

- *StrataClone Blunt PCR Cloning Kit* (Agilent Technologies, Böblingen)

For fast and efficient cloning the pSC-B-amp/kan vector (4.2.1) provided with the *StrataClone* Blunt PCR Cloning Kit was used as target vector for blunt-ended DNA fragments, which were generated with *Phusion™* DNA polymerase (5.5.5.1). The cloning of this standardized system was conducted following the instructions of the manufacturer, with the exception that only half of the recommended reaction mix was used per cloning attempt.

5.5.8.2 Restriction digest

- Restriction enzymes and corresponding 10x buffers (Fermentas, St. Leon Roth)

To obtain linearized DNA fragments and/or to subclone a certain DNA fragment from one vector to another the DNA was digested using appropriate restriction enzymes. These enzymes usually cut palindromic recognition sites to create either blunt or sticky ends. When a vector has been cut with the same restriction enzymes as a certain DNA fragment/insert, then they can easily be joined using a DNA ligase (see ligation: 5.5.8.3).

Protocol for restriction digest preparation (10 µl):

1 µg DNA
1 µl restriction enzyme 1 (10 units/µl)
1 µl restriction enzyme 2 (10 units/µl)
1 µl 10x enzyme buffer (appropriate to enzyme 1 and 2)
ddH₂O to 10 µl

The restriction digest preparation was mixed on ice and incubated at 37°C for two hours. Then the reaction mix was heat-inactivated at 65°C for 20 minutes (temperature and time depend on the used enzymes; here stated for Sall and Ndel). Finally, to purify the needed linearized DNA fragments or vectors, preparative DNA electrophoresis and gel extraction was applied (5.5.7).

5.5.8.3 Ligation

- *T4 DNA ligase* and *T4 10x ligation buffer* (Fermentas, St. Leon Roth)

Ligation is a method to join DNA fragments, like a linearized vector and an insert, that possess complementary ends. In this process, the formation of a

phosphodiester bond between the 3'-hydroxyl end of one DNA fragment and the 5'-phosphate end of the other DNA molecule is catalyzed in an ATP dependent manner by the enzymatic activity of the DNA ligase. For an efficient ligation the insert fragments need to be present in a 5-10 fold molar excess compared to the vector DNA molecules.

Protocol for ligation preparation (20 µl):

200-300 ng vector DNA
X ng insert DNA (6x molar excess compared to vector)
2 µl T4 10x ligation buffer
0.5 µl ATP
1 µl T4 DNA ligase (5 units/µl)
ddH₂O to 20 µl

The ligation preparation was mixed on ice according to the protocol. After incubation for one hour at RT, 1 µl of the T4 DNA ligase was additionally added to the reaction mix and incubated for another hour at RT. This was followed by an enzymatic heat inactivation at 65°C for 20 minutes. Finally the ligation reaction was used to transform competent *E. coli* XL1 blue cells as described previously (5.1.3). Successful ligation and transformation was tested by colony PCR (5.5.5.3) and DNA sequencing (5.5.9).

5.5.9 DNA sequencing

For DNA sequencing the purified DNA was sent to GATC Biotech (Konstanz), who performed Sanger sequencing and provided the results on their webpage for download.

5.6 Biochemical methods

5.6.1 SDS-PAGE

- Solution A: Acrylamide 4K solution (30%) - Mix 37.5 : 1 (Acrylamide : Bisacrylamide) (Applichem, Darmstadt)
- Solution B: 1 M Tris-HCl
adjust to pH 8.7
- Solution C: 1 M Tris-HCl
adjust to pH 6.8
- 20% (w/v) SDS in ddH₂O
- Temed (Applichem, Darmstadt)
- 10% APS (w/v) in ddH₂O
- 10x running buffer:
 - 250 mM Tris-HCl
 - 1.12 M glycine
 - 1% (w/v) SDS
 - pH 8.5
- 2x SDS sample buffer (5.4.1.1)
- *PageRuler™* Prestained Protein ladder (#26616; Fermentas, St. Leon Roth)

Polyacrylamide gel electrophoresis (PAGE) is a technique to separate macromolecules according to their electrophoretic mobility, which is dependent on the length, conformation and charge of the molecule. Because most proteins do not have a sufficient charge on their own, the anionic detergent sodium dodecyl sulfate (SDS) is used to impart the proteins with a negative charge proportional to their molecular mass. The SDS first of all denatures the proteins, so it imparts an evenly distributed negative charge, with which the proteins then can be nicely separated while migrating within a polyacrylamide gel towards the positive pole when an electric field is applied. The separation of the proteins within SDS-PAGE is dependent on their molecular weight, as smaller molecules migrate faster than bigger ones within a gel matrix. The pore size within the gel is dependent on the concentration of the used acrylamide mix (the concentration of the mix in total and the proportion of acrylamide to bisacrylamide) and therefore the resolution of the separated proteins can be adjusted according to the expected size range of the proteins of interest. In a high percentage gel small proteins are separated further; conversely, a low percentage gel is more suitable for separating bigger molecules. To focus all proteins of a sample in the same start line, a stacking gel with a lower pH and a bigger pore size is needed atop of the separating gel. In this way sharp protein bands instead of diffuse ones are produced.

Before preparing the polyacrylamide gel matrix of the SDS-PAGE, two glass plates were cleaned and assembled with a spacer in between at each side using a small metal clamp. After sealing the bottom by attaching adhesive tape, the bottom and sides were further sealed with 0.5-1% preheated agarose. Once the agarose had

cooled the ingredients for the separating gel were mixed according to the required polyacrylamide percentage (Table 5.1) and poured in between the glass plates leaving sufficient space for the stacking gel and the comb. On top of the separating gel a layer of water was carefully pipetted to give the separating gel an even surface and protect it from drying out during polymerization. After 30 minutes, when the separating gel was completely polymerized, the water was discarded and the mixed stacking gel solution (Table 5.2) poured on top. Immediately the comb was inserted into the still liquid stacking gel to create wells for the samples. Though the gel was ready for use after the stacking gel was polymerized it was usually prepared a day in advance and stored in a layer of wet paper at 4°C overnight.

Table 5.1: Pipetting scheme for separating gels according to their different polyacrylamide concentration. The displayed amounts of the mixture is sufficient for 3 gels.

Separating gel	8%	10%	12%	15%
Solution A	4 ml	5 ml	6 ml	7.5 ml
Solution B	5.6 ml	5.6 ml	5.6 ml	5.6 ml
20% SDS	75 µl	75 µl	75 µl	75 µl
ddH₂O	5.215 ml	4.215 ml	3.215 ml	1.715 ml
Temed	10 µl	10 µl	10 µl	10 µl
10% APS	100 µl	100 µl	100 µl	100 µl

Table 5.2: Pipetting scheme for the stacking gel. The displayed amounts of the mixture is sufficient for 3 gels.

Stacking gel	5%
Solution A	1.67 ml
Solution C	1.25 ml
20% SDS	50 µl
ddH₂O	6.925 ml
Temed	10 µl
10% APS	150 µl

Protein samples (derived from co-immunoprecipitation experiments, different mouse tissues or testicular cells) were mixed with 2x SDS sample buffer and heated at 95°C for 5 to 15 minutes. Due to the heat and the SDS and 2-mercaptoethanol in the sample buffer the proteins were denatured (linearized, disulfide bonds reduced, and intramolecular protein interactions broken).

Before placing the gel into the electrophoresis chamber the adhesive tape was removed. The anode and the cathode chambers were filled with 1x running buffer and then the comb was removed. After rinsing the wells using a small syringe the protein

samples and the *PageRuler™* Prestained Protein ladder were loaded. The prestained protein ladder was run in parallel to the protein samples as a reference to estimate the apparent molecular weights of the separated proteins. The SDS-PAGE was run at 60V for approximately 1 hour until the proteins entered the separating gel. Thereafter, 100V were applied to the electrophoresis chamber for another 1 to 1.5 hours depending on the needed separation range of the target proteins.

To visualize the proteins the gel was stained with Coomassie blue (5.6.2) or used for western blot analysis (5.6.3).

5.6.2 Coomassie blue staining

- Coomassie blue staining solution: 0.05% (w/v) *Coomassie Brilliant blue R250* (Applichem, Darmstadt)
10% (v/v) isopropanol
5% (v/v) acetic acid
- Coomassie blue destaining solution: 10% (v/v) isopropanol
5% (v/v) acetic acid

The Coomassie blue staining solution was used to visualize the proteins within a polyacrylamide gel. This is an unspecific staining method, where at the same time the proteins are fixed within the gel with acetic acid, so the proteins do not diffuse within and out of the gel over time.

For this, the stacking gel and the agarose were carefully removed from the separating gel, which was then incubated in the Coomassie blue staining solution for 2 to 4 hours or overnight with continuous agitation. To remove the excess dye from the regions without protein, the gel was incubated in the Coomassie blue destaining solution under continuous agitation until the protein bands were clearly visible in blue and the gel matrix appeared transparent. At the end, the gel was washed in ddH₂O.

If required the protein concentration within the gel could be either estimated or measured (5.6.2.2) and finally the gel was dried for documentation (5.6.2.1).

5.6.2.1 Drying of Coomassie blue stained acrylamide gels

For documentation purposes the gel was dried using cellophane foil. For this the foil was soaked in water until it was fully flexible and then placed on top of a plastic frame. After placing the gel in the middle and adding a small volume of ddH₂O a second foil was placed on top to cover the gel without leaving any air bubbles in

between. A second frame was placed on top congruent to the first one and fixed in place using metal clamps. After overnight drying the gel hardened and could be kept for long-term storage at RT.

5.6.2.2 Measuring protein concentrations in Coomassie blue-stained SDS gels

To estimate protein concentrations a defined amount of the protein was used in one lane and compared with the staining of BSA standards, e.g. 1 µg, 2 µg, 5 µg and 10 µg, in parallel lanes. This estimation was used to calculate the rough amount of protein after purification (5.6.5) and precipitation (5.6.6) or concentration (5.6.7) of especially HIS-tagged fusion proteins.

If the relative concentration of one protein sample in comparison to another was of importance (e.g. when comparing tissue samples), then these samples were quantified by comparison of their Coomassie blue staining intensities using the Odyssey infrared imager from LI-COR® (Bad Homburg). This was used to adjust protein samples in order to load a comparable amount of protein when analyzing the amount of a certain protein (SUN4) in different tissues, or in different ages or genotypes of the same tissue (testis).

5.6.3 Western blot analysis

- CAPS buffer: 50 mM CAPS
 10% (v/v) methanol
 adjust to pH 10
 add 1 mM mercaptopropionic acid
- TBST: 150 mM NaCl
 10 mM Tris-HCl
 0.1% (v/v) Tween®20
 adjust to pH 7.4
- Ponceau S: 0.2% Ponceau S
 in 3% TCA
- Blocking solution: 10% (w/v) milk
 in TBST
- Western Lightning® Plus-ECL Enhanced Chemiluminescence Substrate (PerkinElmer, Waltham)

The western blot is an analytical technique to transfer the proteins from the polyacrylamide gel after SDS-PAGE onto a nitrocellulose (or PVDF) membrane. By performing an immunoblot a certain protein within a tissue sample can then be detected on the membrane using specific antibodies.

Western blotting

To equilibrate the gel for the protein transfer, right after the SDS-PAGE, the gel was incubated with CAPS buffer for 10 minutes under continuous agitation. For blotting, a semi-dry graphite blotting chamber was used. Before assembling the blot 18 whatman papers and the nitrocellulose membrane (0.45 µm, GE Healthcare, Munich) were cut according to the size of the polyacrylamide gel (9 cm x 5 cm) and were soaked with CAPS buffer. To assemble the blot, 9 whatman papers were placed centrally on top of the graphite anode plate; these were followed by the nitrocellulose membrane, the protein gel, and another 9 whatman papers, which were carefully applied to avoid inclusion of air bubbles. Finally the graphite cathode plate was placed on top and fastened using the appropriate screws. The protein transfer was performed at 1 mA/cm² for 50-60 minutes depending on the protein size. In the applied electric field the negatively charged proteins moved towards the anode and were thereby transferred onto the nitrocellulose membrane.

To check for successful protein transfer the nitrocellulose membranes were stained with Ponceau S solution for approximately 3 minutes under continuous agitation. Subsequently, the membranes were washed in ddH₂O to remove the excess dye from regions without protein and visualize the protein bands. If needed, the membranes could be cut or the lanes marked with a graphite pencil as long as the protein lanes were visible in the Ponceau S staining.

Antibody detection

Membranes were washed in TBST twice for 10 minutes, before used for antibody detection. The following incubations were generally performed under continuous agitation. To saturate remaining binding sites the membranes were incubated in blocking solution for two hours at RT and furthermore overnight at 4°C. Subsequently the membranes were incubated with the respective primary antibodies (see Table 4.1 under 4.1.4), which were diluted in blocking solution, for 1.5 hours at RT. After three consecutive washing steps in TBST for 10 minutes each, the membranes were incubated with appropriate secondary antibodies (see Table 4.2 under 4.1.4), which were diluted in blocking solution as well. Finally the membranes were washed three times with TBST for 10 minutes each, before the chemiluminescent antibody detection.

The secondary antibodies used in this approach were coupled to horseradish peroxidase (HRP) and could therefore be visualized with the Western Lightning® Plus-ECL Enhanced Chemiluminescence Substrate, which was applied following the instructions of the manufacturer. HRP catabolizes the substrate, a reaction which is accompanied by the emission of low intensity light (chemiluminescence). This light is enhanced by certain chemicals in the Western Lightning® Plus-ECL kit and can be used for radiographic film exposure. After incubation of the membrane in the ECL solution for one minute the membrane was placed between two layers of transparent plastic foil and covered with a radiographic film (AGFA Cronex 5, Hartenstein Laborversand, Würzburg) for exposure. The exposure time of the radiographic film was dependent on the quality and concentration of the used antibodies, the amount of protein in the membrane, and the needed intensity of the signal. At the beginning the radiographic film was exposed to the emitted light from the membrane for 2 minutes; for optimal results this process could be repeated with an adjusted exposure time until the chemiluminescent reaction ceased. For the following development the film was incubated in the developing and the fixating solutions for one minute each and afterwards washed in ddH₂O and placed to dry. Finally a dark band should be visible showing the existence of the target protein, e.g. within a certain tissue sample.

5.6.3.1 Stripping of a nitrocellulose membrane

- Stripping buffer 1: 100 mM glycine
adjust to pH 2
- Stripping buffer 2: 100 mM Tris-HCl
2% (w/v) SDS
adjust to pH 6.7
- TBST (5.6.3)
- Blocking solution (5.6.3)

In case a particular membrane had to be used for the detection of a different protein as well, the membrane was stripped to remove the previously-bound antibodies. Before the actual stripping the membrane was washed in TBST for 10 minutes. For a rather mild stripping the membrane was then incubated for 30 minutes in stripping buffer 1 and subsequently for another 30 minutes in stripping buffer 2 under continuous agitation. Afterwards the membrane was washed in TBST twice for 10 minutes and then re-blocked by incubation in blocking solution for 2 hours at RT, before a different protein could be detected (5.6.3).

5.6.4 Co-immunoprecipitation

- PBS (5.2.1)
- RIPA-Puffer:
 - 1% (v/v) Triton-X 100
 - 0.5% (w/v) Sodium deoxycholate
 - 0.1% (w/v) SDS
 - 1 mM β -Glycerophosphate
 - 1 mM Na_3VO_4
 - 1 mM EGTA
 - 1 mM EDTA
 - in PBS
 - adjust to pH 7.4
- Proteinase-Inhibitor-Mix: 5 mM α -aminocaproic acid
 - 1 mM Benzamidine
 - 1 mM EDTA
 - 2 $\mu\text{g}/\text{ml}$ Aprotinin
 - 2 $\mu\text{g}/\text{ml}$ Antipain
 - 2 $\mu\text{g}/\text{ml}$ Chymostatin
 - 2 $\mu\text{g}/\text{ml}$ Leupeptin
 - 2 $\mu\text{g}/\text{ml}$ Pepstatin
 - as stock solution (50x in H_2O)
- 2x SDS sample buffer (5.4.1.1)

Co-immunoprecipitation is a method to analyze protein-protein interactions. In this technique a known protein is immunoprecipitated using a specific antibody against the target protein. If the target protein is part of a larger complex and binds tightly to its partners it is possible to pull down the whole protein complex. Afterwards co-immunoprecipitated binding partners of the target protein can be identified by immunoblot analysis.

C- or N-terminal tags can be fused onto the proteins of interest when an antibody specific for the endogenous protein is unavailable or inappropriate. After ectopic expression of these constructs in cell culture, the fusion proteins can be detected using specific antibodies against the tags in western blot analysis.

Production of cell suspensions containing the target proteins for co-immunoprecipitation analysis

Depending on the assay the cell extracts were either produced from cell culture cells ectopically expressing the fusion proteins or from testicular cell suspensions containing endogenous proteins.

Cell culture cells – ectopically expressed proteins

COS-7 cells were co-transfected with 300 ng of the target and 300 ng of the candidate binding partner fusion protein constructs (5.2.2) and were harvested after 24 hours. The transfected COS-7 cells expressing the respective fusion proteins were rinsed with PBS and transferred into a 1.5 ml maximum recoveryTM tube (MCT-150-L-C; Axygen, Inc., Union City, CA) after collecting them using a cell scraper. The cells were then centrifuged at 500 x g for 10 minutes at 4°C to gently pellet the cells.

Testicular cell suspension – endogenous proteins

Testicular cell suspensions were produced as described under 5.4.1.1. After centrifugation in a 50 ml tube the cell pellet was gently resuspended in 1 ml PBS and transferred into a 1.5 ml maximum recoveryTM tube (MCT-150-L-C; Axygen, Inc., Union City, CA). This again was centrifuged at 500 x g for 10 minutes at 4°C to gently pellet the cells.

Lysis of the cell extracts

Cells were resuspended in 500 µl RIPA (radio-immunoprecipitation assay) buffer, which was supplemented with proteinase inhibitor mixture (1:100) and incubated on ice for 10 minutes for lysis. Thereafter lysates were centrifuged at 15,000 x g for 10 minutes at 4°C to pellet the cell debris. The supernatants with the dissolved proteins were further used for the co-immunoprecipitation.

Co-immunoprecipitation

As an input control, 25 µl (~10%) of the supernatant was transferred into a new maximum recovery tube and mixed with 25 µl of the 2x SDS sample buffer. The rest of the supernatant was equally divided (ideally two aliquots of approx. 250 µl) and transferred into new maximum recovery tubes. These lysates were either supplemented with 1.5 µg of the specific antibody for the pulldown or as a control with 1.5 µg of unspecific IgG from the same host species from which the specific antibody was derived (see 4.1.4, Table 4.1). The solutions were incubated at 4°C overnight under continuous agitation. The remaining pellet (after the supernatant has been

divided) was resuspended in 80 µl of 2x SDS sample buffer and together with the input control stored at -20°C until usage in SDS-PAGE.

Following the overnight incubation the protein-antibody solutions were mixed with Dynabeads® Protein G (Invitrogen, Carlsbad) for the pulldown. Protein G binds covalently to all IgG antibodies and is therefore an ideal reagent to pull down antibodies together with their bound antigens and interaction partners. Before usage of the Dynabeads®, 2 x 20 µl of the protein G-coupled Dynabeads® were transferred into new maximum recovery tubes, centrifuged at 500 x g for 1 minute at 4°C and placed onto an appropriate magnetic separator for 1.5 ml tubes for at least one minute. On this magnet the supernatant can be easily discarded, as the magnetic beads are drawn towards the magnet and therefore stay pelleted. The beads were pre-equilibrated with 250 µl of the proteinase inhibitor mix supplemented RIPA buffer. The beads were subsequently always washed by adding RIPA buffer, centrifuging at 500 x g for 1 minute at 4°C, and then placing the preparations for one minute onto the magnet before discarding the solutions. After the RIPA buffer was discarded the protein-antibody solution was transferred to the beads and incubated for 2 hours at 4°C under continuous agitation.

After the antibodies were coupled to the protein G beads, the immune complexes were purified using the magnet, washed three times with 250 µl RIPA buffer and then resuspended in 40 to 50 µl of the 2x SDS sample buffer. Finally the protein samples were heated to 95°C for 15 minutes and placed back onto the magnet for five minutes to separate the immune complexes from the beads, so that the solution could be applied to SDS-PAGE. The supernatant of the immune complexes (after the two hour incubation) was also used as a control, to see how much of the expected binding partner of the target protein was dissolved within the supernatant instead of bound in a protein complex with the target protein. For this, the proteins were precipitated via acetone (5.6.6) and after drying they were resuspended in 80 µl of 2x SDS sample buffer to be used in SDS-PAGE as well.

To detect protein-protein interactions the protein samples and their respective controls (input control, pellet and the supernatants of the immune complexes) were analyzed by SDS-Page (5.6.1) and western/immuno blot (5.6.3) analysis.

5.6.5 Expression and purification of a HIS-tagged fusion protein

- LB medium (5.1.1.1)
- Antibiotic stock solutions (5.1.1.1)
- IPTG (Isopropyl β -D-thiogalactopyranoside) stock solution: 1M IPTG
in ddH₂O
(storage at -20°C)
- Buffer A-D:
8 M urea
100 mM NaH₂PO₄
10 mM Tris-HCl
adjust to pH 8 (A), pH 6.3 (B), pH 5.9 (C) and pH 4.5 (D)
- Neutralization buffer: 1 M Tris-HCl
adjust to pH 9.5
- Ni-NTA (Nickel-nitrilotriacetic) agarose matrix suspension (Qiagen, Hilden)

To generate larger amounts of a particular protein or protein fragments a bacterial vector expression system was used. In this work it was required to express the N-terminal fragment of the murine SUN4 protein (AA 11-127), which was used to immunize animals for antibody production. After bacterial expression the protein needed to be extracted from the bacteria and purified. This was accomplished using nickel affinity chromatography, in which HIS-tagged fusion proteins bind specifically to the Ni-NTA (nickel-nitrilotriacetic) agarose matrix. The protein of interest can then be eluted in pure form from the matrix by lowering the pH.

Bacterial expression

For bacterial protein expression an expression vector including the coding sequence of the particular protein (fragment) was used to transform *E. coli* RosettaTM(DE3) bacteria (5.1.3). The expression vector pET21a(+) was used, in which the coding region of the protein or epitope of interest was cloned in frame to the (His)₆-tag codons to produce His-tag fusion proteins.

To generate sufficient protein, 3 x 200 ml LB medium were prepared with the appropriate antibiotics and inoculated with approximately 3 ml of an overnight liquid culture each. The cultures were incubated on a shaker at 37°C until they reached the exponential growth phase (OD₆₀₀ between 0.5 and 0.8) which took approximately three hours. Expression of the fusion proteins was then induced by adding 1 mM IPTG. After further incubation for another 4 hours the bacteria were pelleted by centrifugation at 3,000 x g for 10 minutes in 50 ml centrifugation tubes. The supernatant was discarded and the bacterial pellets were either immediately resuspended in buffer A or stored at -20°C).

To test for successful protein expression, 1 ml of the culture was taken just before addition of the IPTG and another 1 ml after the 4 hours protein expression period. These samples were centrifuged, the supernatant was discarded, and the pellets were resuspended in 40 µl 2x SDS sample buffer. Successful protein expression was then checked by SDS-PAGE (5.6.1) and Coomassie blue staining (5.6.2).

Lysis of the bacteria

The bacterial pellet was resuspended in 1/20 buffer A, with the volume measured according to the initial culture volume. After overnight incubation at 4°C under continuous agitation the bacterial suspension was sonicated on ice, 3 times for 10 seconds each, with a minute long incubation on ice in between to keep the suspension at a low temperature. The applied ultrasound disrupted the bacterial membranes, so that the protein of interest was released into the lysate. The suspension was incubated under continuous agitation for an additional hour at RT, before centrifugation at 10,000 x g for 15 minutes to pellet insoluble bacterial remains. The supernatant containing the soluble proteins was transferred into a new 50 ml centrifugation tube and placed on ice until loading onto the Ni-NTA agarose matrix.

Affinity purification through Ni-NTA agarose matrix

A 5 ml polypropylene column (Qiagen, Hilden) equipped with an appropriate frit (Qiagen, Hilden) was thoroughly saturated with ddH₂O to replace the air from the frit and ensure a constant flow during the affinity purification. This polypropylene column was filled with 2 ml of the Ni-NTA agarose matrix suspension (1:1 in EtOH) (Qiagen, Hilden) and the matrix was allowed to sediment. From now on the matrix was never allowed to run dry and the solutions were added to the column very carefully in order not to stir up the matrix. The solutions were run through the matrix by gravity flow. First, the prepared matrix was equilibrated by letting 20 ml buffer A pass through. Then the supernatant containing the proteins was loaded onto the column so the HIS-tag fusion proteins would specifically bind to the Ni-NTA agarose matrix while the solution was passing through. Afterwards the matrix was washed with 20 ml of buffer A and 15 ml of buffer B. Finally, the target protein was eluted with 10 ml of buffer C and 10 ml of buffer D. The flow-through was collected in 1.5 ml reaction tubes in 1 ml aliquots. To these aliquots 50 µl of the neutralization buffer was added immediately.

To test in which fraction the target protein was eluted 7.5 µl of each of the fractions from the flow-through of C and D were supplied with 7.5 µl of 2x SDS sample buffer and subjected to SDS-PAGE (5.6.1) and Coomassie blue staining (5.6.2).

5.6.6 Precipitation of proteins

Protein precipitation was used to obtain the pure protein by separating it from its solvent. In this study two different methods were performed to precipitate proteins.

Protein precipitation with methanol and chloroform

- Methanol, p.a.: stored at -20°C
- Chloroform, p.a.: stored at -20°C

150 µl (1-fold volume) of the protein solution was mixed with 600 µl (4-fold volume) ice-cold methanol and 150 µl (1-fold volume) chloroform in a 1.5 ml reaction tube. After vortexing the solution for approximately 10 seconds, 450 µl (3-fold volume) ice-cold ddH₂O was mixed into the solution and incubated on ice for 10 minutes for phase separation before centrifugation at 13,000 x g for 10 minutes at RT. This led to a solution with 3 separated phases: a lower organic chloroform phase containing detergents and lipids, an intermediate phase containing the precipitated protein, and an upper aqueous phase containing salt and nucleic acids. After the upper phase was carefully removed, leaving the intermediate phase intact, another 600 µl of ice-cold methanol was added, and the tube was carefully inverted and centrifuged at 13,000 x g for 10 minutes at RT. Finally, the supernatant was discarded and the protein pellet was air dried and could afterwards be resuspended in any desired solution.

If necessary, in order to resuspend a protein in a certain solution, the mixture could be heated or SDS (up to a total concentration of 4%) could be added.

Protein precipitation with acetone

- Acetone, p.a.: stored at -20°C

Alternatively, proteins were precipitated using acetone. For this, a 9-fold volume of ice-cold acetone was added to the protein solution and, after vigorously shaking, it was incubated at -80°C for one hour. The precipitated protein was then pelleted by

centrifugation at 8,000 x g for 10 minutes at RT. Thereafter, the supernatant was discarded and the protein pellet air dried before resuspension in a chosen solution.

5.6.7 Concentration of proteins

A different method to concentrate a protein (or to exchange the buffer in which a protein is dissolved) was using a centricon (*Amicon® Ultra*, Centrifugal Filter Unit 10K of Millipore, Tullagreen). This basically is a 50 ml tube equipped with a semipermeable membrane through which the protein solution was filtered by centrifugation (3,500 x g for 1 to 1.5 hours each time). Thereby the initial solvent with its molecules and all other dissolved particles (molecules, ions and small protein fragments) pass through the filter as long as they are smaller than the pore size of the filter, which is chosen by the size of the target protein. A minimal volume of 200 µl (for the Centrifugal Filter Unit 10K) should always remain above the filter together with the target protein. Due to the centrifugation the protein, which was dissolved in a large amount of solution, was concentrated up to a minimum of 200 µl of the solvent. The initial solvent could then be replaced by adding a new solvent and thereby diluting the initial one to the desired degree with additional centrifugations.

5.6.8 Dialysis of proteins

- 2 mM EDTA, pH 8.0
- Dialysis buffer (according to use)

Buffer exchange can be performed by dialysis, based on the osmotic potential difference between two solutions, using a dialysis membrane with special cut-off. For this, the protein solution was filled into a semipermeable dialysis tube (Roth, Karlsruhe), which was boiled in 2 mM EDTA for 30 minutes before usage. The filled dialysis tube was then placed into a big jar (~5 L) containing a large volume of dialysis buffer. The overnight incubation under gentle agitation of the dialysis buffer at 4°C allowed sufficient time to exchange the initial buffer from the protein solution with the dialysis buffer until the equilibrium of the solved particle concentrations was reached between the solution in- and outside of the dialysis tube.

5.6.9 Generation of SUN4-specific antibodies

Specific antibodies can be generated in several steps. For this a suitable antigen has to be selected, cloned, expressed and purified. The purified antigen is used to immunize a suitable lab animal, usually a rabbit or guinea pig. After injecting the host animal with the purified antigen it usually takes several weeks before the specific polyclonal antibodies are produced. The specific antibodies can be purified from the obtained immune sera.

Selection and generation of the antigen

SUN4-specific antibodies were generated against the N-terminal domain of the murine SUN4. To select a suitable region the NCBI reference sequence NM_139151 was analyzed for possible interferences, e.g. accessibility and hydrophilicity. Accordingly, the N-terminal region corresponding to amino acids 11 to 127 of the full-length murine SUN4 was identified as a promising antigen. To amplify this part of the coding region, the primers S4_Nterm_5'_Nde and S4_Nterm_3'_Sall (see 4.2.2, Table 4.3) and full-length murine *Sun4* cDNA (Pasch et al., 2015), were used. Thereafter the amplified fragments were ligated into the StrataClone PCR cloning vector pSC-B-amp/kan. They were then excised with NdeI/Sall enzymes and subcloned using the pET21a(+) vector (for a more accurate description see 5.5.8 DNA cloning). The plasmid was used to transform *E. coli* Rosetta bacteria, and the His-tagged N-terminal SUN4 fusion construct was produced using previously-described techniques (see 5.6.5).

Alternatively, a second antibody epitope was selected against a perinuclear domain corresponding to amino acids 246 to 260 of full-length murine SUN4. As an internal control it was important to obtain two different antibodies that, if specific, should always produce co-localizing staining patterns in immunofluorescence experiments.

Immunization

Purified N-terminal SUN4 protein, which was dissolved in PBS and contained 1% SDS, was sent to BioScience (Göttingen) and used for immunization of a guinea pig and a rabbit. The small peptide antigen corresponding to a region within the perinuclear domain was synthesized by BioScience (Göttingen) and used for immunization of two rabbits.

The immunization of the antigens to generate the SUN4-specific antibodies was carried out by Bioscience (Göttingen) following a 2-month protocol. In this protocol the animals received three injections: the first at day 0, then at day 21 and the last at day 49. At primary injection 250 µg and at the following injections 150 µg of the antigen were used to efficiently immunize the guinea pig and rabbits. After a fixed incubation time, during which the immune system of the animals produced different antibodies against the injected antigen, the blood sera, containing the specific polyclonal antibodies were collected. This was accomplished at day 35 for the 1st (test) bleeding, at day 53 for the 2nd (test) bleeding and at day 60 to gather the final bleeding. The obtained sera were forwarded by BioScience (Göttingen) and were then usually affinity purified, because the sera not only contained the specific antibodies generated against the SUN4-specific antigen but also all other antibodies from the animal's immune system. For the purification mainly the final bleedings were used, as 1st and 2nd bleedings, especially from guinea pigs, were small amounts and contained fewer antibodies.

Antibody purification using HiTrap™ NHS-activated HP columns

- Binding buffer: 200 mM NaCO₃
500 mM NaCl
adjust to pH 8.3
- Washing buffer 1: 1 mM HCl, cooled to 4°C
- Buffer A: 500 mM ethanolamine
500 mM NaCl
adjust to pH 8.3
- Buffer B: 100 mM acetic acid
500 mM NaCl
adjust to pH 4.0
- Washing buffer 2: 3.5 M MgCl₂
- Elution buffer: 100 mM glycine, pH 2.5
- Neutralization buffer: 1 M Tris-HCl, pH 9.5
- PBS (5.2.1)
- PBS + 350 mM NaCl, pH 7.4
- Storage buffer: 50 mM Na₂HPO₄
0.1% (w/v) NaN₃ (toxic; addition to a maximum total volume of 1 ml)
adjust to pH 7.0

Affinity purification of antibodies was performed using 1 ml HiTrap™ NHS-activated HP columns (GE Healthcare, Munich). For this, the columns were washed and subsequently coupled with the respective antigen. At all steps it was of importance that the columns never ran dry and air bubbles were excluded from the system. The

columns were washed and loaded using a peristaltic pump with a maximum flowrate of 1 ml/min (if not stated otherwise) or a syringe, respectively.

Antigenic ligand coupling

To covalently couple the antigen onto the HiTrap™ column, the polypeptide was dissolved in binding buffer. Before loading the protein solution onto the column it was centrifuged at 3,000 x g for 5 minutes at 4°C to pellet small insoluble particles. After rinsing the tube by pumping 10 ml of 70% ethanol and subsequently ddH₂O through it, the HiTrap™ column was washed with 6 ml of ice-cold washing buffer via the peristaltic pump, which was equipped with the tube and an adapter to fit onto the column. Subsequently, 1 ml of the protein solution containing 1 to 2 mg of the antigen was filled into an appropriate syringe and loaded onto the column, where the solution was incubated for one hour at RT. During this time the antigen coupled to the NHS-activated sepharose of the HiTrap™ column via its primary amino groups. Thereafter, the column was washed in 6 ml buffer A, 6 ml buffer B and additional 6 ml buffer A, in which it was then further incubated for another hour at RT to inactivate the excessive binding sites (saturation of the active groups with ethanolamine). This was followed by three additional washing steps of 6 ml buffer B, 6 ml buffer A and 6 ml buffer B. Finally, buffer B was replaced by PBS to store the column at 4°C for a few days until antibody purification. If the HiTrap™ column was not needed immediately it was loaded with 1 ml of storage buffer using an appropriate syringe and kept in the fridge until usage.

Affinity purification

For affinity purification the antigen-coupled HiTrap™ column was washed with 10 ml washing buffer 2 and subsequently with 30 ml PBS. During this time the immune serum was centrifuged at 3,000 x g for 10 minutes at 4°C to pellet possible insoluble particles. The supernatant (5 ml guinea pig or 10 ml rabbit final bleeding) was diluted 1:10 in PBS and loaded onto the column. To efficiently and quantitatively bind the antibodies to the column the flow through was reloaded onto the column for another 2 times. To remove unbound material the column was washed with 30 or 50 ml PBS, 30 or 50 ml PBS with 350 mM NaCl for a guinea pig or rabbit serum, respectively. After washing with another 10 ml of PBS the antibody was eluted with 15 ml elution buffer with a flowrate of 3 ml/min. The eluate was collected in 15 ml tubes, where 50 µl

neutralization buffer per ml eluate was added. Finally, the column was washed with 20 ml PBS, before it was loaded with 1 ml storage buffer for long term storage at 4°C.

Dialysis and concentration of the antibody

- PBS (5.2.1)

After the affinity purification the antibody was dialyzed against 5 liter 4°C cold PBS as dialysis buffer (5.6.8). For this the antibody was filled into a dialysis tube with a molecular weight cut-off of 14,000 Da (Roth, Karlsruhe).

Following dialysis the antibody solution was concentrated using a 50K (molecular weight cutoff) centricron (*Amicon® Ultra*, Centrifugal Filter Unit 50K of Millipore, Tullagreen) (5.6.7). Centrifugation at 3,000 x g and 4°C was carried out until the antibody solution reached an OD₂₈₀ of at least 1.48, which is equivalent to a protein concentration of 1 mg/ml. At a minimum concentration of 1 mg protein per ml PBS the antibodies can be stably stored at -80°C, otherwise they could be stabilized by addition of 1 mg/ml BSA. Finally, aliquots of 5 or 10 µl were flash-frozen in liquid nitrogen and stored at -80°C.

5.7 Microscopic methods

5.7.1 Mouse tissue preparation for immunohistochemistry

5.7.1.1 Smear preparation of germ cells or spermatozoa

- PBS (5.2.1)
- Fixation solution (pH 7,4): 2% paraformaldehyde (PFA; w/v) in PBS

10 to 50 µl of testis or epididymis cell suspensions (5.4.1.1) were spread on Superfrost Plus (Menzel Glas, Braunschweig) slides and then dried at RT. Alternatively, the cell suspensions were supplied with an equal volume of 2% PFA and spread on the slides, so the cells were already fixed while drying at RT.

5.7.1.2 Paraffin tissue embedding and sectioning

- PBS (5.2.1)
- Fixation solution (pH 7,4): 1 or 4% formaldehyde in PBS diluted from 37% formaldehyde
- Tert.-Butanol
- EtOH: 50%, 60%, 70%, 80%, 90% and 100% diluted in ddH₂O
- Paraffin (in pastille form)

Testes or epididymes were dissected from the mice and briefly rinsed in PBS. Thereafter, they were transferred into 1% formaldehyde and incubated for three hours for fixation. Following two washing steps in PBS for 30 minutes each the tissue was dehydrated in an increasing ethanol series. For this, the tissue samples were incubated in 50, 60, 70, 80, 90 and 100% ethanol for at least one hour each. Then the tissues were incubated for one hour in tert.-Butanol, and after this directly transferred into preheated paraffin and incubated overnight at 58-60°C in the liquid paraffin. Finally the tissues were transferred into a labeled and preheated Peel-a-way® tissue embedding mould filled with liquid paraffin, and positioned using a warm needle or tweezers. After further incubation for approximately two hours the moulds were taken out of the incubator, cooled down to RT, and stored at 4°C.

For immunofluorescence on paraffin-embedded tissues, the tissues were usually sectioned a day in advance to give the sections sufficient time to dry. Using a sliding microtome (Leitz) the tissues were cross-sectioned at 4-7µm. These sections were transferred from the microtome blade onto a water droplet, which had been placed on a Superfrost Plus (Menzel Glas, Braunschweig) slide. Together with the slide, the sections were placed on a heating plate warming the sections to 58°C to gently remove folds and stretch the sections atop of the water. Once the paraffin

became transparent and the sections were fully stretched, the slide was removed from the heating plate. Subsequently the water was removed using a paper towel to absorb the water from underneath the tissue section on the tilted slide. Remaining water between the sections and the slide was removed by rigorously shaking it off. Finally, the sections were dried overnight at RT.

5.7.1.3 Frozen tissue embedding and sectioning

- PBS (5.2.1)
- Fixation solution (pH 7,4): 1% PFA (w/v) in PBS
- Sucrose solution: 15 and 30% (w/v) in PBS
- Tissue-Tek® O.C.T.™ Compound (Sakura, Staufen)
- Liquid nitrogen (LN₂)
- Methyl butane

Following the dissection of the testes, the organs were cut in two halves and immediately transferred into 1% PFA to fix the tissue. After fixation for one hour at RT the tissue samples were washed twice in PBS for 30 minutes each. Subsequently, the tissues were dehydrated using consecutive 15% and 30% sucrose solutions until the samples sank to the bottom, indicating that they were completely infiltrated with the sucrose solution. Tissues were embedded in Tissue-Tek® with the cut surface facing the bottom of the Peel-a-way® tissue embedding moulds to facilitate later sectioning. The testes halves were placed onto a single drop of Tissue-Tek® avoiding that air bubbles form underneath the tissue. The samples were completely covered with the embedding compound, and finally cryo-embedded by transferring the moulds in methylbutane, which was precooled to approximately -140°C with liquid nitrogen. The tissues were stored at -80°C in the freezer.

Frozen tissues were sectioned at 6 or 7µm using a cryomicrotome (2800 Frigocut E, Reichert-Jung). The sections were collected onto Superfrost Plus (Menzel Glas, Braunschweig) slides by gently placing the slide atop of the sections on the blade of the cryomicrotome. Afterwards the sections were air dried at RT for at least 30 minutes.

5.7.2 Immunofluorescence analysis

5.7.2.1 Immunofluorescence analysis on paraffin tissue sections

- Roti-Histol
- EtOH: 50%, 60%, 70%, 80%, 90% and 100% diluted in H₂O
- PBS (5.2.1)
- Antigen unmasking solution (H-3300; Vector Laboratories, Burlingame): 1:100 in ddH₂O
- Permeabilization solution: 0.1% Triton X-100 (v/v) in PBS
- PBT:
 - 0.15% (w/v) BSA
 - 0.1% Tween 20
 - in PBS
- Hoechst stock solution: 5 µg Hoechst 33258 (Roche) in ddH₂O
→working dilution: 1:333 in PBS
- Embedding medium: 50% glycerol in PBS

Paraffin removal and rehydration of the sections

First the paraffin was removed from the sections by incubating them twice for 10 minutes in Roti-Histol at RT. Afterwards the sections were rehydrated in a decreasing ethanol series (100%, 90%, 80%, 70%, 60% and 50%). For this they were incubated in 100% ethanol for 10 minutes, in the following steps for 2 minutes each, then for 5 minutes in 50% ethanol and finally in ddH₂O for at least 3 minutes.

Antigen retrieval

After rehydration antigen retrieval was performed to increase the accessibility of antibody epitopes. For this antigen unmasking solution (1:100 in ddH₂O) was preheated to 100°C in a table autoclave (CertoClav autoclave CV-EL 10L/12L, Certo Clav, Traun). The sections were transferred into the hot solution and incubated at 125°C and 1 to 1.5 bar for up to 20 minutes depending on the used antibodies and thickness of the sections. After guarded releasing the pressure of the autoclave the samples were carefully removed and placed in PBS for at least 5 minutes.

Antibody staining

To permeabilize the tissue (cellular membranes), the sections were incubated in 0.1% Triton X-100 in PBS for 10 minutes. After washing the samples twice for 5 minutes in PBS they were blocked in PBT for 1 to 2 hours. To stain the proteins of

interest, the samples were placed in a humidified chamber and incubated with respective primary antibodies. For this, the slides were dried around the tissue sections using an absorbing paper towel and placed in the chamber. Subsequently, 50 to 200 µl of primary antibodies appropriately diluted in PBT were added atop of the sections and incubated for one hour at RT or overnight at 4°C (for antibody dilutions and incubation times see Table 4.1 under 4.1.4). If the tissue sections were double-labeled with two different antibodies, the antibodies were either incubated together or one after another with two 5 minutes washing steps in between. When the antibodies were used consecutively, the antibody with the lower affinity was used first. In some cases the tissues were then refixed for 3 minutes in 1% formalin in PBS to protect the antibodies from displacement, before incubating with the second primary antibody with higher affinity. Thereafter the samples were washed twice in PBS for 5 minutes each and incubated with the appropriate secondary antibodies for 30 minutes under the same conditions as described above. For the last 10 minutes of the incubation, 2 drops of Hoechst were added to co-stain for DNA. Finally, the sections were washed three times in PBS for 5 minutes each, embedded in 50% glycerol in PBS and covered with a coverslip to protect from drying. The samples were stored at 4°C until they were analyzed with the confocal laser scanning microscope (CLSM; 5.8.1).

5.7.2.2 Immunofluorescence analysis on frozen tissue sections, germ cell or spermatozoa smear, and cultured COS-7 cells

- PBS (5.2.1)
- Fixation solution (pH 7,4): 1% PFA or formaldehyde in PBS
- Permeabilization solution (5.7.2.1)
- PBT (5.7.2.1)
- Hoechst stock solution (5.7.2.1)
- Embedding medium (5.7.2.1)

Tissue fixation

All materials that so far were not previously fixed, such as the dried cell smears on slides or cultured COS-7 cells grown on cover slips, were fixed with 1% PFA for 3 to 10 minutes.

Antibody staining

To permeabilize the cellular membranes the samples were incubated in 0.1% Triton X-100 for 5 to 10 minutes and after washing in PBS (twice for 5 minutes) blocked with PBT for at least one hour. The antibody staining was conducted as described above for the paraffin sections (5.7.2.1), thereby the optimal antibody concentrations were adjusted according to the performed method (e.g. staining cultured cells or tissue sections). The primary antibodies' concentrations for the frozen tissue sections were the same as used for the paraffin-embedded tissue sections (Table 4.1 under 4.1.4). In contrast to tissue sections and cell smear on slides, which were embedded using a coverslip, COS-7 cells were grown on coverslips and then mounted in the embedding medium on Superfrost Plus (Menzel Glas, Braunschweig) slides at the end. The immunofluorescence stainings were analyzed using a CLSM (5.8.1) or structured illumination microscope (SIM; 5.8.2).

5.7.3 Hematoxylin and Eosin staining

- Hematoxylin solution according to Mayer
- Eosin stock solution (1983)
- EtOH (50%, 60%, 70%, 80%, 90% and 100% in ddH₂O)
- Roti-Histol

The Hematoxylin/Eosin staining is a histological staining method to gain insight into the morphologic structure of thin sliced tissue preparations, commonly applied to examine pathological tissues. By this method cellular and tissue-specific details can be resolved using a normal light microscope. Hematoxylin is a basic/positive blue stain that binds to basophilic substances like the acidic and negatively charged DNA or RNA. Therefore it preferentially stains nuclei, which contain mainly DNA (and RNA). Eosin is an acidic/negative red stain that binds to basic and positively charged substances. It labels the basic cytoplasm due to its mostly positively charged proteins.

Histological analysis using the Hematoxylin/Eosin staining was performed on paraffin-embedded testis tissue that was fixed with 4% paraformaldehyde overnight (5.7.1.2). After the paraffin was removed from the 5 µm testis tissue sections, they were rehydrated (5.7.2.1). The sections were then placed in a humidified chamber and incubated in 150 µl Hematoxylin solution for 8 minutes at RT. Subsequently, the slides with the sections were quickly rinsed with and then placed into tap water, where the staining reaction was observed. After approximately 8 minutes, when the nuclei showed a strong blue color, the staining reaction was stopped by transferring the slides

into ddH₂O. Following a 5 minutes washing step in ddH₂O the sections were placed back into the humidity chamber and counterstained with 150 µm diluted Eosin solution (Eosin stock solution diluted 1:100 in ddH₂O) for approximately 30 minutes at RT. After washing in ddH₂O for 2 minutes, the sections were dehydrated. For this, the slides were incubated in an increasing ethanol series (50%, 70% and 100%) for 1 minute each step. Then they were dipped into Roti-Histol to replace the EtOH and finally embedded by covering with Roti®-Histokitt (Carl Roth GmbH & Co. KG, Karlsruhe) and a coverslip. After drying for at least one hour the samples were analyzed using the Olympus CX41 microscope equipped with a Leica EC3 camera.

5.7.4 Tissue preparation for electron microscopy

5.7.4.1 Tissue embedding

- PBS (5.2.1)
- Buffered glutaraldehyde solution:
2.5% glutaraldehyde
50 mM KCl
2.5 mM MgCl₂
50 mM cacodylate
adjust to pH 7.2
- Cacodylate buffer:
50 mM cacodylate
adjust to pH 7.2
- Osmium tetroxide:
2% osmium tetroxide
in 50 mM cacodylate buffer
- 0.5% Uranyl acetate in ddH₂O
- EtOH p.a. (50, 70, 90, 96 and 100% in ddH₂O)
- Propylene oxide
- Epon 812

Testis or epididymis samples were rinsed in PBS. Small pieces were separated from the tissue, transferred to buffered glutaraldehyde solution, and fixed for 45 minutes at RT. By the end of the fixation time the tissues were transferred onto ice and the following steps performed at approximately 0 - 4°C. Subsequently, the tissue pieces were washed in cacodylate buffer 5 times for 3 minutes each. Following a postfixation incubation with osmium tetroxide solution for 1.5 to 2 hours the samples were washed in ddH₂O 5 times for 3 minutes each. Then the tissues were stained in 0.5% uranyl acetate overnight. The following day the samples were washed 5 times for 3 minutes in ddH₂O and dehydrated in an increasing ethanol series. For this the tissue pieces were incubated in 50%, 70%, 90% and three times in 100% ethanol in ddH₂O for 30 minutes each. Before the last incubation in 100% ethanol the tissue pieces were taken from the ice. Following three incubations in propylene oxide at RT for 30 minutes each, the tissues were incubated overnight in a 1:1 mixture of propylene oxide and

Epon. After two changes of Epon every two hours on the next day the tissue pieces were finally embedded in Epon, which was then polymerized at 60°C for at least 48 hours. After polymerization the tissue samples were stored at RT.

5.7.4.2 Embedding of testicular cells according to Russell et al. (1991)

- PBS:
150 mM NaCl
5 mM KCl
3.2 mM Na₂HPO₄
0.8 mM KH₂PO₄
adjust to pH 7.3
- Sodium cacodylate buffer:
50 mM sodium cacodylate
adjust to pH 7.4
- Glutaraldehyde solution 1:
3% glutaraldehyde
0.5% Triton X 100
50 mM lysine
50 mM sodium cacodylate
adjust to pH 7.4
- Glutaraldehyde solution 2:
3% glutaraldehyde
50 mM EDTA
50 mM sodium cacodylate
adjust to pH 7.4
- Sodium barbital buffer:
0.1 M sodium barbital
adjust to pH 8.4
- Osmium tetroxide:
2% osmium tetroxide
in 50 mM cacodylate buffer
- 2% Uranyl acetate in ddH₂O
- EtOH p.a. (50, 70, 90, 96 and 100% in ddH₂O)
- Propylene oxide
- Epon 812

To specifically analyze the connection between the NE and the microtubule manchette, testicular cell suspensions were prepared for electron microscopy (EM) (5.4.1.1). Testicular cell suspensions were treated according to the protocol by Russell et al. (1991), who first described rod-like linkers that interconnect the NE with the spermatid manchette. For this, the testicular cells were resuspended in 1 ml PBS containing 5 mM EDTA (pH 7.3). This suspension was divided into three 2 ml reaction tubes to obtain smaller pellets after centrifugation at 400 x g for 5 minutes at 4°C. After the supernatant was discarded, cells were resuspended in sodium cacodylate buffer containing 5 mM EDTA (pH 7.4). Following centrifugation at 600 x g for 5 minutes at 4°C cell pellets were fixed for 1.5 hours at RT in glutaraldehyde solution 1. After the first hour of incubation the cell pellets were subdivided into 4 small pieces using a needle. Then the fragments were further fixed for 50 minutes at RT in glutaraldehyde solution 2. Subsequently, the samples were washed three times in sodium barbital

buffer for 5 minutes each on ice. Following five washing steps in ddH₂O for 3 minutes each the cells were stained in 2% uranyl acetate overnight at 4°C and processed further as described above.

5.7.4.3 Sectioning and contrasting of Epon-embedded tissue samples

- 2% Uranyl acetate in EtOH p.a.
- EtOH p.a. (50 and 100% in ddH₂O)
- Reynold's lead citrate: 80 mM lead nitrate
 - 120 mM sodium citrate
 - 160 mM NaOH
- ddH₂O: boiled!

For electron microscopic analysis the samples were sectioned ultrathin (55 – 65 nm) using a Leica EM UC7 ultramicrotome equipped with a diamond cutter. The ultrathin sections were placed on small copper grids (50 mesh), which were precoated with Pioloform FN65 (Plano, Wetzlar) (0.8% in chloroform). For a better contrast the tissue sections were double stained with uranyl acetate and lead citrate. For this the grids were placed upside down onto a drop of 2% uranyl acetate on parafilm and covered with a glass petri dish to protect the section from drying-out. Following 20 minutes incubation in uranyl acetate the grids were dipped into 100% ethanol, then 50% ethanol solution and twice in ddH₂O. Afterwards the grids were placed upside down into Reynold's lead citrate solution, which was diluted 1:1 in degassed ddH₂O before usage. Samples were incubated for 8 minutes, whereby the grids were not only covered by a glass petri dish to protect them from drying out as before, but NaOH pellets were also added underneath the petri dish to bind the free CO₂ from the air. Finally, the grids were washed three times in ddH₂O and excess water was carefully removed using a filter paper. The grids with the contrasted sections were stored in a grid box at RT until they were analyzed using the JEM-2100 transmission electron microscope (Jeol, Eching, Germany).

5.8 Image acquisition and analysis

5.8.1 Confocal laser scanning microscopy

Immunofluorescence stainings on sections were visualized using a Leica TCS-SP2 AOBS confocal laser scanning microscope (Leica Microsystems AG, Wetzlar, Germany) equipped with an argon/krypton laser used for the emission at 488nm and three diode lasers covering the wavelengths at 405nm, 561nm and 633nm. Images were taken with the 63x/1.40 HCX PL APO oil immersion objective and depending on the needed detail, an additional digital zoom (2-, 4- or 8-fold) was applied using the Leica LCS Lite confocal software. Usually three proximate consecutive confocal sections were scanned in a z-distance of 0.122 µm. If the whole cell nuclei needed to be analyzed up to approximately 60 consecutive confocal sections were recorded. The confocal images shown in this study represent calculated maximum 2D z-projections of the optical stack.

5.8.2 Structured illumination microscopy

Structured illumination microscopy in this study was performed on testis cell suspensions, which were spread in 2% PFA fixation solution on Superfrost Plus (Menzel Glas, Braunschweig) slides. Single spermatids were imaged with a Zeiss ELYRA S.1 structured illumination microscope equipped with a Zeiss Plan-APOCHROMAT 63x/1.4 oil DIC objective using the Zeiss ZEN 2012 software package including Superresolution Structured Illumination plugin (Carl Zeiss Microscopy GmbH, Jena, Germany).

5.8.3 Transmission electron microscopy

Ultrastructural analysis was performed using the transmission electron microscope JEM-2100 (Jeol; Eching bei München, Germany). The images were taken with a TemCam F416 camera using the associated software EMMENU Version 4.0.9.31 (Tietz Video and Image Processing Systems (TVIPS), Gauting, Germany).

5.8.4 Image processing

Image processing was carried out using ImageJ (National Institutes of Health, version 1.42q; <http://rsbweb.nih.gov/ij>) and/or Adobe Photoshop CS5 (Adobe Systems).

5.9 Statistics

The statistical analysis of the testis weight was performed using Microsoft Excel 2010 and R (Version 2.10.1; <http://www.r-project.org>). After gathering sufficient data of testes of wild type (n=14), heterozygous (n=16) and homozygous (n=12) *Sun4* mutant mice the mean values and standard deviations of the corresponding groups were calculated (Microsoft Excel 2010). Then the grouped values were tested for normal distribution (Shapiro-Wilk-Test; R). The distribution pattern between the different groups was compared accordingly (Kruskal-Wallis-Test; R).

6 References

- Akhmanova, A., Mausset-Bonnefont, A. L., van Cappellen, W., Keijzer, N., Hoogenraad, C. C., Stepanova, T., Drabek, K., van der Wees, J., Mommaas, M., Onderwater, J. et al. (2005). The microtubule plus-end-tracking protein CLIP-170 associates with the spermatid manchette and is essential for spermatogenesis. *Genes Dev* **19**, 2501-15.
- Alsheimer, M., Drewes, T., Schutz, W. and Benavente, R. (2005). The cancer/testis antigen CAGE-1 is a component of the acrosome of spermatids and spermatozoa. *Eur J Cell Biol* **84**, 445-52.
- Alsheimer, M., Fecher, E. and Benavente, R. (1998). Nuclear envelope remodelling during rat spermiogenesis: distribution and expression pattern of LAP2/thymopoietins. *J Cell Sci* **111**, 2227-2234.
- Beck, C. (2013). Master Thesis: Functionelle Charakterisierung des spermatogenese-spezifischen SUN-Proteins Sun4. University of Würzburg, Würzburg.
- Behrens, T. W., Jagadeesh, J., Scherle, P., Kearns, G., Yewdell, J. and Staudt, L. M. (1994). Jaw1, A lymphoid-restricted membrane protein localized to the endoplasmic reticulum. *J Immunol* **153**, 682-90.
- Bellve, A. R., Cavicchia, J. C., Millette, C. F., O'Brien, D. A., Bhatnagar, Y. M. and Dym, M. (1977). Spermatogenic cells of the prepuberal mouse. Isolation and morphological characterization. *J Cell Biol* **74**, 68-85.
- Brinkley, B. R. (1985). Microtubule organizing centers. *Annu Rev Cell Biol* **1**, 145-72.
- Cain, N. E., Tapley, E. C., McDonald, K. L., Cain, B. M. and Starr, D. A. (2014). The SUN protein UNC-84 is required only in force-bearing cells to maintain nuclear envelope architecture. *J Cell Biol* **206**, 163-72.
- Calvi, A., Wong, A.S., Wright, G., Wong, E.S., Loo, T.H., Stewart, C.L. and Burke, B. (2015). SUN4 is essential for nuclear remodeling during mammalian spermiogenesis. *Dev Biol* **407**, 321-30.
- Cartwright, S. and Karakesisoglu, I. (2014). Nesprins in health and disease. *Semin Cell Dev Biol* **29**, 169-79.
- Chambliss, A. B., Khatau, S. B., Erdenberger, N., Robinson, D. K., Hodzic, D., Longmore, G. D. and Wirtz, D. (2013). The LINC-anchored actin cap connects the extracellular milieu to the nucleus for ultrafast mechanotransduction. *Sci Rep* **3**, 1087.
- Chang, W., Worman, H. J. and Gundersen, G. G. (2015). Accessorizing and anchoring the LINC complex for multifunctionality. *J Cell Biol* **208**, 11-22.
- Chikashige, Y., Haraguchi, T. and Hiraoka, Y. (2007). Another way to move chromosomes. *Chromosoma* **116**, 497-505.
- Clermont, Y. (1963). The cycle of the seminiferous epithelium in man. *Am J Anat* **112**, 35-51.

- Clermont, Y.** (1972). Kinetics of spermatogenesis in mammals: seminiferous epithelium cycle and spermatogonial renewal. *Physiol Rev* **52**, 198-236.
- Clermont, Y. and Leblond, C. P.** (1955). Spermiogenesis of man, monkey, ram and other mammals as shown by the periodic acid-Schiff technique. *Am J Anat* **96**, 229-53.
- Clermont, Y., Oko, R. and Hermo, L.** (1993). Cell biology of mammalian spermiogenesis. In: Desjardin C, Ewing LL, editors. *Cell and molecular biology of the testis*. New York: Oxford University Press. pp. 332-376.
- Cole, A., Meistrich, M. L., Cherry, L. M. and Trostle-Weige, P. K.** (1988). Nuclear and manchette development in spermatids of normal and azh/azh mutant mice. *Biol Reprod* **38**, 385-401.
- Conrad, M.N., Lee, C.Y., Chao, G., Shinohara, M., Kosaka, H., Shinohara, A., Conchello, J.-A. and Dresser, M.E.** (2008). Rapid telomere movement in meiotic prophase is promoted by NDJ1, MPS3, and CSM4 and is modulated by recombination. *Cell* **133**, 1175-87
- Crisp, M., Liu, Q., Roux, K., Rattner, J. B., Shanahan, C., Burke, B., Stahl, P. D. and Hodzic, D.** (2006). Coupling of the nucleus and cytoplasm: role of the LINC complex. *J Cell Biol* **172**, 41-53.
- Dadoune, J. P.** (2003). Expression of mammalian spermatozoal nucleoproteins. *Microsc Res Tech* **61**, 56-75.
- Dam, A. H., Feenstra, I., Westphal, J. R., Ramos, L., van Golde, R. J. and Kremer, J. A.** (2007). Globozoospermia revisited. *Hum Reprod Update* **13**, 63-75.
- Dam, A. H., Ramos, L., Dijkman, H. B., Woestenenk, R., Robben, H., van den Hoven, L. and Kremer, J. A.** (2011). Morphology of partial globozoospermia. *J Androl* **32**, 199-206.
- Dang, R., Zhu, J.Q., Tan, F.Q., Wang, W., Zhou, H., et al.** (2012). Molecular characterization of a KIF3B-like kinesin gene in the testis of *Octopus tankahkeei* (Cephalopoda, Octopoda). *Mol Biol Rep* **39**, 5589-5598.
- de Boer, P., de Vries, M. and Ramos, L.** (2015). A mutation study of sperm head shape and motility in the mouse: lessons for the clinic. *Andrology* **3**, 174-202.
- Ding, X., Xu, R., Yu, J., Xu, T., Zhuang, Y. and Han, M.** (2007). SUN1 is required for telomere attachment to nuclear envelope and gametogenesis in mice. *Dev Cell* **12**, 863-72.
- Djinovic-Carugo, K., Gautel, M., Ylanne, J. and Young, P.** (2002). The spectrin repeat: a structural platform for cytoskeletal protein assemblies. *FEBS Lett* **513**, 119-23.
- Dooher, G. B. and Bennett, D.** (1973). Fine structural observations on the development of the sperm head in the mouse. *Am J Anat* **136**, 339-61.
- Duong, N. T., Morris, G. E., Lam le, T., Zhang, Q., Sewry, C. A., Shanahan, C. M. and Holt, I.** (2014). Nesprins: tissue-specific expression of epsilon and other short isoforms. *PLoS One* **9**, e94380.

- Fan, J. and Beck, K.A.** (2004). A role for the spectrin superfamily member Syne-1 and kinesin II in cytokinesis. *J Cell Sci* **117**, 619-629
- Fawcett, D. W.** (1975). The mammalian spermatozoon. *Dev Biol* **44**, 394-436.
- Fawcett, D. W., Anderson, W. A. and Phillips, D. M.** (1971). Morphogenetic factors influencing the shape of the sperm head. *Dev Biol* **26**, 220-51.
- Fawcett, D. W. and Phillips, D. M.** (1969). The fine structure and development of the neck region of the mammalian spermatozoon. *Anat Rec* **165**, 153-64.
- Fischer-Vize, J. A. and Mosley, K. L.** (1994). Marbles mutants: uncoupling cell determination and nuclear migration in the developing *Drosophila* eye. *Development* **120**, 2609-18.
- Fridkin, A., Mills, E., Margalit, A., Neufeld, E., Lee, K. K., Feinstein, N., Cohen, M., Wilson, K. L. and Gruenbaum, Y.** (2004). Matefin, a *Caenorhabditis elegans* germ line-specific SUN-domain nuclear membrane protein, is essential for early embryonic and germ cell development. *Proc Natl Acad Sci U S A* **101**, 6987-92.
- Fridkin, A., Penkner, A., Jantsch, V. and Gruenbaum, Y.** (2009). SUN-domain and KASH-domain proteins during development, meiosis and disease. *Cell Mol Life Sci* **66**, 1518-33.
- Fridolfsson, H. N., Ly, N., Meyerzon, M. and Starr, D. A.** (2010). UNC-83 coordinates kinesin-1 and dynein activities at the nuclear envelope during nuclear migration. *Dev Biol* **338**, 237-50.
- Frohnert, C., Schweizer, S. and Hoyer-Fender, S.** (2011). SPAG4L/SPAG4L-2 are testis-specific SUN domain proteins restricted to the apical nuclear envelope of round spermatids facing the acrosome. *Mol Hum Reprod* **17**, 207-18.
- Göb, E., Meyer-Natus, E., Benavente, R. and Alsheimer, M.** (2011). Expression of individual mammalian Sun1 isoforms depends on the cell type. *Commun Integr Biol* **4**, 440-2.
- Göb, E., Schmitt, J., Benavente, R. and Alsheimer, M.** (2010). Mammalian sperm head formation involves different polarization of two novel LINC complexes. *PLoS One* **5**, e12072.
- Graumann, K., Runions, J. and Evans, D. E.** (2010). Characterization of SUN-domain proteins at the higher plant nuclear envelope. *Plant Journal* **61**, 134-44.
- Gruenbaum, Y., Margalit, A., Goldman, R. D., Shumaker, D. K. and Wilson, K. L.** (2005). The nuclear lamina comes of age. *Nat Rev Mol Cell Biol* **6**, 21-31.
- Gruenbaum, Y., Wilson, K. L., Harel, A., Goldberg, M. and Cohen, M.** (2000). Review: nuclear lamins--structural proteins with fundamental functions. *J Struct Biol* **129**, 313-23.
- Grünewald, L.** (2015). Master Thesis: Analyse von molekularen und biochemischen Eigenschaften von hodenspezifischen LINC-Komplexen. University of Würzburg, Würzburg.
- Hagan, I. and Yanagida, M.** (1995). The product of the spindle formation gene sad1+ associates with the fission yeast spindle pole body and is essential for viability. *J Cell Biol* **129**, 1033-47.

- Haque, F., Lloyd, D. J., Smallwood, D. T., Dent, C. L., Shanahan, C. M., Fry, A. M., Trembath, R. C. and Shackleton, S.** (2006). SUN1 interacts with nuclear lamin A and cytoplasmic nesprins to provide a physical connection between the nuclear lamina and the cytoskeleton. *Mol Cell Biol* **26**, 3738-51.
- Haque, F., Mazzeo, D., Patel, J. T., Smallwood, D. T., Ellis, J. A., Shanahan, C. M. and Shackleton, S.** (2010). Mammalian SUN protein interaction networks at the inner nuclear membrane and their role in laminopathy disease processes. *J Biol Chem* **285**, 3487-98.
- Hasan, S., Guttinger, S., Muhlhausser, P., Anderegg, F., Burgler, S. and Kutay, U.** (2006). Nuclear envelope localization of human UNC84A does not require nuclear lamins. *FEBS Lett* **580**, 1263-8.
- Heller, C. G. and Clermont, Y.** (1963). Spermatogenesis in man: an estimate of its duration. *Science* **140**, 184-6.
- Hermo, L., Pelletier, R. M., Cyr, D. G. and Smith, C. E.** (2010a). Surfing the wave, cycle, life history, and genes/proteins expressed by testicular germ cells. Part 1: background to spermatogenesis, spermatogonia, and spermatocytes. *Microsc Res Tech* **73**, 241-78.
- Hermo, L., Pelletier, R. M., Cyr, D. G. and Smith, C. E.** (2010b). Surfing the wave, cycle, life history, and genes/proteins expressed by testicular germ cells. Part 2: changes in spermatid organelles associated with development of spermatozoa. *Microsc Res Tech* **73**, 279-319.
- Hermo, L., Pelletier, R. M., Cyr, D. G. and Smith, C. E.** (2010c). Surfing the wave, cycle, life history, and genes/proteins expressed by testicular germ cells. Part 3: developmental changes in spermatid flagellum and cytoplasmic droplet and interaction of sperm with the zona pellucida and egg plasma membrane. *Microsc Res Tech* **73**, 320-63.
- Hermo, L., Pelletier, R. M., Cyr, D. G. and Smith, C. E.** (2010d). Surfing the wave, cycle, life history, and genes/proteins expressed by testicular germ cells. Part 5: intercellular junctions and contacts between germs cells and Sertoli cells and their regulatory interactions, testicular cholesterol, and genes/proteins associated with more than one germ cell generation. *Microsc Res Tech* **73**, 409-94.
- Hetzer, M. W.** (2010). The nuclear envelope. *Cold Spring Harb Perspect Biol* **2**, a000539.
- Hetzer, M. W. and Wente, S. R.** (2009). Border control at the nucleus: biogenesis and organization of the nuclear membrane and pore complexes. *Dev Cell* **17**, 606-16.
- Hiraoka, Y. and Dernburg, A. F.** (2009). The SUN rises on meiotic chromosome dynamics. *Dev Cell* **17**, 598-605.
- Ho, H. C.** (2010). Redistribution of nuclear pores during formation of the redundant nuclear envelope in mouse spermatids. *J Anat* **216**, 525-32.
- Hodzic, D.M., Yeater, D.B., Bengtsson, L., Otto, H. and Stahl, P.D.** (2004). Sun2 is a novel mammalian inner nuclear membrane protein. *J Biol Chem* **279**, 25805-25812.
- Isermann, P. and Lammerding, J.** (2013). Nuclear mechanics and mechanotransduction in health and disease. *Curr Biol* **23**, R1113-21.

- Ito, C., Suzuki-Toyota, F., Maekawa, M., Toyama, Y., Yao, R., Noda, T. and Toshimori, K.** (2004). Failure to assemble the peri-nuclear structures in GOPC deficient spermatids as found in round-headed spermatozoa. *Arch Histol Cytol* **67**, 349-60.
- Jahed, Z., Shams, H. and Mofrad, M.R.K.** (2015). A Disulfide Bond Is Required for the Transmission of Forces through SUN-KASH Complexes. *Biophys J* **109**, 501-509.
- Jaspersen, S. L. and Ghosh, S.** (2012). Nuclear envelope insertion of spindle pole bodies and nuclear pore complexes. *Nucleus* **3**, 226-36.
- Jaspersen, S. L., Martin, A. E., Glazko, G., Giddings, T. H., Jr., Morgan, G., Mushegian, A. and Winey, M.** (2006). The Sad1-UNC-84 homology domain in Mps3 interacts with Mps2 to connect the spindle pole body with the nuclear envelope. *J Cell Biol* **174**, 665-75.
- Juneja, S. C. and van Deursen, J. M.** (2005). A mouse model of familial oligoasthenoteratozoospermia. *Hum Reprod* **20**, 881-93.
- Kato, A., Nagata, Y. and Todokoro, K.** (2004). Delta-tubulin is a component of intercellular bridges and both the early and mature perinuclear rings during spermatogenesis. *Dev Biol* **269**, 196-205.
- Ketema, M., Wilhelmsen, K., Kuikman, I., Janssen, H., Hodzic, D. and Sonnenberg, A.** (2007). Requirements for the localization of nesprin-3 at the nuclear envelope and its interaction with plectin. *J Cell Sci* **120**, 3384-94.
- Kierszenbaum, A. L., Rivkin, E. and Tres, L. L.** (2003). Acroplaxome, an F-actin-keratin-containing plate, anchors the acrosome to the nucleus during shaping of the spermatid head. *Mol Biol Cell* **14**, 4628-40.
- Kierszenbaum, A. L., Rivkin, E. and Tres, L. L.** (2011). Cytoskeletal track selection during cargo transport in spermatids is relevant to male fertility. *Spermatogenesis* **1**, 221-230.
- Kierszenbaum, A. L. and Tres, L. L.** (2004). The acrosome-acroplaxome-manchette complex and the shaping of the spermatid head. *Arch Histol Cytol* **67**, 271-84.
- Kierszenbaum, A. L., Tres, L. L., Rivkin, E., Kang-Decker, N. and van Deursen, J. M.** (2004). The acroplaxome is the docking site of Golgi-derived myosin Va/Rab27a/b- containing proacrosomal vesicles in wild-type and Hrb mutant mouse spermatids. *Biol Reprod* **70**, 1400-10.
- King, M.C., Drivas, T.G. and Blobel, G.** (2008). A network of nuclear envelope membrane proteins linking centromeres to microtubules. *Cell* **134**, 427-38.
- Kracklauer, M. P., Banks, S. M., Xie, X., Wu, Y. and Fischer, J. A.** (2007). Drosophila klaroid encodes a SUN domain protein required for Klarsicht localization to the nuclear envelope and nuclear migration in the eye. *Fly (Austin)* **1**, 75-85.
- Kracklauer, M. P., Link, J. and Alsheimer, M.** (2013). LINCing the nuclear envelope to gametogenesis. *Curr Top Dev Biol* **102**, 127-57.

- Kracklauer, M. P., Wiora, H. M., Deery, W. J., Chen, X., Bolival, B., Jr., Romanowicz, D., Simonette, R. A., Fuller, M. T., Fischer, J. A. and Beckingham, K. M.** (2010). The Drosophila SUN protein Spag4 cooperates with the coiled-coil protein Yuri Gagarin to maintain association of the basal body and spermatid nucleus. *J Cell Sci* **123**, 2763-72.
- Krausz, C.** (2011). Male infertility: pathogenesis and clinical diagnosis. *Best Pract Res Clin Endocrinol Metab* **25**, 271-85.
- Krausz, C., Escamilla, A. R. and Chianese, C.** (2015). Genetics of male infertility: from research to clinic. *Reproduction* **150**, R159-74.
- Leblond, C. P. and Clermont, Y.** (1952a). Definition of the stages of the cycle of the seminiferous epithelium in the rat. *Ann N Y Acad Sci* **55**, 548-73.
- Leblond, C. P. and Clermont, Y.** (1952b). Spermiogenesis of rat, mouse, hamster and guinea pig as revealed by the periodic acid-fuchsin sulfurous acid technique. *Am J Anat* **90**, 167-215.
- Lee, K. K., Starr, D., Cohen, M., Liu, J., Han, M., Wilson, K. L. and Gruenbaum, Y.** (2002). Lamin-dependent localization of UNC-84, a protein required for nuclear migration in *Caenorhabditis elegans*. *Mol Biol Cell* **13**, 892-901.
- Lei, K., Zhang, X., Ding, X., Guo, X., Chen, M., Zhu, B., Xu, T., Zhuang, Y., Xu, R. and Han, M.** (2009). SUN1 and SUN2 play critical but partially redundant roles in anchoring nuclei in skeletal muscle cells in mice. *Proc Natl Acad Sci U S A* **106**, 10207-12.
- Lindeman, R. E. and Pelegri, F.** (2012). Localized products of futile cycle/Irmp promote centrosome-nucleus attachment in the zebrafish zygote. *Curr Biol* **22**, 843-51.
- Link, J., Leubner, M., Schmitt, J., Gob, E., Benavente, R., Jeang, K. T., Xu, R. and Alzheimer, M.** (2014). Analysis of meiosis in SUN1 deficient mice reveals a distinct role of SUN2 in mammalian meiotic LINC complex formation and function. *PLoS Genet* **10**, e1004099.
- Liu, Q., Pante, N., Misteli, T., Elsagga, M., Crisp, M., Hodzic, D., Burke, B. and Roux, K. J.** (2007). Functional association of Sun1 with nuclear pore complexes. *J Cell Biol* **178**, 785-98.
- Lu, W., Gotzmann, J., Sironi, L., Jaeger, V. M., Schneider, M., Luke, Y., Uhlen, M., Szigyarto, C. A., Brachner, A., Ellenberg, J. et al.** (2008). Sun1 forms immobile macromolecular assemblies at the nuclear envelope. *Biochim Biophys Acta* **1783**, 2415-26.
- MacKinnon, E. A. and Abraham, J. P.** (1972). The manchette in stage 14 rat spermatids: a possible structural relationship with the redundant nuclear envelope. *Z Zellforsch Mikrosk Anat* **124**, 1-11.
- Malkov, M., Fisher, Y. and Don, J.** (1998). Developmental schedule of the postnatal rat testis determined by flow cytometry. *Biol Reprod* **59**, 84-92.
- Malone, C. J., Fixsen, W. D., Horvitz, H. R. and Han, M.** (1999). UNC-84 localizes to the nuclear envelope and is required for nuclear migration and anchoring during *C. elegans* development. *Development* **126**, 3171-81.

- Malone, C. J., Misner, L., Le Bot, N., Tsai, M. C., Campbell, J. M., Ahringer, J. and White, J. G.** (2003). The *C. elegans* hook protein, ZYG-12, mediates the essential attachment between the centrosome and nucleus. *Cell* **115**, 825-36.
- Mascarenhas, M.N., Flaxman, S.R., Boerma, T., Vanderpoel, S. and Stevens G.A.** (2012). National, regional, and global trends in infertility prevalence since 1990: a systematic analysis of 277 health surveys. *PLoS Med* **9**, e1001356
- Matzuk, M. M. and Lamb, D. J.** (2008). The biology of infertility: research advances and clinical challenges. *Nat Med* **14**, 1197-213.
- McGee, M. D., Rillo, R., Anderson, A. S. and Starr, D. A.** (2006). UNC-83 IS a KASH protein required for nuclear migration and is recruited to the outer nuclear membrane by a physical interaction with the SUN protein UNC-84. *Mol Biol Cell* **17**, 1790-801.
- Meinke, P. and Schirmer, E. C.** (2015). LINC'ing form and function at the nuclear envelope. *FEBS Lett* **589**, 2514-21.
- Meistrich, M. L., Trostle-Weige, P. K. and Russell, L. D.** (1990). Abnormal manchette development in spermatids of azh/azh mutant mice. *Am J Anat* **188**, 74-86.
- Mejat, A. and Misteli, T.** (2010). LINC complexes in health and disease. *Nucleus* **1**, 40-52.
- Mellad, J.A., Warren, D.T. and Shanahan, C.M.** (2011). Nesprins LINC the nucleus and cytoskeleton. *Current opinion in cell biology* **23**, 47-54.
- Meyerzon, M., Fridolfsson, H. N., Ly, N., McNally, F. J. and Starr, D. A.** (2009). UNC-83 is a nuclear-specific cargo adaptor for kinesin-1-mediated nuclear migration. *Development* **136**, 2725-33.
- Miki, F., Kurabayashi, A., Tange, Y., Okazaki, K., Shimanuki, M. and Niwa, O.** (2004). Two-hybrid search for proteins that interact with Sad1 and Kms1, two membrane-bound components of the spindle pole body in fission yeast. *Mol Genet Genomics* **270**, 449-61.
- Mislow, J. M., Holaska, J. M., Kim, M. S., Lee, K. K., Segura-Totten, M., Wilson, K. L. and McNally, E. M.** (2002). Nesprin-1alpha self-associates and binds directly to emerin and lamin A in vitro. *FEBS Lett* **525**, 135-40.
- Mochida, K., Tres, L. L. and Kierszenbaum, A. L.** (1998). Isolation of the rat spermatid manchette and its perinuclear ring. *Dev Biol* **200**, 46-56.
- Mochida, K., Tres, L. L. and Kierszenbaum, A. L.** (1999). Structural and biochemical features of fractionated spermatid manchettes and sperm axonemes of the azh/azh mutant mouse. *Mol Reprod Dev* **52**, 434-44.
- Moriguchi, K., Suzuki, T., Ito, Y., Yamazaki, Y., Niwa, Y. and Kurata, N.** (2005). Functional isolation of novel nuclear proteins showing a variety of subnuclear localizations. *Plant Cell* **17**, 389-403.
- Morimoto, A., Shibuya, H., Zhu, X., Kim, J., Ishiguro, K., Han, M. and Watanabe, Y.** (2012). A conserved KASH domain protein associates with telomeres, SUN1, and dynein during mammalian meiosis. *J Cell Biol* **198**, 165-72.

- Mosley-Bishop, K. L., Li, Q., Patterson, L. and Fischer, J. A.** (1999). Molecular analysis of the klarsicht gene and its role in nuclear migration within differentiating cells of the Drosophila eye. *Curr Biol* **9**, 1211-20.
- Mylonis, I., Drosou, V., Brancorsini, S., Nikolakaki, E., Sassone-Corsi, P. and Giannakouras, T.** (2004). Temporal association of protamine 1 with the inner nuclear membrane protein lamin B receptor during spermiogenesis. *Journal of Biological Chemistry* **279**, 11626-11631.
- Nebel, B. R., Amarose, A. P. and Hacket, E. M.** (1961). Calendar of gametogenic development in the prepuberal male mouse. *Science* **134**, 832-3.
- O'Donnell, L. and O'Bryan, M. K.** (2014). Microtubules and spermatogenesis. *Semin Cell Dev Biol* **30**, 45-54.
- Oakberg, E. F.** (1956a). A description of spermiogenesis in the mouse and its use in analysis of the cycle of the seminiferous epithelium and germ cell renewal. *Am J Anat* **99**, 391-413.
- Oakberg, E. F.** (1956b). Duration of spermatogenesis in the mouse and timing of stages of the cycle of the seminiferous epithelium. *Am J Anat* **99**, 507-16.
- Oakberg, E. F.** (1957). Duration of spermatogenesis in the mouse. *Nature* **180**, 1137-8.
- Oda, Y. and Fukuda, H.** (2011). Dynamics of Arabidopsis SUN proteins during mitosis and their involvement in nuclear shaping. *Plant Journal* **66**, 629-641.
- Olins, A. L., Hoang, T. V., Zwerger, M., Herrmann, H., Zentgraf, H., Noegel, A. A., Karakesisoglou, I., Hodzic, D. and Olins, D. E.** (2009). The LINC-less granulocyte nucleus. *Eur J Cell Biol* **88**, 203-14.
- Padmakumar, V. C., Libotte, T., Lu, W., Zaim, H., Abraham, S., Noegel, A. A., Gotzmann, J., Foisner, R. and Karakesisoglou, I.** (2005). The inner nuclear membrane protein Sun1 mediates the anchorage of Nesprin-2 to the nuclear envelope. *J Cell Sci* **118**, 3419-30.
- Pasch, E., Link, J., Beck, C., Scheuerle, S. and Alsheimer, A.** (2015). The LINC complex component Sun4 plays a crucial role in sperm head formation and fertility. *Biol Open* **4**, 1792-802
- Perey, B., Clermont, Y. and Leblond, C.P.** (1961). The wave of the seminiferous epithelium in the rat. *Am J Anat* **108**, 47-77.
- Perez, F., Diamantopoulos, G. S., Stalder, R. and Kreis, T. E.** (1999). CLIP-170 highlights growing microtubule ends in vivo. *Cell* **96**, 517-27.
- Petersen, C., Füzesi, L. and Hoyer-Fender, S.** (1999). Outer dense fibre proteins from human sperm tail: molecular cloning and expression analyses of two cDNA transcripts encoding proteins of approximately 70 kDa. *Mol Hum Reprod* **5**, 627-35.
- Pierre, P., Scheel, J., Rickard, J. E. and Kreis, T. E.** (1992). CLIP-170 links endocytic vesicles to microtubules. *Cell* **70**, 887-900.

- Rattner, J. B. and Brinkley, B. R.** (1971). Ultrastructure of mammalian spermiogenesis. II. Elimination of the nuclear membrane. *J Ultrastruct Res* **36**, 1-7.
- Rattner, J. B. and Brinkley, B. R.** (1972). Ultrastructure of mammalian spermiogenesis. III. The organization and morphogenesis of the manchette during rodent spermiogenesis. *J Ultrastruct Res* **41**, 209-18.
- Rattner, J. B. and Olson, G.** (1973). Observations on the fine structure of the nuclear ring of the mammalian spermatid. *J Ultrastruct Res* **43**, 438-44.
- Razafsky, D. and Hodzic, D.** (2009). Bringing KASH under the SUN: the many faces of nucleo-cytoskeletal connections. *J Cell Biol* **186**, 461-72.
- Rosenberg-Hasson, Y., Renert-Pasca, M. and Volk, T.** (1996). A Drosophila dystrophin-related protein, MSP-300, is required for embryonic muscle morphogenesis. *Mech Dev* **60**, 83-94.
- Rothballer, A. and Kutay, U.** (2013). The diverse functional LINCs of the nuclear envelope to the cytoskeleton and chromatin. *Chromosoma* **122**, 415-29.
- Rothballer, A., Schwartz, T. U. and Kutay, U.** (2013). LINCing complex functions at the nuclear envelope: what the molecular architecture of the LINC complex can reveal about its function. *Nucleus* **4**, 29-36.
- Roux, K. J., Crisp, M. L., Liu, Q., Kim, D., Kozlov, S., Stewart, C. L. and Burke, B.** (2009). Nesprin 4 is an outer nuclear membrane protein that can induce kinesin-mediated cell polarization. *Proc Natl Acad Sci U S A* **106**, 2194-9.
- Russell, L. D., Ettlin, R. A., Sinha Hikim, A. P. and Clegg, E. D.** (1990). Histological and Histopathological Evaluation of the Testis. Clearwater, Fl: Cache River Press.
- Russell, L. D., Russell, J. A., MacGregor, G. R. and Meistrich, M. L.** (1991). Linkage of manchette microtubules to the nuclear envelope and observations of the role of the manchette in nuclear shaping during spermiogenesis in rodents. *American Journal of Anatomy* **192**, 97-120.
- Schirmer, E. C. and Foisner, R.** (2007). Proteins that associate with lamins: many faces, many functions. *Exp Cell Res* **313**, 2167-79.
- Schirmer, E. C. and Gerace, L.** (2005). The nuclear membrane proteome: extending the envelope. *Trends Biochem Sci* **30**, 551-8.
- Schultz, N., Hamra, F. K. and Garbers, D. L.** (2003). A multitude of genes expressed solely in meiotic or postmeiotic spermatogenic cells offers a myriad of contraceptive targets. *Proc Natl Acad Sci U S A* **100**, 12201-6.
- Schütz, W., Alsheimer, M., Ollinger, R. and Benavente, R.** (2005a). Nuclear envelope remodeling during mouse spermiogenesis: postmeiotic expression and redistribution of germline lamin B3. *Exp Cell Res* **307**, 285-91.
- Schütz, W., Benavente, R. and Alsheimer, M.** (2005b). Dynamic properties of germ line-specific lamin B3: the role of the shortened rod domain. *Eur J Cell Biol* **84**, 649-62.

- Shao, X., Tarnasky, H. A., Lee, J. P., Oko, R. and van der Hoorn, F. A.** (1999). Spag4, a novel sperm protein, binds outer dense-fiber protein Odf1 and localizes to microtubules of manchette and axoneme. *Dev Biol* **211**, 109-23.
- Shimanuki, M., Miki, F., Ding, D. Q., Chikashige, Y., Hiraoka, Y., Horio, T. and Niwa, O.** (1997). A novel fission yeast gene, kms1+, is required for the formation of meiotic prophase-specific nuclear architecture. *Mol Gen Genet* **254**, 238-49.
- Sosa, B. A., Kutay, U. and Schwartz, T. U.** (2013). Structural insights into LINC complexes. *Curr Opin Struct Biol* **23**, 285-91.
- Sosa, B. A., Rothbauer, A., Kutay, U. and Schwartz, T. U.** (2012). LINC complexes form by binding of three KASH peptides to domain interfaces of trimeric SUN proteins. *Cell* **149**, 1035-47.
- Starr, D. A.** (2009). A nuclear-envelope bridge positions nuclei and moves chromosomes. *J Cell Sci* **122**, 577-86.
- Starr, D. A. and Fischer, J. A.** (2005). KASH 'n Karry: the KASH domain family of cargo-specific cytoskeletal adaptor proteins. *Bioessays* **27**, 1136-46.
- Starr, D. A. and Fridolfsson, H. N.** (2010). Interactions between nuclei and the cytoskeleton are mediated by SUN-KASH nuclear-envelope bridges. *Annu Rev Cell Dev Biol* **26**, 421-44.
- Starr, D. A. and Han, M.** (2002). Role of ANC-1 in tethering nuclei to the actin cytoskeleton. *Science* **298**, 406-9.
- Starr, D. A., Hermann, G. J., Malone, C. J., Fixsen, W., Priess, J. R., Horvitz, H. R. and Han, M.** (2001). unc-83 encodes a novel component of the nuclear envelope and is essential for proper nuclear migration. *Development* **128**, 5039-50.
- Stewart-Hutchinson, P. J., Hale, C. M., Wirtz, D. and Hodzic, D.** (2008). Structural requirements for the assembly of LINC complexes and their function in cellular mechanical stiffness. *Exp Cell Res* **314**, 1892-905.
- Strambio-De-Castillia, C., Niepel, M. and Rout, M. P.** (2010). The nuclear pore complex: bridging nuclear transport and gene regulation. *Nat Rev Mol Cell Biol* **11**, 490-501.
- Suzuki-Toyota, F., Ito, C., Toyama, Y., Maekawa, M., Yao, R., Noda, T., Lida, H. and Toshimori, K.** (2007). Factors maintaining normal sperm tail structure during epididymal maturation studied in Gopc(-/-) mice. *Biol Reprod* **77**, 71-82.
- Suzuki-Toyota, F., Ito, C., Toyama, Y., Maekawa, M., Yao, R., Noda, T. and Toshimori, K.** (2004). The coiled tail of the round-headed spermatozoa appears during epididymal passage in GOPC-deficient mice. *Arch Histol Cytol* **67**, 361-71.
- Tarsounas, M., Pearlman, R. E. and Moens, P. B.** (2001). CLIP-50 immunolocalization during mouse spermiogenesis suggests a role in shaping the sperm nucleus. *Dev Biol* **236**, 400-10.
- The ESHRE Capri Workshop Group.** (2010). Europe the continent with the lowest fertility. *Hum Reprod Update* **16**, 590-602.
- Toshimori, K. and Ito, C.** (2003). Formation and organization of the mammalian sperm head. *Arch Histol Cytol* **66**, 383-96.

- Tzur, Y. B., Wilson, K. L. and Gruenbaum, Y.** (2006). SUN-domain proteins: 'Velcro' that links the nucleoskeleton to the cytoskeleton. *Nat Rev Mol Cell Biol* **7**, 782-8.
- Wang, Q., Du, X., Cai, Z. and Greene, M. I.** (2006). Characterization of the structures involved in localization of the SUN proteins to the nuclear envelope and the centrosome. *DNA Cell Biol* **25**, 554-62.
- Wang, W., Zhu, J. Q., Yu, H. M., Tan, F. Q. and Yang, W. X.** (2010). KIFC1-like motor protein associates with the cephalopod manchette and participates in sperm nuclear morphogenesis in Octopus tankahkeei. *PLoS One* **5**, e15616.
- Ward, W. S. and Coffey, D. S.** (1991). DNA packaging and organization in mammalian spermatozoa: comparison with somatic cells. *Biol Reprod* **44**, 569-74.
- Warren, D. T., Zhang, Q., Weissberg, P. L. and Shanahan, C. M.** (2005). Nesprins: intracellular scaffolds that maintain cell architecture and coordinate cell function? *Expert Rev Mol Med* **7**, 1-15.
- Wilhelmsen, K., Ketema, M., Truong, H. and Sonnenberg, A.** (2006). KASH-domain proteins in nuclear migration, anchorage and other processes. *J Cell Sci* **119**, 5021-9.
- Wilhelmsen, K., Litjens, S. H., Kuikman, I., Tshimbalanga, N., Janssen, H., van den Bout, I., Raymond, K. and Sonnenberg, A.** (2005). Nesprin-3, a novel outer nuclear membrane protein, associates with the cytoskeletal linker protein plectin. *J Cell Biol* **171**, 799-810.
- Wilson, M. H. and Holzbaur, E. L.** (2015). Nesprins anchor kinesin-1 motors to the nucleus to drive nuclear distribution in muscle cells. *Development* **142**, 218-28.
- Wolosewick, J. J. and Bryan, J. H.** (1977). Ultrastructural characterization of the manchette microtubules in the seminiferous epithelium of the mouse. *Am J Anat* **150**, 301-31.
- Xiong, H., Rivero, F., Euteneuer, U., Mondal, S., Mana-Capelli, S., Larochelle, D., Vogel, A., Gassen, B. and Noegel, A. A.** (2008). Dictyostelium Sun-1 connects the centrosome to chromatin and ensures genome stability. *Traffic* **9**, 708-24.
- Yamamoto, A.** (2014). Gathering up meiotic telomeres: a novel function of the microtubule-organizing center. *Cell Mol Life Sci* **71**, 2119-34.
- Yan, W.** (2009). Male infertility caused by spermiogenic defects: Lessons from gene knockouts. *Molecular and Cellular Endocrinology* **306**, 24-32.
- Yang, W. X., Jefferson, H. and Sperry, A. O.** (2006). The molecular motor KIFC1 associates with a complex containing nucleoporin NUP62 that is regulated during development and by the small GTPase RAN. *Biol Reprod* **74**, 684-90.
- Yang, W. X. and Sperry, A. O.** (2003). C-terminal kinesin motor KIFC1 participates in acrosome biogenesis and vesicle transport. *Biol Reprod* **69**, 1719-29.
- Yassine, S., Escoffier, J., Abi Nahed, R., Pierre, V., Karaouzene, T., Ray, P. F. and Arnoult, C.** (2015). Dynamics of Sun5 localization during spermatogenesis in wild type and Dpy19l2 knock-out mice indicates that Sun5 is not involved in acrosome attachment to the nuclear envelope. *PLoS One* **10**, e0118698.

- Yu, J., Lei, K., Zhou, M., Craft, C. M., Xu, G., Xu, T., Zhuang, Y., Xu, R. and Han, M.** (2011). KASH protein Syne-2/Nesprin-2 and SUN proteins SUN1/2 mediate nuclear migration during mammalian retinal development. *Hum Mol Genet* **20**, 1061-73.
- Zhang, Q., Skepper, J. N., Yang, F., Davies, J. D., Hegyi, L., Roberts, R. G., Weissberg, P. L., Ellis, J. A. and Shanahan, C. M.** (2001). Nesprins: a novel family of spectrin-repeat-containing proteins that localize to the nuclear membrane in multiple tissues. *J Cell Sci* **114**, 4485-98.
- Zhang, X., Xu, R., Zhu, B., Yang, X., Ding, X., Duan, S., Xu, T., Zhuang, Y. and Han, M.** (2007). Syne-1 and Syne-2 play crucial roles in myonuclear anchorage and motor neuron innervation. *Development* **134**, 901-8.
- Zhen, Y. Y., Libotte, T., Munck, M., Noegel, A. A. and Korenbaum, E.** (2002). NUANCE, a giant protein connecting the nucleus and actin cytoskeleton. *J Cell Sci* **115**, 3207-22.
- Zhou, X., Graumann, K., Evans, D. E. and Meier, I.** (2012a). Novel plant SUN-KASH bridges are involved in RanGAP anchoring and nuclear shape determination. *Journal of Cell Biology* **196**, 203-211.
- Zhou, X., Groves, N. R. and Meier, I.** (2015). Plant nuclear shape is independently determined by the SUN-WIP-WIT2-myosin XI-i complex and CRWN1. *Nucleus* **6**, 144-53.
- Zhou, Z., Du, X., Cai, Z., Song, X., Zhang, H., Mizuno, T., Suzuki, E., Yee, M. R., Berezov, A., Murali, R. et al.** (2012b). Structure of Sad1-UNC84 homology (SUN) domain defines features of molecular bridge in nuclear envelope. *J Biol Chem* **287**, 5317-26.

7 Appendix

7.1 Abbreviations

AA	amino acid
bp	base pairs
cDNA	complementary DNA
CLSM	confocal laser scanning microscopy
EM	electron microscopy
ER	endoplasmic reticulum
gp	guinea pig
HRP	horseradish peroxidase
IF	immunofluorescence
INM	inner nuclear membrane
m	mouse
mRNA	messenger RNA
MTOC	microtubule organizing center
NE	nuclear envelope
NPCs	nuclear pore complexes
o/n	overnight
ODF	outher dense fiber
ONM	outer nuclear membrane
P	<i>Phusion™</i> DNA Polymerase
PCR	polymerase chain reaction
PNS	perinuclear space
rb	rabbit
RNE	redundant nuclear envelope
RT	room temperature
RT-PCR	reverse transcription – polymerase chain reaction
SIM	structured illumination microscopy
T	Taq DNA Polymerase
WB	western blot

Erklärung

Hiermit versichere ich an Eides statt,

dass ich die Dissertation eigenständig angefertigt habe und keine anderen als die von mir angegebenen Quellen oder Hilfsmittel benutzt habe,

und dass ich die Gelegenheit zur Promotion nicht kommerziell vermittelt bekommen habe und ich keine Person oder Organisation eingeschaltet habe, die gegen Entgelt einen Betreuer bzw. eine Betreuerin für die Anfertigung der Dissertation sucht.

Darüber hinaus erkläre ich,

dass ich die Regeln der Universität Würzburg über gute wissenschaftliche Praxis eingehalten habe,

dass die Dissertation nicht in gleicher oder ähnlicher Form bereits in einem anderen Prüfungsverfahren vorgelegen hat,

und dass ich früher keine weiteren akademischen Grade erworben oder zu erwerben versucht habe.

Würzburg, den _____

(Elisabeth Pasch)

Danksagung

Die Zeit der Doktorarbeit war eine ganz besondere Zeit in meinem Leben und insofern gilt mein Dank all denjenigen, die zum Gelingen dieser Arbeit beigetragen haben.

Im Besonderen möchte ich mich bei Manfred Alsheimer bedanken, der mir das Vertrauen schenkte, das spannende und abwechslungsreiche Thema, „The role of SUN4 and related proteins in sperm head formation and fertility“, zu bearbeiten. Vielen Dank dafür, dass du jederzeit ein so großes Interesse an meiner Arbeit gezeigt hast und mir immer mit zahlreichen Hilfestellungen, ob an der Bench oder am „Schreibtisch“ beiseite gestanden hast. Dank dir habe ich in den vergangenen Jahren sehr viel lernen können, nicht zuletzt von den zahlreichen interessanten Diskussionen, die sich nicht immer nur um die Wissenschaft drehten. Des Weiteren bedanke ich mich bei Prof. Dr. Dr. Manfred Schartl für die freundliche Übernahme des Zweitgutachtens meiner Doktorarbeit.

Ohne ein funktionierendes Labor mit einer so guten Atmosphäre wäre ich wohl bis heute noch nicht fertig geworden. Ein riesen Dankschön geht daher an die Mitglieder der Arbeitsgruppen Alsheimer und Benavente für die wertvollen Tipps, Tricks, Diskussionen oder einfach nur benötigte Ablenkung. Es war großartig, euch alle als Kollegen gehabt zu haben. Viele von euch sind nicht nur die besten Kollegen die man sich wünschen kann, sondern auch wertvolle Freunde geworden. Ein besonderes Dankeschön im Labor „Alsavente“ geht dabei an Jana, Hanna, Katharina, Irene und Marie, aber auch an meine großartigen Masterstudenten Caro und Luisa, und natürlich auch an Silke für die Unterstützung und Arbeitserleichterung (beim Genotypisieren und Ultradünnschnitte anfertigen) und an alle anderen Praktikanten unseres Labors. Des Weiteren danke ich natürlich auch Ricardo Benavente für die „süße“ Unterstützung im Labor, die Motivation, wenn ich sie brauchte und das Angebot, auf die „eisernen Reserven“ zurückgreifen zu dürfen. Vielen Dank, Ricardo, deine Anwesenheit hat das Labor stets erhellt.

Ein großes Dankschön geht neben Markus, Uli, Patrick und Kathrin für die großartige Organisation des Lehrstuhls, und Sarah und Carina für ihre Freundschaft auch an alle anderen Mitglieder der Zoologie I, die ich hier leider nicht alle im Einzelnen erwähnen kann. Ein großer Dank gebührt auch der EM-Abteilung für die Unterstützung und die vielfachen Hilfestellungen und natürlich auch dem Personal des Tierstalls des Biozentrums für ihre leidenschaftliche Arbeit.

Doch trotz der guten Bedingungen am Lehrstuhl und in den dazugehörigen Einrichtungen wäre die Abgabe dieser Arbeit wohl niemals zustande gekommen, wenn ich nicht auch im privaten den nötigen Rückhalt bekommen hätte. An dieser Stelle möchte ich all meinen Freunden danken, die jederzeit für mich dagewesen sind und mich in allen Entscheidungen unterstützt haben. Danke für all eure Motivation und vor allem Freundschaft, Danke für alle Ablenkung und aufbauenden Gespräche, und ich danke dir, Jan, zusätzlich für deinen kleinen Exkurs in „R“. ;)

Und zu guter Letzt, geht ein ganz besonderer Dank an meine Familie. Danke Mama und Papa, dass ihr mich in allem unterstützt, was ich mir in den Kopf gesetzt habe. Und ich danke euch auch, dass ihr mir immer das Gefühl gebt, jederzeit mit allem was mich bedrückt, zu euch zu kommen. Dafür möchte ich mich auch bei meinen Geschwistern Caroline und Friedrich bedanken. Es ist das beste Gefühl der Welt zu wissen, dass ihr alle immer hinter mir steht und den Rücken stärkt. „Ohana“. :D Und nicht zu vergessen natürlich auch ein riesen Dankeschön an meinen Mann Michi. Was soll ich sagen, ich danke dir für alles, ich liebe Dich!